Universitetet i Stavanger

FACULTY OF SCIENCE AND TECHNOLOGY

MASTER'S THESIS

Study program/specialization: Petroleum Engineering/ Reservoir Engineering	Spring semester, 2019 Open
Author: Katarina Radenkovic	…… (signature of author)
Faculty Supervisors: Skule Strand Tina Puntervold	
Title of master's thesis: The effect of wettability on waterflooding and relative permeability at quite water-wet conditions in chalk core	
Credits: 30	
Keywords: Smart Water Wettability Relative permeability Acid number Spontaneous imbibition Waterflooding Oil recovery Carbonates Chalk	Number of pages: 145 + Enclosure: 19 Stavanger, June 14, 2019

Acknowledgment

I would like to express my special and sincere thanks to my supervisors Associate Professors Skule Strand and Tina Puntervold who gave me a golden opportunity to do this project. They gave me invaluable guidance, support and assistance in completing my project. Their visions and motivations have deeply inspired me. It was a great privilege and honor to study and work under their guidance. I would also like to thank them for their friendship and amazing sense of humor.

I would also like to extend my deep gratitude to the post-doctoral fellow, Iván Darío Piñerez Torrijos and Associate Professor Pål Østebø Andersen, for all the time they spent helping me with laboratory work. My completion of this project could not be accomplished without his support.

I thank my friends and research colleagues in Smart Water group, Amalie Harestad and Agnes Kahlbom Wathne, for all the days we spent together in the lab, for all hard discussions and decisions we made together, for all the fun we had during the past six months and for all the support they provided during my research work.

I would like to express my deep and sincere gratitude to my dear friend PhD student Jaspreet Singh Sachdeva for helping me finalize my work and for the patience during my thesis finalization.

I am extremely grateful to my parents, sister and brother for their love, prayers, support, caring and sacrifices for my education. I am very thankful to my husband, his love, prayers, understanding, and support to complete this research work.

Radenkovic Katarina

Abstract

The effect of performing waterflooding in chalk has been previously tested with a purpose of Enhanced Oil recovery. Regarding oil recovery processes, rock wettability is the key parameter determining transport of fluid flow through porous media. This work shows how the core wettability affect the relative permeability in carbonate reservoirs and hence impact the oil recovery.

In this project, carbonate chalk material from Stevns Klint is used as a porous media to evaluate the effect of wettability on unsteady state relative permeability estimations at room temperature of 23°C. For the experiment, two chalk cores were prepared as reference water-wet cores and used as examples of the optimum cases after a completely successful waterfloods and two other cores were used with modified wettability. All the cores were saturated to 20% of initial water saturation, cores were saturated fully by synthetic model oil/crude oil to establish initial conditions. Cores were afterwards subjected to flooding by a formation water and flooded two artificial versions of seawater (SW0T and SW1/2T brines) to measure wettability by chromatography wettability method. The reference water-wet cores showed quite high oil recovery while mixed-wet cores showed insignificantly lower oil recovery during both forced and spontaneous imbibition tests. Pressure drop curve behave more or less the same for the reference water-wet cores SK-R1, SK-R2 and mixed-wet core SK-C3, while core SK-C6 behave slightly different during forced imbibition test. Production history and pressure drop from cores SK-R1, SK-R2 and SK-C3 were used to do the history matching of relative permeability curves by Sendra modeling tool.

Spontaneous imbibition was introduced in order to gather information about cores' wettability and forced imbibition was introduced to monitor behavior of fluid flow through core under a viscous force dominated environment, while pressure drop across all cores and oil production measurements were recorded. Collected data was combined with end-points of relative permeability curves to calculate the effect of wettability on relative permeabilities. As synthetic model oil used in this project contained the polar organic components (POC) responsible for wettability alteration towards an oil-wet state, it was used with a purpose of changing the carbonate cores' wettability through flooding. POC is quantified by the acid and base numbers, AN and BN, which are

measured in mg KOH/g. In carbonate reservoirs, the acidic POC plays a major role on determining wetting state.

After spontaneous imbibition tests, wetting state of the cores was analyzed by chromatographic wettability test, through which we obtain the water-wet surface area of all chalk cores.

The experimental measurements acquired during the flooding processes will contribute to increase our understanding of how significantly wettability changes affect relative permeabilities and oil/water saturations during oil production. The concept of wettability is of great importance to the industry and academia, specially to check for its effect on enhanced oil recovery, where diverse mechanisms have been proposed to increase recovery by changing the wetting state of reservoir rocks, as it impacts reserve volumes and flooding performance.

Table of Contents

List of figures

List of tables

Symbols and abbreviations

A	*Adsorption area*
A_1	*The area between the forced drainage curve and the saturation axis*
A_2	*The area between the forced imbibition curve and the saturation axis*
a_o	*Constant (oil), dimensionless*
a_w	*Constant (water), dimensionless*
A_{wett}	*The area between the SCN^- and SO_4^{2-} curves of a wetted core sample*
A_{ref}	*The area between the SCN^- and SO_4^{2-} curves of a completely water-wet reference core sample*
AN	*Acid number*
BN	*Base number*
c_o	*Constant for the entry pressure of water phase*
$COBR$	*Crude oil, brine and rock system*
c_w	*Constant for the entry pressure of water phase*
CWT	*Chromatography Wettability Test*
C/C_o	*Relative concentration of ions*
D	*Core diameter*
DI	*Deionized water*
EOR	*Enhanced oil recovery*
E	*The total efficiency of oil displacement*
E_D	*Microscopic displacement efficiency*
E_V	*Macroscopic displacement efficiency*
FI	*Forced imbibition*
F_v	*Viscous force*
Fc	*Capillary force*
fw	*Fractional flow*
FW	*Formation water*
g_c	*Conversion factor*
g	*Gravitational acceleration*
H	*Height of the liquid column*

I_{AH}	*Amott–Harvey relative displacement index*
I_{USBM}	*USBM relative displacement index*
IFT	*Interfacial tension*
IC	*Ion chromatography*
I_O	*Displacement-by-oil-ratio*
I_w	*Displacement-by-water-ratio*
J	*Dimensionless value for capillary pressure calculation*
k	*Absolute permeability*
k_o	*Effective permeability of oil*
k_w	*Effective permeability of water*
k_g	*Effective permeability of gas*
k_{ro}	*Relative permeability of oil*
k_{rw}	*Relative permeability of water*
k_{nw}	*Permeability of non-wetting phase*
k_w	*Permeability of wetting phase*
KOH	*Potassium hydroxide*
L	*Core length*
M	*Mobility ratio*
N_{ca}	*Capillary number*
N_w	*Corey exponent for water phase*
N_o	*Corey exponent for oil phase*
$OOIP$	*Original oil in place*
P_c	*Capillary pressure*
P_o	*Pressure of oil phase*
P_w	*Pressure of water phase*
P_{tc}	*Capillary pressure threshold*
PSD	*Pore size distribution*
PV	*Pore volume*
PV/d	*Pore volume per day*
r	*The radius of the cylindrical pore channel*
q	*The flow rate*
ROW	*Rock, oil and water system*
R_1	*The largest curving radii*

R_2	*The smallest curving radii*
S_o	*Saturation of oil phase*
S_g	*Saturation of gas phase*
S_w	*Saturation of water phase*
S_{wc}	*The connate water saturation*
S_{wr}	*The residual water saturation*
S_{or}	*Residual oil saturation*
S_{wi}	*Initial water saturation*
S_{oi}	*Initial oil saturation*
S_{gi}	*Initial gas saturation*
S_n	*Normalized saturation*
SW	*Seawater*
$SW0T$	*Synthetic seawater without* SO_4^{2-}
$SW½T$	*Synthetic seawater with equal concentration of* SCN^- *and* SO_4^{2-}
SK	*Stevns Klint*
SI	*Spontaneous imbibition*
TOC	*Total organic content*
$USBM$	*United States Bureau of Mines*
WI	*The wettability index*
φ	*Porosity*
ΔS_{WS}	*Saturation change during spontaneous imbibition of water*
ΔS_{WF}	*Saturation change during forced imbibition of water;*
ΔS_{OS}	*Saturation change during spontaneous drainage of oil;*
ΔS_{OF}	*Saturation change during forced drainage of oil.*
ΔP	*Pressure drop*
ΔP_g	*Pressure difference between oil and water due to gravity*
$\Delta\rho$	*Density difference between oil and water*
μ_w	*Viscosity of water*
μ_o	*Viscosity of oil*
ρ	*Density of single phase*
θ	*Contact angle*
θ_a	*Advancing contact angle*
θ_r	*Receding contact angle*

dP/dx	*The pressure gradient*
λ_D	*Mobility of the displacing fluid*
λ_d	*Mobility of the displaced fluid*
λ_w	*Mobility of water*
λ_o	*Mobility of oil*
σ	*Interfacial tension*
σ_{ow}	*Interfacial tension between oil phase and water phase*
σ_{os}	*Interfacial tension between oil phase and solid surface*
σ_{sw}	*Interfacial tension between solid surface and water phase*
μ	*The viscosity*
μ_w	*Viscosity of water phase*
μ_o	*Viscosity of oil phase*
υ_{avg}	*Average flow velocity in the capillary tube*

1. Introduction

1.1. Background

Crude oil, also known as “Black Gold”, represents the primary source of energy nowadays. According to the U.S. Energy Information Administration, intensive consumption of hydrocarbons has led to a reduction in global reserves (EIA, 2019). Acknowledging that this form of fossil fuel, also the largest energy source in the world, is depleting, scientists and researchers are dedicated to new inventions and discoveries that would contribute to better exploitation of remaining oil reserves. On this path of research work, different methods are being tested and developed in which “Enhanced Oil Recovery (EOR) by Smart Water” represents the youngest one. The Smart water concept represents injection of modified seawater into the carbonate reservoir to alter its wettability.

Presently about 50% of the global petroleum reserves are stored in carbonate reservoirs, which generally give low oil recovery (Høgnesen, 2005). Manrique et al. (2007) claims that the reason for such low recovery stays in carbonates’ fragile nature. Fractures in the rock matrix result in low hydrocarbon recovery. This occurs as a result of early breakthrough of water after fluid injection due to unbalanced sweeping. Thus, carbonate reservoirs become the hot topic for scientists with a main goal of determining their heterogeneity.

The wetting state of rock matrix appears to be a major parameter for carbonate reservoirs. According to Chilingar & Yen (1983) and Høgnesen (2005), about 80% of the world’s carbonate reservoirs have been determined as oil-wet. Therefore, wettability is a crucial parameter for determining the impact of waterflooding on oil recovery from carbonate reservoirs (Hirasaki & Zhang, 2004; Morrow & Mason, 2001; Tong, 2002). Since carbonate reservoirs are often fractured, spontaneous imbibition of water from the fractures and into the matrix is important to produce the oil from the matrix. Fractures hold a relatively small amount of crude oil.

Oil recovery processes can be classed into primary, secondary and tertiary methods. Primary methods include natural flow and artificial lift, secondary methods include waterflooding, while the tertiary method involves thermal method, gas and chemical

injection. Primary recovery methods give low ultimate recovery. That is why the industry nowadays is more and more focused on secondary and tertiary recovery methods.

The secondary method of waterflooding is defined as water injection into the hydrocarbon-rich reservoir, with an aim of maintaining pressure and displacing the residual oil. This process has been used as a synonym for improved oil recovery (IOR)'s secondary recovery method (Green & Willhite, 1998; Speight, 2017). Water injection appears to be widely used all across the globe in the oil reservoirs due to water's price, availability, environmental impact and good injectivity in oil-bearing formations (Yousef, Al-Saleh, & Al-Jawfi, 2012). Injecting a brine, which has a composition different from the formation water, can be considered an EOR-method. For carbonate reservoirs this implies to seawater or modified seawater, Smart water. The optimized composition of Smart water alters the wettability of carbonate reservoirs and improves oil recovery (Standnes & Austad, 2000).

Spontaneous imbibition of water into the matrix is important and is dependent on the wettability. Wettability is also affecting not only the location of fluids in the pore space, but also the relative permeability of the fluids. Relative permeability is an input parameter in reservoir simulation to evaluate the success or potential for e.g. Smart Water EOR.

The present study deals with estimation and analysis of the impact of waterflooding on carbonate rock petrophysical properties when the fluids with modified compositions are injected into the reservoir. Especially the impact of wettability and wettability alteration will have on relative permeability and oil recovery.

1.2. Objectives

This project deals with the with waterflooding as a recovery process in carbonate reservoirs. The main objective of this study is to discover how the relative permeability curves are influenced by wettability changes in selected chalk materials with same initial water saturations. The purpose of this experimental work is to acquire knowledge about the adsorption of acidic components of the crude oil onto the chalk rock surface and how this adsorption influences wetting properties of the rock and relative permeabilities during water injection. Various methods, such as forced imbibition, spontaneous imbibition and chromatography, have been used in the experimental work.

Experimentally, the initial water saturation of chalk cores was stablished using desiccator method. Two reference cores were flooded by model oil, while two other cores were flooded with crude oil containing polar organic components, giving two completely water-wet reference cores and two less water-wet cores due to crude oil adsorption. Thereafter, cores were subjected to forced and spontaneous imbibition by formation water (deionized water). Investigating core wettability by forced imbibition of formation water (DI), permeability data and oil recovery data were generated, while spontaneous imbibition (SI) provides information about capillary forces present in a system. The tests were performed on cores with initial water saturation $S_{wi} = 0.2$ established by dessicator.

Additionally, the chromatography wettability test was performed on effluent samples to confirm the accuracy of results giving the information about wetting state, obtained by forced and spontaneous imbibition tests. The test gives the fraction of water-wet area inside the core. If wettability index, WI= 1, the areas between SCN^- and SO_4^{2-} are the same and the core is completely water-wet. If WI <1, the areas are different and the fraction of water-wet surface area inside the core is lower.

Finally, obtained results were used to simulate the relative permeability curves with an aim of confirming the effect of different wetting states on relative permeability curves and the location of their intersection point.

1.3 Thesis Outline

The work presented in this thesis is organized into six sections. The detailed description of sections is briefly described as follows:

- Section 1 gives an introduction to the experimental work and describes projects importance and objectives.
- Section 2 presents a literature review on oil recovery processes, mechanisms for fluid displacement, theoretical aspects of wettability and defines carbonate reservoirs. Subsections gives deeper explanation about how wettability affect the relative permeability curves.
- Section 3 describes the materials, methods and analytical methods used to investigate the reasons for different relative permeabilities. The work is based on waterflooding in Hassler cell and utilizes water-wet Stevens Klint chalk cores saturated with formation water under vacuum and flooded by synthetic model oil and crude oil. The brines used to carry out experiments were SW0T and SW1/2T.
- Section 4 briefly describes the experimentally obtained results and discussion on chalk cores and comparison with the results obtained on other cores processed by other two students from group.
- Section 5 covers simulated results and discussion.
- Section 6 provides the overall conclusions and recommendations for future work.

2. Literature Review

This section covers the general principles and briefly describes fundamental concepts related to oil recovery, mechanisms for fluid displacement, the concept of wettability and the ways of determining wettability and a general background about carbonate rocks.

2.1 Oil recovery

The life cycle of a reservoir is given by the following structure: exploration, discovery, delineation, development, production, and abandonment (Dake, 1983). Production of oil and gas from a reservoir, in itself, requires detailed planning. There are several methods of oil recovery and basic subdivision is presented in Table 1 and Figure 1.

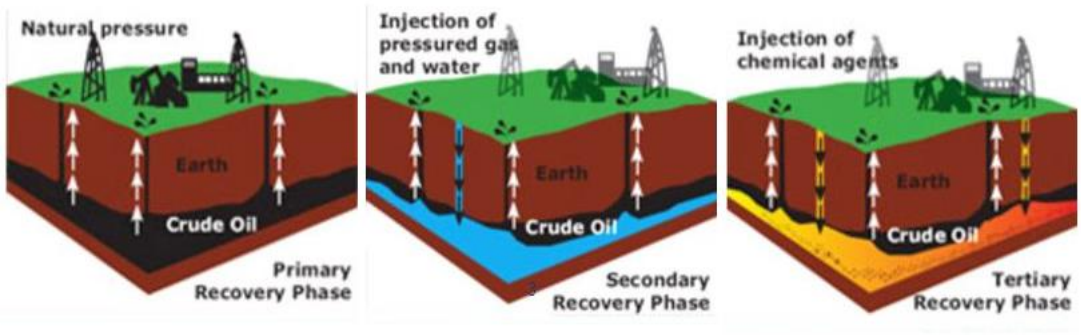

Figure 1. Primary (left), Secondary (middle) and Tertiary (right) Oil Recovery Stages (SlidePlayer, 2017)

Table 1. Methods for Petroleum Recovery (Speight, 2017)

Conventional Oil Recovery	Primary Recovery	Natural Flow Artificial Lift	Pump Gas Lift Other	
	Secondary Recovery	Waterflood Pressure Maintenance	Water Gas Injection	
Enhanced Oil Recovery	Tertiary Recovery	Thermal Method	Steam Soak Steam Drive Steam Flood Cyclic Steam Injection Hot Water Drive Combustion	
		Gas Injection	Miscible/Immiscible	Hydrocarbon Injection CO_2 Injection Flue Gas Injection
		Chemicals Injection	Alkali Flood Polymer Flood Micellar Flood	

			Foam Injection	
		Other	Microbial Injection Oil Mining	

2.1.1 Primary Recovery

Primary recovery represents the first stage in oil recovery process. The main principle for this stage is usage of natural reservoir energy such as water/gas drive, fluid/rock expansion or gravity drainage to displace the hydrocarbons from the formation to the production facilities (Green & Willhite, 1998). The reservoir pressure is usually higher than the bottom hole pressure inside wellbore. Consequently, the positive pressure difference will be high enough to transport hydrocarbons towards production well and surface (Figure 1). Furthermore, the production will reduce the reservoir pressure, i.e. differential pressure. This will lead to lowered hydrocarbon production in self flowing wells. As a support for reservoir pressure it will be necessary to install artificial lift systems, which can result in big costs. The primary recovery mostly reaches its maximum when the reservoir pressure is too low. Finally, only 5-30 % of the original oil in place (OOIP) is recovered during the primary phase production (Baviere, 1991).

2.1.2 Secondary Recovery

The secondary oil recovery begins right after primary recovery starts decreasing. To maintain the reservoir pressure and aid in the further displacement of hydrocarbons towards the production wells (Green & Willhite, 1998), water or gas injection is carried out (Figure 2). The secondary stage will last until the injected gas or water is produced in an amount which is not profitable. According to Baviere (1991), 30 to 70% of OOIP is left in the reservoir at the end of secondary recovery phase. Hence, the oil recovered is in the range 20-40% of OOIP (Castor, 1981; Muggeridge, 2014). The reason for such a low percentage of oil recovery (Zolotuchin & Ursin, 2000) is explained by reservoir fractures, non-favorable wettability, capillary-trapped oil or considerable permeability variations with layered depths. Gas injection is not so commonly used as it is less effective than waterflooding (Green & Willhite, 1998). Waterflooding, sometimes used as a synonym for secondary recovery (Green & Willhite, 1998), replaces the pressure loss of the reservoir through water injection and displaces the oil towards producing wells (Speight, 2017).

2.1.2.1 Waterflooding

Waterflooding has been performed in the fields around the world for more than a century. As already mentioned in section 2.1.2, water injection or waterflooding is one of two main conventional methods referring to secondary oil recovery. The main goal of water injection process is to displace the residual oil from the pore spaces, maintain reservoir pressure and improve sweep efficiency of the reservoir. Efficiency of such displacement will depend on factors such as oil viscosity and rock characteristics. On the other hand, to obtain successful water injection into the reservoir, the water entering the system must satisfy reservoir standards (Lyons, 1996). Considering this, the injected water should have the same composition as the water that is already present in the reservoir, i.e. the formation water. If for some reason the injected water has the same composition as seawater, the process can be classified either as secondary or tertiary oil recovery method. Brownscombe and Dyes (1952) observed that water flooding could be used in a highly fractured rock only if the system is water-wet. If the rock is not water-wet, no positive capillary forces exist to imbibe the water into the rock. Consequently, the gravity drainage process will take place.

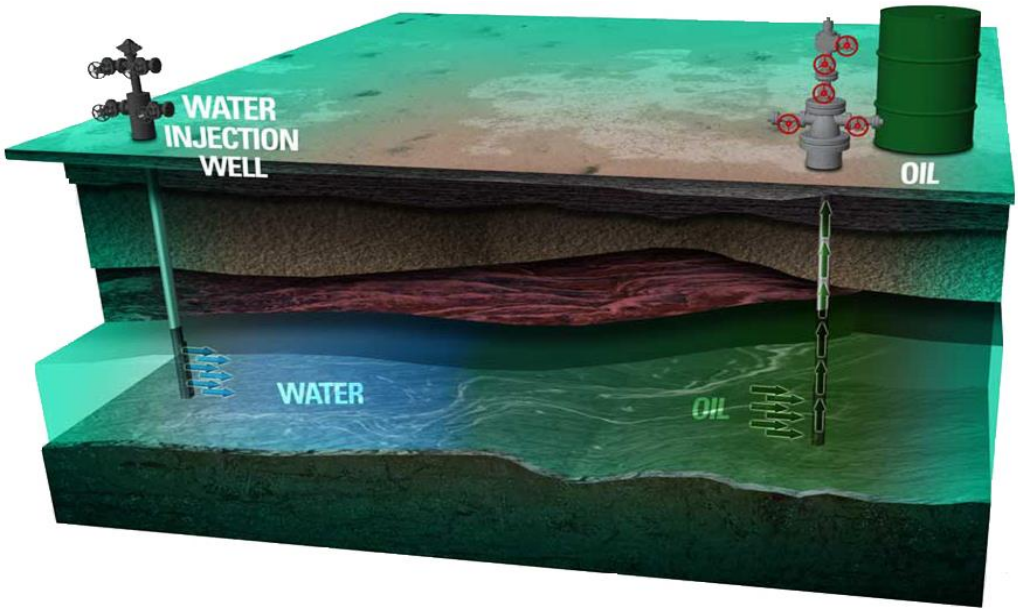

Figure 2. Waterflooding process of an oil reservoir (PNG, 2019).

Waterflooding, however, is not always the best oil displacement process and it can have complications. The most known disadvantage with water injection is the so-called viscous fingering (Figure 3). This problem occurs due to viscosity difference between oil and water (Ahmed, 2010). The unfavorable mobility ratio of these two fluids result in fingering of water through the more viscous oil and consequently the efficiency of oil displacement is reduced due to poor sweep efficiency. In the fingering pattern shown in Figure 3, when the oil is swept out from the reservoir, some sections are missed along the way leaving residual oil behind (Willhite, 1986). In later stages of waterflooding, when less oil is recovered per barrel of water injected into the reservoir, the surfactants may be introduced to the injection fluid. This leads to a reduction in the surface energy between water and oil causing oil droplets to flow more efficiently through the rock formations to the producing wells.

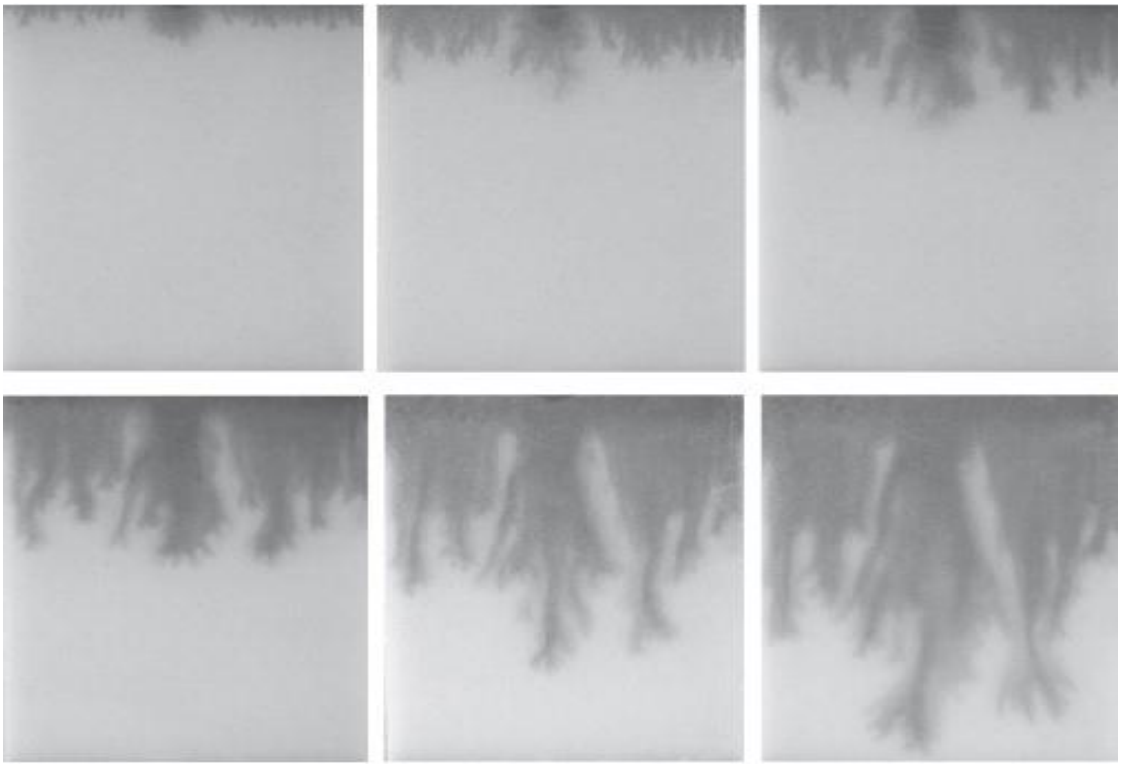

Figure 3. Viscous Fingering profile during waterflooding[i]

In fractured reservoirs, it is paramount to understand the importance of viscous and capillary displacements to better interpret the recovery mechanisms, including and not limited to waterflooding (Figure 4). Figure illustrates the waterflooding process in fractured reservoir over the time of 200 days, where the oil recovery for is shown on

[i] https://www.sciencedirect.com/topics/engineering/viscous-fingering

Figure 4.c. Graue et al. (2001) performed waterflooding studies on both strongly water-wet and moderately water-wet fractured chalk materials and showed that:

- Fractures can significantly affect the water movement during waterflooding in case of water-wet conditions (not a case at moderately water-wet conditions).
- For strongly water-wet and moderately water-wet chalks, the oil recovery was similar after performing waterflooding processes due to increase in permeability after low fracturing.
- At strongly water-wet conditions, the fractures do not have a great impact on the total oil recovery. On the other hand, at moderately water-wet conditions, the recovery appeared to be reduced when the permeability increased after fracturing was too high.
- Open fractures act as barriers to flow at both wetting conditions.
- The recovery mechanisms changed towards more viscous dominant flow regimes at less water-wet conditions.

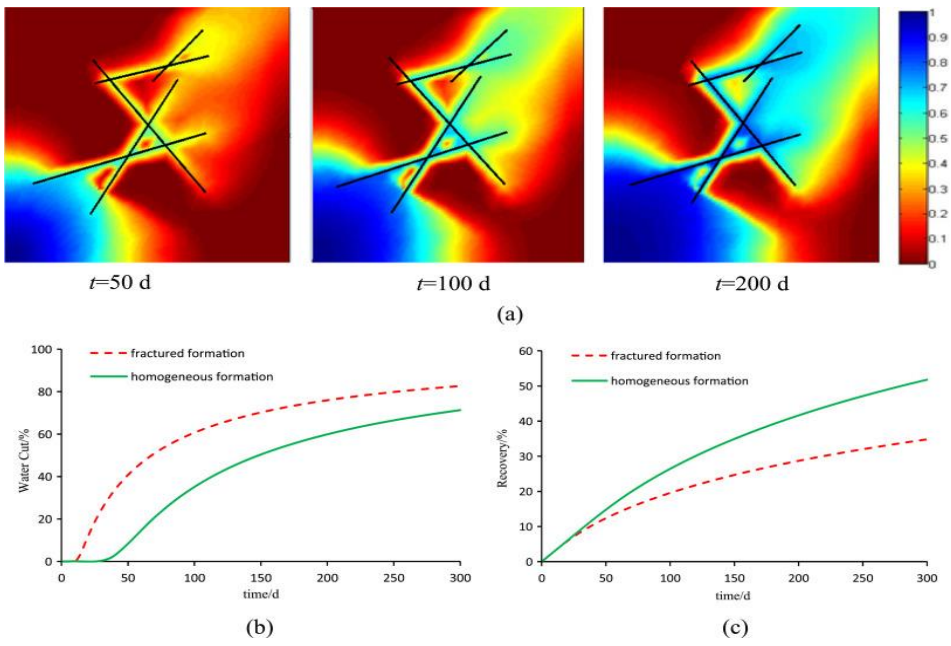

Figure 4 The effect of fractures on Water cut and Oil Production (Zhanga, 2016); a) waterflooding through a fractured reservoir over a period of 200 days, b) water cut % in fractured and homogeneous formation, c) oil recovery % in fractured and homogeneous formation.

Moreover, understanding of waterflooding process is the basis for studying the impact of wettability on relative permeability in terms of oil displacement.

2.1.3 Tertiary Recovery – Enhanced Oil Recovery (EOR)

Nowadays, tertiary recovery is replaced by the term "Enhanced Oil Recovery (EOR)". The main goal with this last oil recovery stage is to recover the residual oil that is left in the reservoir after the primary and secondary recovery stages. Many researchers have tried to define EOR in their own words. Baviere states that (1991), "EOR consists of methods aimed at increasing ultimate oil recovery by injecting appropriate agents not normally present in the reservoir, such as chemicals, solvents, oxidizers and heat carriers in order to induce new mechanisms for displacing oil." In the tertiary stage the various fluids injected into the reservoir have an aim of changing rock and crude oil properties (Green & Willhite, 1998), (Figure 1). This means changing of wettability, interfacial tension, fluid density, viscosity, permeability, porosity and pore size that could ultimately lead to enhanced oil recovery (Zhang, 2006). Tertiary stage is subdivided into five methods: chemical, miscible, immiscible gas drives, thermal and other processes (Taber, 1997), as given in Table 2.

Table 2. Classification of EOR methods (Taber, 1997)

Chemical	*Surfactant* *Alkaline* *Polymer* *Micellar* *Emulsion*
Miscible	*Slug Process* *Enriched* *Vaporizing Gas Drive* *CO_2* *N2 Miscible* *Alcohol*
Immiscible gas drives	*CO_2* *Flue* *Inert Gas*
Thermal	*Hot Water* *In-Situ Combustion* *Steam* *Electrical Heating*
Wettability alteration	*Low Salinity Water Injection in Sandstones* *Smart Water in Carbonates* *Cationic Surfactants in Carbonates*
Other	*Microbial EOR* *Foam* *Water Alternating Gas*

Wettability alteration was proposed recently as a new EOR method. It has the ability to increase capillary forces and improve microscopic sweep efficiency. Proposed processes for water-based wettability alteration are subdivided into: Smart Water, Low Salinity (sandstones) and Seawater/modified Seawater (carbonates).

2.1.3.1 Smart Water as Tertiary Method

The composition of the injection brine is an important parameter for oil displacement. Through several studies it has been shown that modified injection water can alter the wettability in oil reservoirs to a more water-wet state (Standnes & Austad, 2000). The modified seawater is then called "Smart Water". Injection of optimized brine improves the wetting properties of oil reservoirs and optimizes fluid flow and oil recovery. Smart water disturbs the chemical equilibrium of the initial crude oil, brine and rock (CBR) system, and hence alter the wettability. In the same way it will have positive effects on the capillary pressure and relative permeability of oil and water. When injected, smart water makes oil more mobile resulting in better oil production, Figure 5.

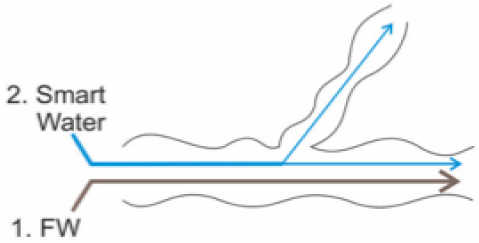

Figure 5. Wettability Alteration by Smart Water (Strand, Puntervold, & Austad, 2016)

The main advantages of this method are that this method is economical and does not require addition of expensive chemicals and that it is environmentally friendly. Studies so far have shown no injection problems with smart water (Austad, 2013). For this reason, Austad (2013) claims that it would be desirable to flood with smart water from the beginning of the waterflooding process. To fully understand the smart water concept, it is important to keep in mind the initial wettability of the system and the factors influencing it, as well as the fact that hydrocarbons are stored in both sandstones and carbonates which generally have different rock properties.

2.2 Mechanisms for fluid displacement

The displacement forces present the crucial factor when considering oil production and fluid flow in porous media. The oil displacement through reservoir can be obtained

using many different methods. Still, Morrow (1979) claims that during the oil production process there are three most important displacing forces determining the flow of oil and water through porous media. These are viscous forces, gravity forces and capillary forces. The oil recovery has two stages: spontaneous imbibition and forced imbibition. For these two stages there will be different necessary driving forces, such as capillary and gravity forces in spontaneous imbibition stage (Strand, 2005) and viscous forces in forced imbibition stage. The interplay between these forces is very important in situations where the wettability approaches neutral state or the interfacial tension (IFT) decreases. With a decrease in IFT in several orders of magnitude, the gravity forces may dominate the flow pattern in the porous media (Strand, 2005).

The overall displacement during an EOR process can be divided into microscopic and macroscopic scale. The product of microscopic and macroscopic displacement efficiencies give the total efficiency (E) of oil displacement, defined by equation:

$$E = E_D E_V \tag{2.1}$$

where E_D is the microscopic displacement efficiency and E_V is the macroscopic (volumetric) displacement efficiency, both expressed as a fraction. The microscopic displacement specifies the mobilization of hydrocarbons at pore scale. E_D is, in general, presented in the magnitude of the residual oil saturation reached (S_{or}). The macroscopic (volumetric) displacement efficiency specifies the volumetric interpretation of reservoir displacement and the sweep efficiency. Also, E_V is defined as a measure of how efficient the volumetric sweep is (Green & Willhite, 1998).

Without fluid flow, there will be no oil recovery. The permeability is one of the most important rock properties. Its role is to determine how the fluid will flow through a porous medium. Darcy's law is used to define the fluid flow in porous media for unfractured reservoirs by following equation:

$$q = -\frac{k\, dP}{\mu\, dx} \tag{2.2}$$

Where,

- k Permeability $[m^2]$
- q Flow rate $[m^3/s]$

μ Viscosity $[Pa \cdot s]$

dP/dx pressure gradient $[Pa/m]$.

If two fluids are present in the reservoir system, such as waterflooding of oil reservoir, displacement efficiency will depend on the wettability of reservoir rock. The displacement process is defined through mobility ratio concept. Mobility ratio, M, is defined as the mobility of the displacing fluid λ_D behind the flooding front divided by the mobility of the displaced fluid λ_d ahead of the flooding front and can be estimated from:

$$M = \frac{\lambda_D}{\lambda_d} = \frac{\lambda_w}{\lambda_o} = \frac{\left(\frac{k_{rw}}{\mu_w}\right)_{S_{or}}}{\left(\frac{k_{ro}}{\mu_o}\right)_{S_{wi}}} \tag{2.3}$$

Where,

M Mobility ratio

λ_D Mobility of the displacing fluid ($m^2/ Pa \cdot s$)

λ_d Mobility of the displaced fluid ($m^2/ Pa \cdot s$)

λ_w Mobility of water ($m^2/ Pa \cdot s$)

λ_o Mobility of oil ($m^2/ Pa \cdot s$)

k_{rw} Relative permeability of water (m^2)

k_{ro} Relative permeability of oil (m^2)

μ_w Water viscosity ($Pa \cdot s$)

μ_o Oil viscosity ($Pa \cdot s$)

S_{or} Residual oil saturation

S_{wi} Irreducible water saturation

To obtain better sweep and favorable mobility of oil during waterflooding process, surfactants are very often added to the injected water.

2.2.1 Viscosity forces

The viscous forces represent one of the three main active displacing forces when waterflooding is taking place in a reservoir system. They are defined as the magnitude of the pressure drop caused by flow of fluids over a certain length through the porous

medium. The estimation of such a force can be done through either laminar (Figure 6) or turbulent flow (Figure 7). In laminar flow a viscous fluid moves in parallel layers, having a constant velocity at any point in the fluid. During turbulent flow the fluid mixes irregularly and it has no constant flow rate.

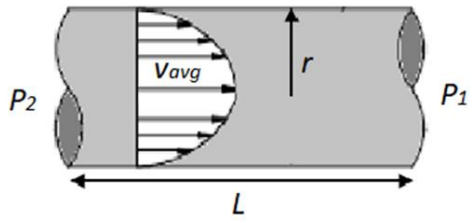

Figure 6. Effect of Viscous Forces on Laminar Fluid Flow (modified after (Power, 2018))

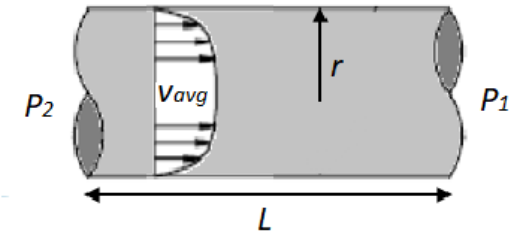

Figure 7. Effect of viscous forces on Turbulent fluid flow (modified after (Power, 2018))

Considering laminar flow (Figure 6), described as the flow through a bundle of a parallel capillary tubes, the pressure drop through a single tube can be calculated by Poiseuille´s law (Green & Willhite, 1998):

$$\Delta P = \frac{-8\mu L v_{avg}}{r^2 g_c} \tag{2.4}$$

Where,

ΔP	pressure drop across the capillary tube [Pa]
μ	viscosity [Pa·s]
L	length of the capillary tube [m]
v_{avg}	average flow velocity in the capillary tube [m/s]
r	radius of the capillary tube [m]
g_c	conversion factor

During waterflooding process, a term capillary number, denoted N_{ca}, is introduced. This number is the dimensionless ratio of viscous to capillary forces. N_{ca} is mathematically defined by equation (2.5):

$$N_{ca} = \frac{F_v}{F_c} = \frac{v\mu_w}{\sigma_{ow}} \quad (2.5)$$

Where,

F_v	Viscous force
F_c	Capillary force
v	Interstitial pore velocity
μ_w	Viscosity of the water/Viscosity of displacing fluid
σ_{ow}	Interfacial tension between displaced (oil) and displacing (water) fluid

From equation (2.5), we observe that N_{ca} will increase as the viscosity of the displacing fluid increases, interfacial tension between displacing and displaced fluid decreases or when the flow rate of the displacing fluid increases (Green & Willhite, 1998). The most common values of N_{ca} for successful waterflooding will be $N_{ca} < 10^{-7}$ (Melrose, 1974.)

So, in order to produce more oil under the same waterflooding conditions, viscous forces have to overcome capillary forces (Morrow, 1979) responsible for trapping oil in a way that either the viscous forces within the pores or the pressure gradient should be increased (Abdallah, 2007).

2.2.2 Gravity forces

Lake (2010) claims that the effects of gravity forces on droplets of oil within a pore space are determined by the density of the fluid. These forces have a major role in multiphase systems where there may be large differences in the densities of the fluids. In a water-oil system, the pressure difference due to gravity is given by:

$$\Delta P_g = \Delta\rho g H \quad (2.6)$$

Where,

ΔP_g	pressure difference between oil phase and water phase, due to the gravity [Pa]
$\Delta\rho$	density difference between oil phase and water phase [kg/m^3]

g gravity acceleration (9.81) [m^2/s]

H height of the liquid column [m]

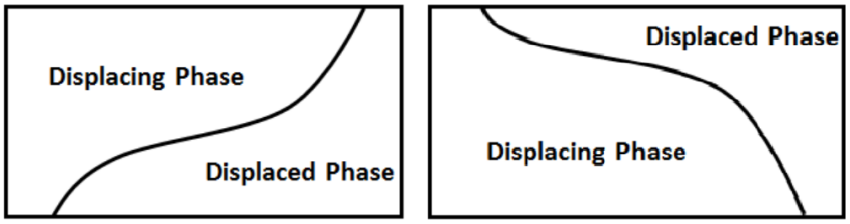

Figure 8. Gravity effects on Displacement profile (PERMInc, 2012)

2.2.3 Capillary forces

Capillary forces (P_c) are the active forces of a system where two or more immiscible fluids are present. They are very important for further optimization of oil recovery. There are several ways to define capillary forces. By one of definitions, P_c is "the pressure difference across a curved interface between two immiscible fluids" (Zolotuchin & Ursin, 2000). Generally, they represent the pressure difference between non-wetting and wetting phases (Strand, 2005), and are given by the equation (2.7):

$$P_c = P_o - P_w \tag{2.7}$$

Where,

P_c Capillary pressure
P_o Oil phase pressure
P_w Water phase pressure

Now, to force water into the matrix and mobilize the trapped oil droplets, the capillary threshold pressure should be overcome by the imbibing forces. Such a relation is defined by Leveret J-function:

$$P_{tc} = \sigma\sqrt{\frac{\varphi}{k}J} \tag{2.8}$$

Where,

P_{tc} Capillary pressure threshold
σ Interfacial tension between the phases
φ Porosity
k Permeability
J Dimensionless value (often the value 0.25)

Moreover, the threshold capillary pressure can also be exceeded by viscous and gravity forces and eventually eliminated by modifying the wettability of the rock (Al-Hadhrami & Blunt, 2001).

The interface of two immiscible fluids in a single capillary tube is, in most of the cases, shaped in meniscus form which is defined by the two radii R_1 and R_2 (Figure 9).

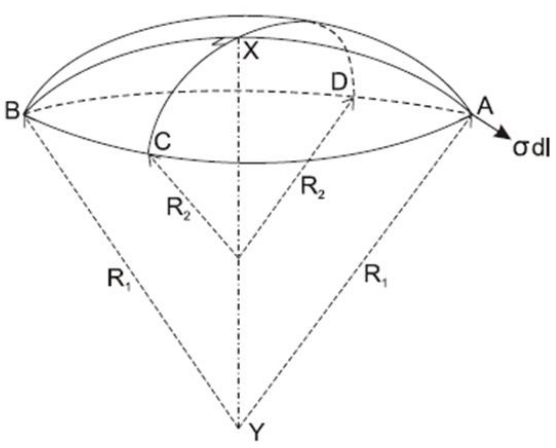

Figure 9. Curved surface with the largest R1 and the smallest R2 curving (modified after (Hunter, 1996)).

The curved shape of meniscus comes as the result of pressure difference between these two fluids. Also, the interface of curvature will be convex towards the wetting fluid, supported by higher internal pressure. The capillary pressure in such a case is given by Laplace equation, that gives the relation between the two radii,

$$P_c = \sigma\left(\frac{1}{R_1} + \frac{1}{R_2}\right) \qquad (2.9)$$

Where,

P_c	Capillary pressure
σ	The interfacial tension
R_1	The largest curving radii
R_2	The smallest curving radii

Assuming that the droplet of water/oil is of spherical shape and equal to pore size, this implies that $R_1 = R_2$ and hence, P_c equals $2\sigma/r$. The capillary pressure can have both positive and negative values, depending on which phase will have a lower pressure. In

most of the cases, the fluid that is wetting the capillary tube is the one with a lower pressure (Green & Willhite, 1998). For a water-wet capillary tube, the water phase will displace the oil phase. For an oil-wet capillary tube, it will be opposite displacing. The cylindrical tube model is often used to idealize the complexity of a porous media (Figure 10) (Mørk, 2001; Green & Willhite, 1998).

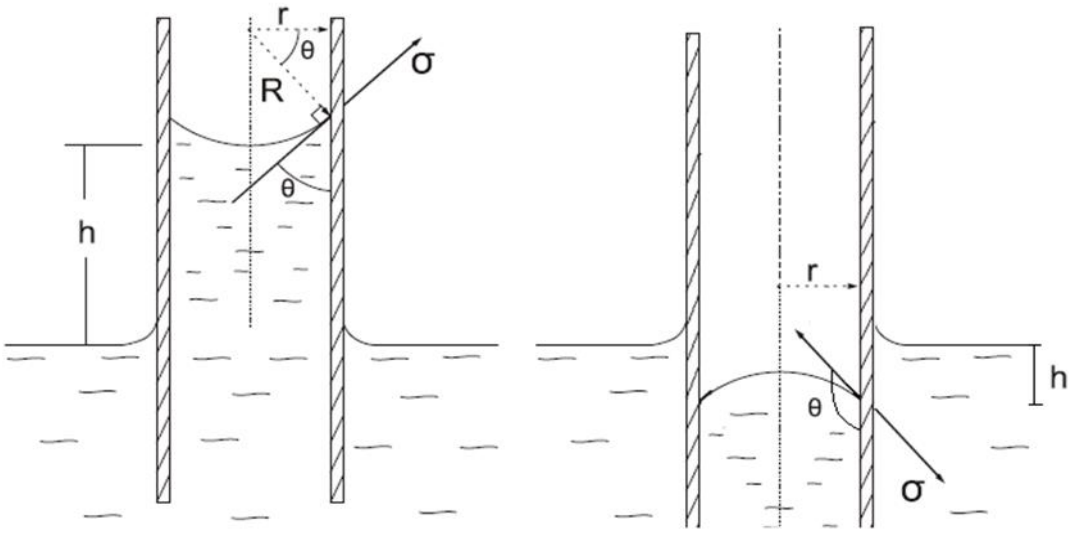

Figure 10. The cylindrical tube model for oil/water vs. mercury (modified from (Mørk, 2001))

Hence, to specify P_c we need to employ the interfacial tension for a water/oil system. To determine capillary pressure in this case, the following formula should be used:

$$P_c = \frac{2\sigma_{ow}\, cos\theta}{r} \qquad (2.10)$$

where,

σ_{ow}	The interfacial tension (IFT) between oil and water phase
θ	The contact angle defined as the tangent to the oil-water surface in the triple-point rock-water-oil.
r	The radius of the cylindrical pore channel

The function of capillary forces is fundamentally different in fractured and non-fractured reservoirs. In the non-fractured reservoirs, the oil is trapped by capillary forces resulting in a high residual oil saturation (Anderson, 1987). To displace trapped oil droplets the IFT should be reduced (Taugbøl, 1995). On the other hand, in fractured

reservoirs these forces will lead to spontaneous imbibition (SI) of water. This mechanism is crucial for improving the displacement efficiency (Strand, 2005).

2.2.3.1 Relative permeability concept

To fully understand how waterflood works, we should consider the main properties of reservoir rocks. These are (Craig, 1993):

1. Properties of the rock such as permeability, porosity, surface area or pore size distribution.
2. Rock-fluid properties such as capillary pressure and relative permeability.

Numerous experimental studies (Craig, 1993; Torsæter & Abtahi, 2000) have confirmed that effective permeability for a given reservoir is presented as the function of the wetting characteristics of the rock and fluid saturations of the reservoir. The effective permeability is the capacity of transmitting fluids under the condition of saturation equal to less than 100 % peculiar to a porous medium (Torsæter & Abtahi, 2000). This parameter is denoted by k_w, k_o, k_g respectively for water, oil and gas phases and is measured in mD. To fully define and understand the reservoir conditions at which effective permeability stands, the saturation should be determined for each phase. Saturations are denoted by So, Sg, S_w for the phases water, oil and gas, respectively. Another major parameter is absolute permeability, denoted by k. Ahmed (Ahmed, 2010) defines absolute permeability as "a measure of the capacity of the medium to transmit the fluids". It can be calculated from the Darcy's law for linear incompressible fluid flow as follows:

$$k = -\frac{q\ \mu\ dP}{A\ L} \tag{2.11}$$

Hence, the relative permeability is defined as the ratio of effective permeability of a given phase to the absolute permeability (Anderson, 1987) as can be seen in the following equations:

$$k_{rw} = \frac{k_w}{k} \tag{2.12}$$

$$k_{ro} = \frac{k_o}{k} \tag{2.13}$$

$$k_{rg} = \frac{k_g}{k} \tag{2.14}$$

Where,

k_{rw}	Relative permeability of oil phase
k_{ro}	Relative permeability of oil phase
k_{rg}	Relative permeability of gas phase
k_w	Effective permeability of water phase
k_o	Effective permeability of oil phase
k_g	Effective permeability of gas phase
k	Absolute permeability.

Overall, there are various factors that can affect relative permeability. The most important factors are active forces (viscous, capillary and gravitational), pore geometry, temperature, saturation history, saturation and wettability (Torsæter & Abtahi, 2000). Moreover, referring to the wettability, the relative permeability is usually denoted as k_{nw} for the non-wetting phase and k_w for the wetting phase. For an oil/water system, the relative permeabilities for oil and water phase can be plotted as a function of water saturation as shown in Figure 11.

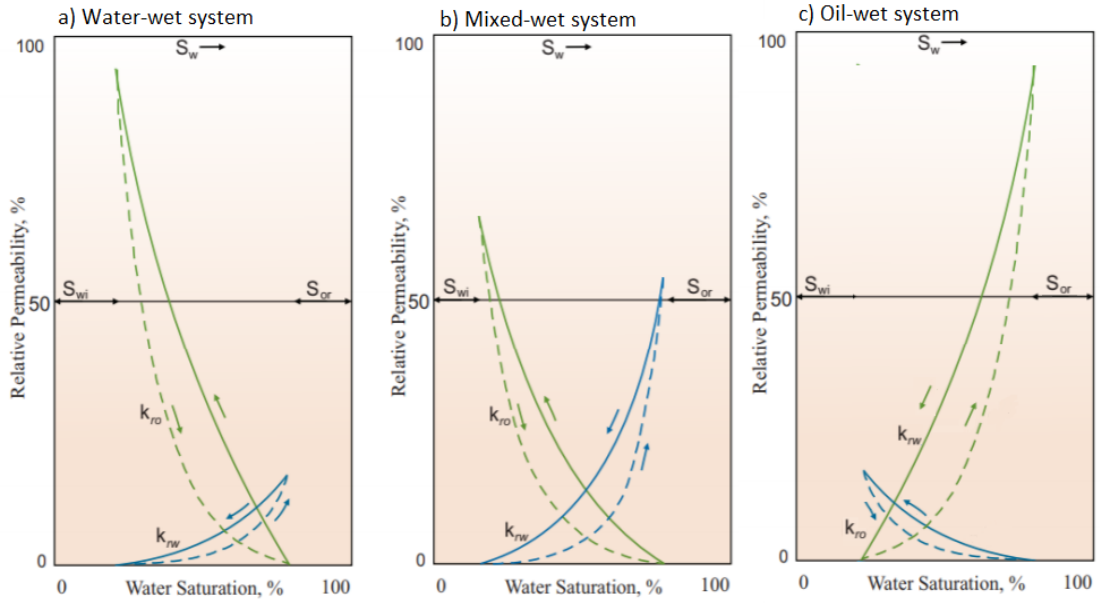

Figure 11. Relative permeability curves, k_{ro} (green) and k_{rw} (blue) for (a) water-wet and (b) mixed-wet system for and c) oil-wet system, k_{ro} (blue) and k_{rw} (green), (modified after (Donaldson & Alam, 2008)). Drainage process when k_{ro} arrow moves upward and Imbibition when moves downward.

The saturation history for these curves is based on drainage and imbibition processes. When the saturation of the wetting phase decreases in magnitude, drainage process will be employed. Otherwise, when the saturation of the wetting phase increases in magnitude, imbibition will take place. Figure 11 clearly shows that each relative permeability curve contains three elements that describe them:

1. The end point fluid saturations.
2. The end point permeabilities.
3. The curvature of the relative permeability functions.

The importance of each element is different. The end point fluid saturations give the information about the amount of recoverable oil. For determining sweep efficiency in the reservoir, the mobility ratio term containing the end point permeabilities, should be considered. Also, the placement of the cross-point gives the information about the wetting state of the core. If the cross-point is placed to the left of 0.5 on water saturation axis, the system is said to be more oil-wet and if it is placed to the right of 0.5, the system is preferentially water-wet. Finally, the shape of the curvature for the relative permeability functions may also have an important bearing on recovery efficiency.

2.2.3.2 Fractional flow concept

Fractional flow should be mentioned when introducing waterflooding and relative permeability concepts. The fractional flow can be predicted from relative permeability and capillary pressure data. The fraction of water and oil flowing is given by the fractional flow curve. It depends on the properties of both the porous media and the fluids. The viscosity is the main fluid property affecting the fluid flow. If two fluids have the same relative permeability, for example oil and gas, more gas than oil will flow because of the significant difference in viscosity. For the simplest case of horizontal flow, with negligible capillary pressure, the fractional flow is given by equation (2.15):

$$fw = \frac{1}{\left[1 + \frac{(k_{ro}\mu_o)}{(k_{rw}\mu_w)}\right]} \qquad (2.15)$$

Where,

fw Fractional flow

k_{ro}	Relative permeability of oil phase
μ_o	Viscosity of oil phase
k_{rw}	Relative permeability of water phase
μ_w	Viscosity of water phase

As mentioned in section 2.2.3.1, the cross point of relative permeability curves gives information about the wetting state of a system. Similarly, the shape of the fractional flow curve can also give us information about the wetting state. Figure 12 illustrates the fractional flow curves for strongly water-wet and strongly oil-wet rocks.

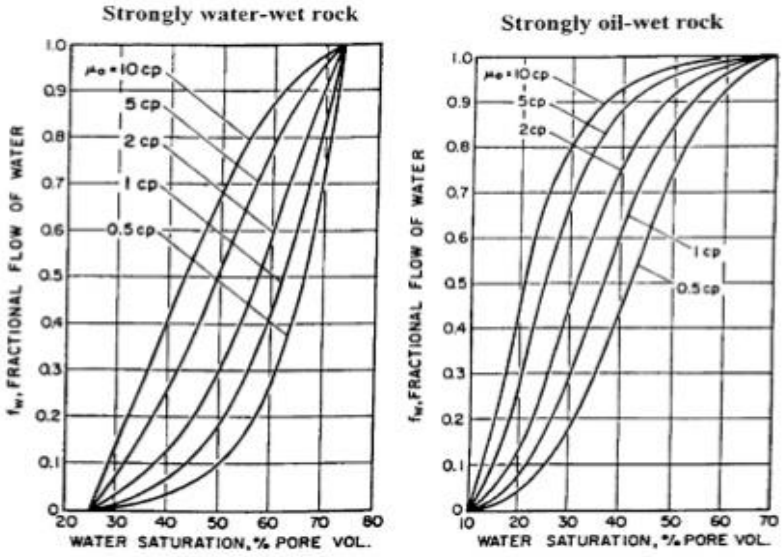

Figure 12. Effect of viscosity on fractional flow curve for strongly water-wet rock and strongly oil-wet rock (Satter & Iqbal, 2015).

To determine water saturation at the front, the tangent is drawn from $S_{wi} = 0$ (Figure 13).

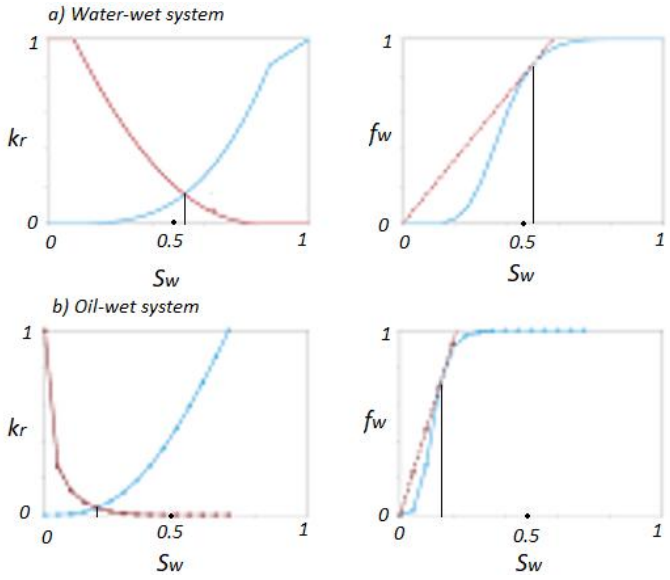

Figure 13. Relative permeability and fractional flow curves for a) water-wet system and b) oil-wet system. Relative permeability: blue line-k_{rw}, red line-k_{ro}. Fractional flow: blue line-fractional flow curve, red line-tangent (Ganesh & Mishra, 2015)

When the tangent line meets up the fractional flow curve, the front saturation at breakthrough is obtained (Figure 13). When the fractional flow curve is placed as in Figure 13 (a), the tangent line gives the water saturation value higher than 0.5. The same value gives the cross point of relative permeability curves. Consequently, the system is defined water-wet (Craig, 1993) and opposite in Figure 13 (b) for oil-wet systems.

2.3 Theoretical aspects of wettability

Wettability directly affects the fluid flow characteristics and hydrocarbon displacement efficiency. Craig (1971) defined wettability as "the tendency of one fluid to spread on or to adhere to a solid surface in the presence of other immiscible fluids" (Craig, 1971). Applying this definition to reservoir engineering, the solid surface will be reservoir rock, either sandstones or carbonates. Wettability plays a major role when defining the waterflooding potential of a reservoir system. As reported by Strand (2005), it is a crucial factor while defining multiphase flow in reservoir rock, and fluid distribution and trapping (Strand, 2005).

2.3.1 Classification

According to Anderson classification (1986b), the wetting state of a reservoir is divided into homogeneous and heterogeneous wetting states (Anderson, 1986b). In the homogenous state, the reservoir rock has affinities to the wetting and non-wetting phases. Based on this, Donaldson (Donaldson & Alam, 2008) described the wettability

state of water/oil/rock system in four different states, water-wet, oil-wet, mixed-wet and fractional wet state (Figure 14). Wettability as such can be determined through contact angle method with respect to the present phases.

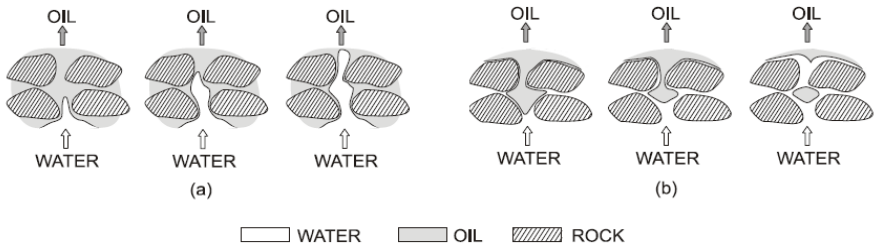

Figure 14. Composition of a rock when the system is water-wet (a) and oil-wet (b)

2.3.1.1 The Four Wetting states

The reservoir rock can have four different wetting states, water-wet, oil-wet, mixed-wet or fractional wet. These reservoir rock conditions are described in the following sections:

Water-wet

The system is called water-wet when more than 50% of rock surface is covered by water phase. In water-wet reservoir systems, water fills up the smaller pores and is present as a thin film on the surface of preferentially water-wet larger pores in the rock. Oil is found in the larger pores but in the form of being placed on the surface of water film. Consequently, water is the continuous (wetting) phase while oil is the discontinuous (non-wetting) phase in a water-wet system. If the water saturation of rock is equal to the initial water saturation, S_{wi}, then the discontinuous phase can become continuous, but as soon as the water saturation starts increasing, the non-wetting phase becomes discontinuous. So, if a water-wet core is saturated with oil and water is injected through it, water will spontaneously imbibe into the rock. As the result, the water will displace the oil. The process will continue until a state of static equilibrium is achieved between the capillary and surface energy forces between the rock/fluid surface.

Oil-wet

In an oil-wet system, the conditions are reversed. As reported by Donaldson (2008), this implies that oil occupies the smaller pores and will be present as a thin film on the surface of preferentially oil-wet larger pores in the rock and water will exist mainly in the large pores, resting on the film of oil. In such a system water, as the nonwetting phase, can be present as the continuous phase. This occurs in large pores when the

saturation is almost equal to the residual oil saturation, S_{or}, but the continuity of water phase can decrease when the oil is injected, i.e. the water saturation is decreased. After injection, the water will stay trapped in large pores surrounded by oil phase. Thus, an oil-wet system will have oil as the continuous phase just in cases where all the saturations will be either equal to or higher than the residual oil saturation.

Fractional wet

Brown and Fatt (1956) proposed this term with an aim of characterizing wetting state of the pore surfaces where the preferential wetting is randomly distributed throughout the rock. There are some areas which are either water-wet or oil-wet and are scattered throughout the rock with no continuous oil networks. This comes as the result of random distribution of minerals that are exposed to the surfaces in the rock pores.

Mixed-wet

Salathiel (1973) defines the mixed-wet system as "*a condition where the small pores in the rock are water-wet and saturated with water, but the larger pores are oil-wet and filled with oil in contact with the pore walls that form a continuous path through the length of the rock"*. This definition was based on the fact that such a condition could occur during the original oil accumulation if the connate water is moved out of the large rock pores in presence of oil-containing surface-active compounds. These components will then progressively displace the remaining films of water placed on the surfaces of rock pores. Hence, due to large capillary threshold pressure for a water displacement, the oil droplets will not be able to enter the smaller pores.

2.3.2 Wettability determination methods

Several techniques have been proposed and developed with an aim to measure the wettability in a given reservoir system. The existence of wettability determination methods is presented in many documents (Anderson, 1986b). For evaluation of wetting state for a given system, two methods are of significant importance. These are quantitative and qualitative methods. Quantitative methods, known as direct methods, are based on Contact Angle, Amott, USBM and Chromatographic wettability measurements. According to Anderson (1986b), indirect methods, or qualitative methods, include measurements obtained from imbibition rates, microscope examination, flotation, glass slide method, relative permeability curves,

permeability/saturation relationships, capillary pressure curves, capillarimetric method, displacement capillary pressure, reservoir logs, nuclear magnetic resonance and dye adsorption. Moreover, none of the abovementioned methods is allowed to change the wetting condition of a surface when introduced into the system. This is the reason why the compatibility between the fluids and surfaces should be taken into consideration, as it is well known that the wettability can be influenced by the minerals that compose the rocks providing different surface charges. For the purpose of this project, newly developed chromatographic wettability method (Strand, Standnes, & Austad, 2006) was used with an aim of determining the wetting state in artificial chalk cores. The principle of this method as well as for the other methods is briefly described in upcoming sections:

2.3.2.1 Contact Angle Method

When two immiscible fluids are present and both contact a solid surface, the less wetting fluid will retreat from contact with the solid while the stronger wetting fluid will be attracted to the solid surface. The intersection point between different phases and solid surface will create the different contact angles (Strand, 2005), (Figure 15).

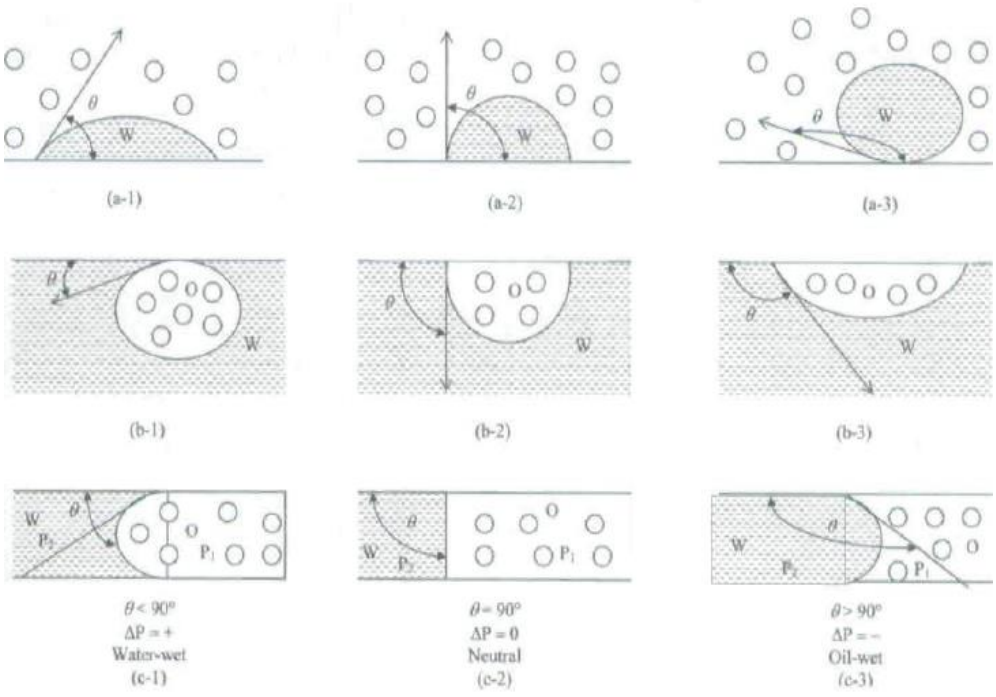

Figure 15. Contact angles for various wetting conditions of water and oil: (a) drops of water in oil on a plane surface, (b) drops of oil on a plane surface, and (c) water and oil in a capillary tube (Donaldson & Alam, 2008).

The Figure 15 illustrates contact angle for various wetting conditions of water and oil: (a) drops of water in oil on a plane surface, (b) drops of oil on a plane surface, and (c) water and oil in a capillary tube. The contact angle method directly quantifies the wetting state of the rock and can be evaluated through the Young's equation (1855) as follows:

$$\sigma_{ow} cos\theta = \sigma_{os} - \sigma_{ws} \qquad (2.15)$$

Where,

σ_{os}	Interfacial tension between a solid surface and oil
σ_{ws}	interfacial tension between a solid surface and water
σ_{ow}	interfacial tension between water and oil
θ	The contact angle

These notations are also presented on Figure 16:

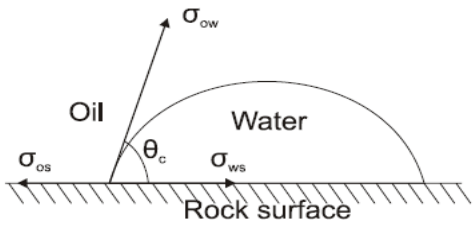

Figure 16. Water-wet condition (The parameters ($\sigma_{os}, \sigma_{ws}, \sigma_{ow}$) needed for contact angle determination) (Raza, Treiber, & Archer, 1968)

There are various methods for determining rock wettability through contact angle method such as tilting plate method, sessile drop or bubble method, vertical rod method, tensiometric method, cylinder method and capillary rise method. Among them, two generally well-defined and most commonly used methods for wettability measurements on smooth surfaces are sessile drop as static method and modified sessile drop as dynamic method.

Sessile drop - static measurement

In static measurement, the contact angle is being calculated out of the equilibrium between the interfacial tensions of present fluids and their adhesive attractions to the surface, already given by Young's equation (2.15), Figure 17.

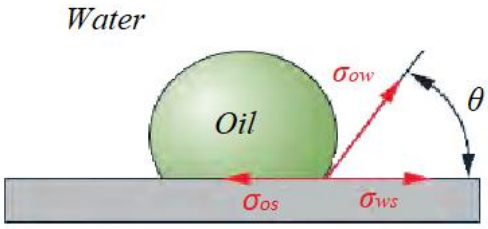

Figure 17. A droplet of oil surrounded by water; The static measurement of contact angle (modified after (Abdallah, 2007)).

In this case, when the fluid drop is placed onto the flat minerally charged surface, the angle is formed only as the result of applied gravity forces, when no other forces are present in the system (Anderson, 1986b). Hence, there will be no fluid displacement with respect to the solid surface. In rock/oil/water (ROW) system, the water phase is used as a reference phase for contact angle determination, as water is a denser fluid than oil. The values that can be obtained are in the range from 0° to 180°, depending on fluid's attraction towards solid surface. As already mentioned in section 2.3.2, this measurement directly contributes to determination of wetting state in reservoir (Morrow, 1990; Anderson, 1986b; Rao & Girard, 1996). Consequently, Table 3 describes the different wetting states related to contact angle measurements.

Table 3. Measurement of contact angles and wetting states on carbonate rock surfaces (Modified after (Donaldson & Alam, 2008))

Wettability	Contact Angle	Carbonate Rocks Reservoirs
(Treiber & Owens, 1972)		
Water-wet	0° – 75°	8%
Intermediate-wet	75° – 105°	4%
Oil-wet	105° – 180°	88%
(Chilingar & Yen, 1983)		
Water-wet	0° – 80°	8%
Intermediate-wet	80° – 100°	12%
Oil-wet	100° – 180°	80%
(Anderson, 1986b)		
Water-wet	0° – 90°	
Intermediate-wet	90°	
Oil-wet	90° – 180°	

When the contact angle is less than 90°, the surface is preferentially water-wet, as the water spreads uniformly over the solid surface (Abdallah, 2007). If the angle is greater than 90°, the system is preferentially oil–wet. The oil is the spreading fluid that occupies the smallest pores in this case. Finally, when the rock has no specific preference towards

solid surface, it is said to be intermediate-wet or mixed-wet, with contact angle equal to 90° (Anderson, 1986b).

Modified Sessile drop - dynamic measurement

The characteristics of modified sessile drop contact angles were studied by Leach et al. (1962). Initially, two minerally charged parallel plates were simultaneously immersed into pure brine. After aging them for some period, the fluid droplet is placed in between them in a way that droplet is in contact with both plates. Applied force displaces initially parallelly placed plates opposite to each other and the fluid droplet moves. Dynamic contact angles are gradually changed from the static case generating two angles, advancing and receding angles, Figure 18.

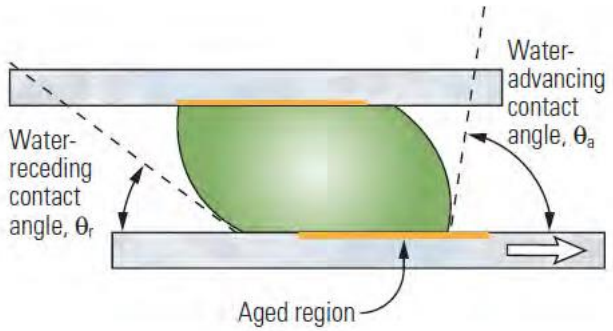

Figure 18. Dynamic measurement of contact angle (Abdallah, 2007)

Advancing contact angles, denoted as (θ_a), are formed at the front of the encroaching wetting phase (Rao, 1999). Likewise, receding contact angles, denoted as (θ_r), are formed at the front of the encroaching nonwetting phase. Treiber (1972) found that the advancing contact angle is greater than the receding angle by as much as 75°. The difference between them represents the hysteresis, i.e. delay of the equilibrium values when the forces acting on the oil droplet are changed.

2.3.2.2 Amott Method

Contrary to contact angle measurements, the Amott method is used for average wettability determination in a porous media. The Amott method (Amott, 1959) is based on saturation changes by spontaneous imbibition, forced displacement and drainage process of water and oil (Donaldson & Alam, 2008). Likewise, the main principle of the proposed method is established in a way that the wetting fluid imbibes spontaneously into the artificial core resulting in non-wetting fluid to be displaced. According to Amott (1959), the forced displacement is, for the most part, done by

centrifugation or by flooding (Cuiec, 1984). Anderson et al. (1986b) claims that the influence of relative permeability, viscosity and initial water saturation (S_{wi}) of the rock is decreased after establishing the ratio between spontaneous imbibition and forced imbibition. Since the method is time consuming and will result in having two concepts "displacement-by-oil-ratio", IO, and "displacement-by-water-ratio", IW. To obtain these values, some preparation steps should be done to the core sample (Donaldson & Alam, 2008). Initially, the core sample is pre-flushed with water and kerosene to remove the crude oil components and formation water. Then it is immersed in DI water and the volume of oil spontaneously released is measured. The corresponding increase in water saturation is denoted as ΔS_{WS} (equation 2.16). Thereafter, the core sample is subjected to forced displacement by centrifuging/waterflooding. The increase in water saturation by forced displacement is given by ΔS_{WF} (equation 2.16). When all necessary input data are defined, the Amott wettability index to water (I_W) can be calculated using equation (2.16). The procedure for Amott oil wettability index (I_O) is similar, but in this case it is followed by notations ΔS_{OS} for the corresponding saturation change during spontaneous drainage of oil and ΔS_{OF} for saturation change during forced drainage of oil (equation 2.17). The Amott wettability indexes can be presented by equations 2.16 and 2.17:

$$I_W = \frac{\Delta S_{WS}}{\Delta S_{WS} + \Delta S_{WF}} \tag{2.16}$$

$$I_O = \frac{\Delta S_{OS}}{\Delta S_{OS} + \Delta S_{OF}} \tag{2.17}$$

Where,

ΔS_{WS}	saturation change during spontaneous imbibition of water
ΔS_{WF}	saturation change during forced imbibition of water;
ΔS_{OS}	saturation change during spontaneous drainage of oil;
ΔS_{OF}	saturation change during forced drainage of oil.

Sometimes, a modification of this method called "Amott-Harvey Relative Displacement Index" is utilized. The procedure of modified method is quite identical to the Amott method, except an additional step is included prior to preparation of the core, which consists of centrifuging the core first under brine and then under crude oil in order to reduce the plug to irreducible water saturation. The Amott-Harvey index can

be calculated using the difference between Amott indexes for water and oil by equation (2.18):

$$I_{AH} = I_w - I_o \tag{2.18}$$

The modified Amott test cycle is divided into five segments, Figure 19:

1. Primary drainage of water by oil to establish initial water saturation, S_{wi}
2. Spontaneous imbibition of water
3. Forced imbibition of water
4. Spontaneous imbibition (drainage) of oil
5. Forced imbibition (drainage) of oil

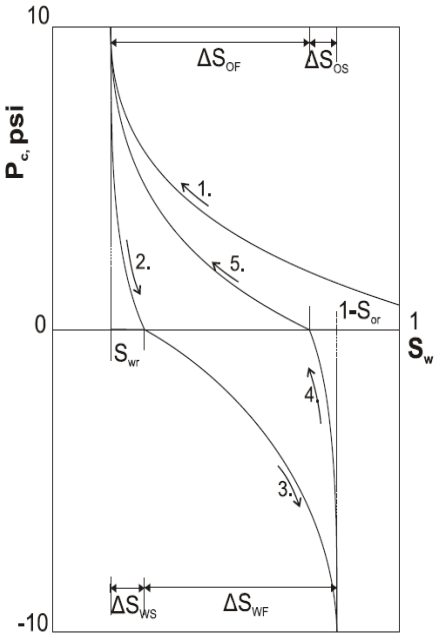

Figure 19. Five segments of the modified Amott test cycle.(modified after (Omland, 2015)

The values for Amott-Harvey index (Anderson, 1986b) are placed in a range from -1 (completely oil-wet system) to +1 (completely water-wet system). In addition, Cuiec (1984), defined systems to be water–wet when $+0.3 < I_{AH} < 1$, intermediate-wet when $-0.3 < I_{AH} < +0.3$, and oil–wet when $-1 < I_{AH} < -0.3$.

The biggest disadvantages of this method are that (a) this method is insensitive near neutral wettability (Anderson, 1986b), (b) it is not able to distinguish sufficiently between systems that reach residual non-wetting phase without change in sign of imbibition capillary pressure (Ma, 1999), and it does not identify between degrees of strong water wetness in a system satisfactorily (Morrow, 1990).

2.3.2.3 United States Bureau of Mines (USBM) Method

As with the Amott method, the USBM method, developed by Donaldson (1969), is used for wettability determination in a porous media. Generally, the measurement principle is identical to the Amott method and is based on measuring the average wetting state of the core, but, compared to Amott, USBM does not provide clear measurements in spontaneous imbibition process and can eventually have improvement at low pressures, when centrifuge process is considered (McPhee, 2015). From thermodynamic point of

view, due to favorable free energy of a proposed system, the displacing fluid or the wetting fluid will require less energy than the displaced fluid, which is the non-wetting fluid. This energy is said to be proportional to the two areas under imbibition and drainage capillary pressure curves plotted against the water saturation in an oil/water system as shown in Figure 20. The shape of these curves will strongly depend on two major parameters: rock wettability towards water/oil phase and the pore-size distribution. The following steps are performed (Abdallah, 2007):

1. Initially, the core is saturated with brine and placed in a glass holder filled with oil. It is centrifuged until the residual water saturation is obtained (line 1 in Figure 20)
2. Then, the core is placed in another core holder filled with pure brine and centrifuged at different gradually increased speeds with a goal of oil displacement. This volume is measured, and the capillary pressure curve is obtained (line 2 in Figure 20).
3. Finally, the core is placed in an oil-filled core holder. The brine volume is recorded at each incremental speed increase. The second capillary pressure curve is obtained (line 3 in Figure 20).

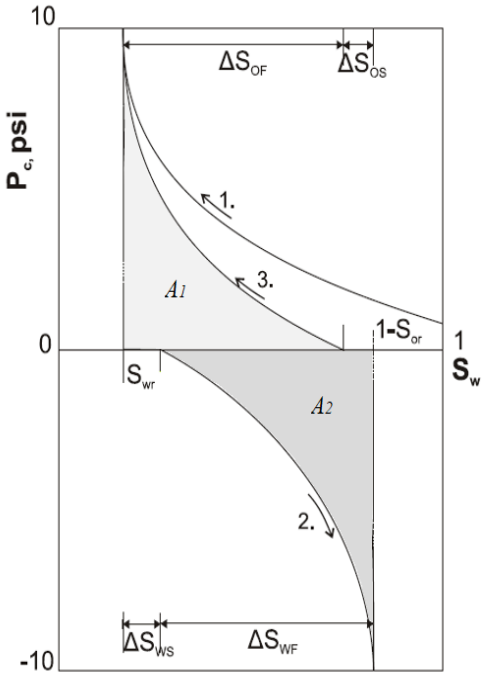

Figure 20. The USBM method for wettability determination. Capillary pressure curves for drainage and imbibition processes: 1. Primary (Forced) Drainage; 2. Secondary (Forced) Drainage; 3. Forced Imbibition (modified after (Omland, 2015))

The ratio between the obtained areas (A_1 and A_2) is used to calculate the wettability index (I_{USBM}), using equation (2.19):

$$I_{USBM} = log\left(\frac{A_1}{A_2}\right) \tag{2.19}$$

where,

A_1 The area between the forced drainage curve and the saturation axis

A_2 The area between the forced imbibition curve and the saturation axis

When $I_{USBM} > 0$, the core is characterized water-wet, and when $I_{USBM} < 0$, the core will be oil-wet .When the values are close to zero, the core is characterized as neutral-wet (Anderson, 1986b). The range of wettability index goes therefore from - ∞ (strongly oil-wetting) to + ∞ (strongly water-wetting), but mostly values are placed in range of -1 and +1 (Abdallah, 2007). If, for example, the core sample is taken to be water-wet, and water is displacing fluid, the area under the brine-drive capillary pressure curve is smaller than area under the capillary pressure curve for the water displacement by oil (Anderson, 1986b). In addition, the comparison of wettability indexes for Amott and USBM method is given in Table 4 for different wetting states of a system.

Table 4.Comparison of wettability indexes for Amott and USBM methods in case of different wetting state of a system (Anderson, 1986b)

	Oil-wet	Neutral-wet	Water-wet
Amott wettability index water ratio	0	0	>0
Amott wettability index oil ratio	>0	0	0
Amott-Harvey wettability index	-0.1 to -0.3	-0.3 to 0.3	0.3 to 1.0
USBM wettability index	About -1	About 0	About 1
Minimum contact angle	$105° - 120°$	$60° - 75°$	0°
Maximum contact angle	180°	$105° - 120°$	$60° - 75°$

However, this method has both advantages and disadvantages. It is time efficient and highly sensitive to near neutral-wetting cores (Anderson, 1986b), but the test must be applied to plug-sized cores and exposed to the centrifuge process (Abdallah, 2007) which may cause damage of core plugs due to very high spin velocities. Since chalk cores are weak material and very sensitive to fractures, the USBM method has not been used in this study.

2.3.2.4 Spontaneous imbibition

Studies have shown that spontaneous imbibition (SI) plays a huge role for oil recovery processes in water-wet fractured reservoirs, especially in low-permeable rock formations (Brownscombe & Dyes, 1952; Morrow & Mason, 2001). This mechanism represents spontaneous take up of a fluid into a porous formation. Moreover, the fluid, initially placed within the porous rock, is by definition displaced by corresponding imbibing (displacing) fluid, only as the result of present attractive capillary forces as the main driving forces in the system. For this reason, SI measurements are said to have the same magnitude as capillary pressure (Morrow, 1990). Observed phenomena is moreover explained as the result of differential attraction forces between the fluids present in SI cell and the rock pore walls.

The spontaneous imbibition process can be easily explained by . The chalk core is initially placed inside the SI cell made of glass. The upper part of SI cell has a volumetric tube used to sample the produced oil and measure its volume. The formation water, which is the most commonly used imbibing brine, is used to fill the SI cell. The procedure of oil displacement occurs at the ambient temperature of $23°C$. Typically, the oil recovery process by spontaneous imbibition will depend on the strength of capillary forces driving the mechanism. The amount of oil produced is recorded with time.

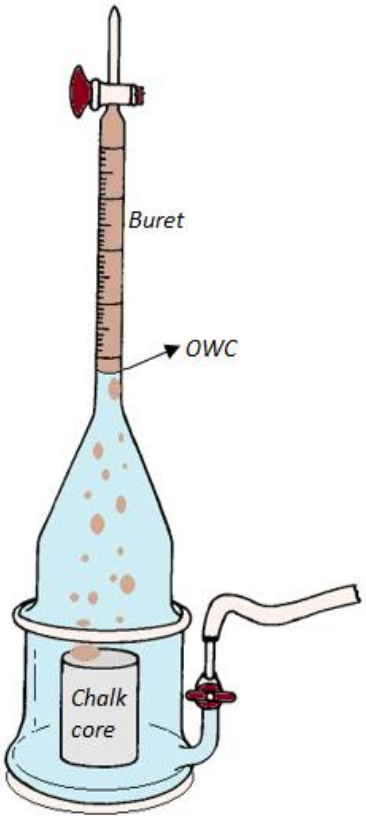

Figure 21. Cell for spontaneous imbibition process. On the figure, water phase displaces the oil phase out of chalk core sample. Correspondng oil production can be read out from byrette with oil column.

This method has proved to be capable of determining wettability easily in systems with various degrees of water-wetness (Morrow, 1979). Moreover, this determination is considered when compared to the reference samples with nearly perfectly wetting conditions for a given core sample (Morrow, 1990). Hence, for the strongly water-wet systems, the oil recovery after the SI test will be significantly higher than the oil recovery in significantly water-wet systems as shown in Figure 22.

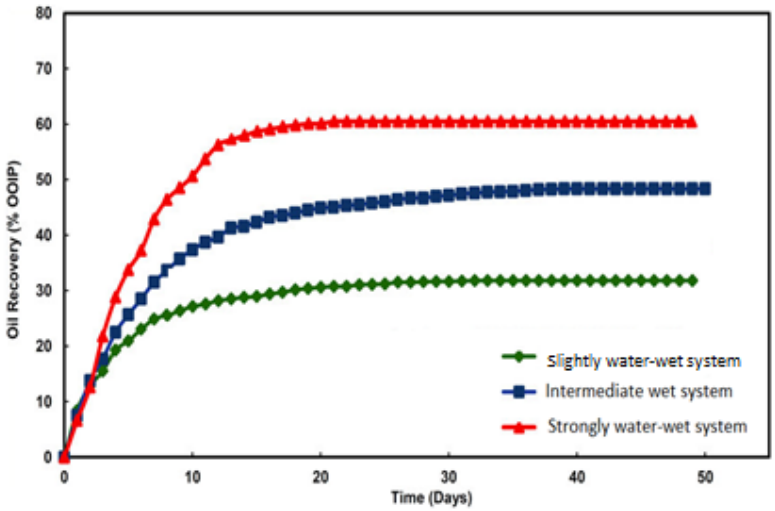

Figure 22. Oil recovery curves for different wetting states obtained by SI test (modified from (Shehata & Nasr-El-Din, 2014)

A simplified wetting index based on SI experiments can be calculated based on equation for modified Amott water index (I^*_{W-SI}).

$$I^*_{W-SI} = \frac{SI_c}{SI_{ww}} \tag{2.20}$$

Where,

I^*_{W-SI}	Simplified Amott wetting index only based on SI
SI_c	The oil recovery (%OOIP) by SI from the assessed core
SI_{ww}	The oil recovery (%OOIP) by SI from the reference, strongly water-wet core

If the index values approaches 1, the core is characterized as a strongly water-wet. If the value was equal 0 the core is characterized as a fractional- or neutral-wet (Pinerez, 2019).

2.3.2.5 Chromatographic Wettability Test

The new chromatographic wettability test (CWT) for carbonates was developed and proposed by Strand (2006) with an aim of determining the fraction of water-wet surface area of the carbonate surface. The model by itself is constructed to work on the principle of chromatographic separation between a non-adsorbing tracer, thiocyanate (SCN^-),

with no affinity towards chalk, and adsorbing sulphate (SO_4^{2-}), with high affinity towards the chalk surface (Figure 23). On the other hand, the thiocyanate tracer, besides having no affinity towards carbonate surface, is also not expected to engage in any chemical interactions with the chalk core. That is why thiocyanate ions are produced in the effluent samples before sulphate ions which gets adsorbed on the available chalk surface sites (tracer follows the fluid front as illustrated in Figure 24). The CWT allows to be run at S_{or} and 25 °C, as well as on 100% saturated cores.

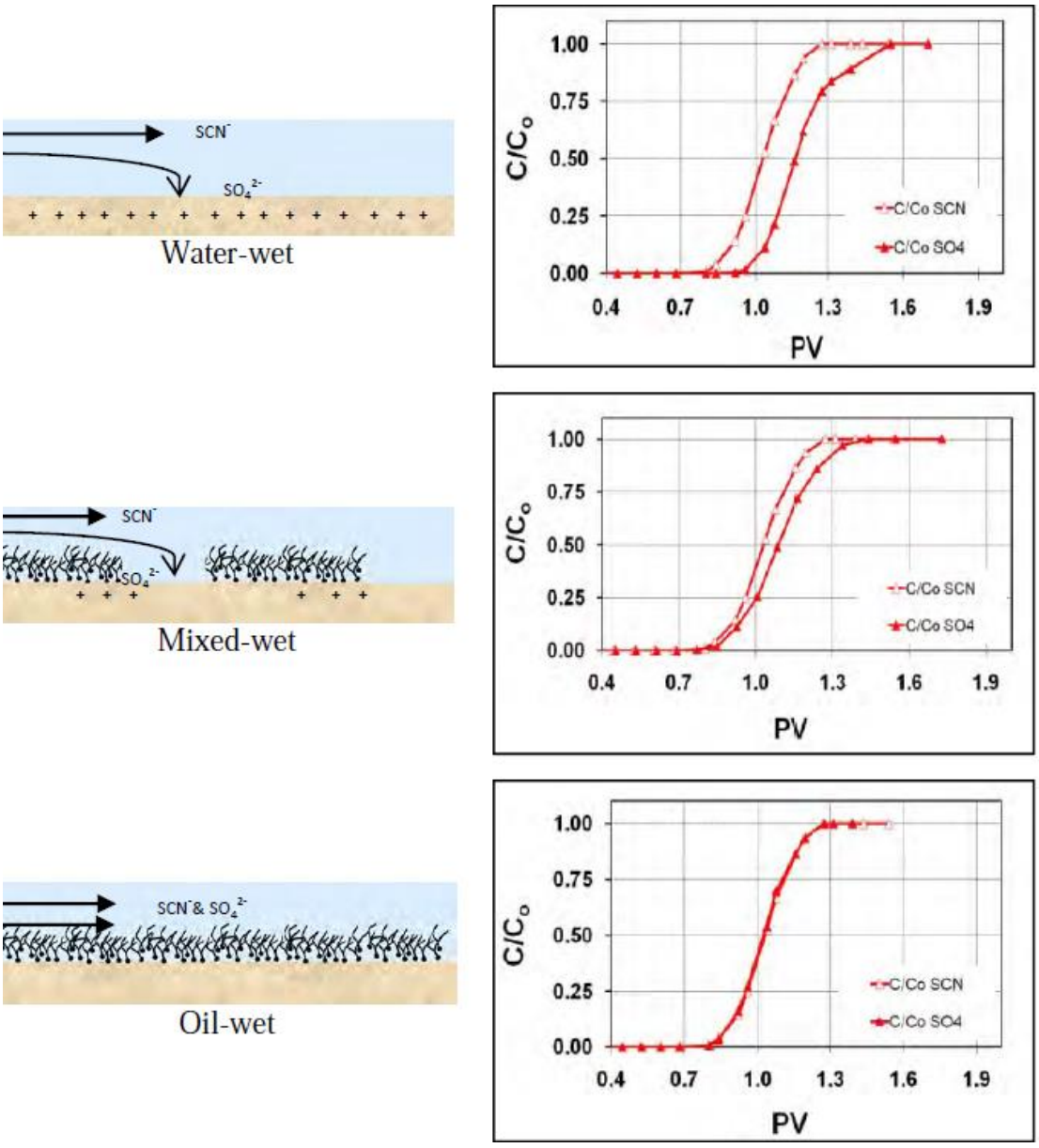

Figure 23. Schematic illustration of chromatographic wettability test for water-wet, mixed-wet and oil-wet system. Adsorption of sulphate onto each of mentioned systems. No separation – oil wet surface, large separation – water wet surface (Shariatpanahi, 2012)

The brines used for core flooding during the chromatographic wettability test were SW0T, without thiocyanate and sulfate, and SW1/2T, which is enriched with equal amounts of thiocyanate and sulfate. After performing ion chromatography (IC) of the effluent samples, it is observed that the sulfate concentration is delayed compared to the thiocyanate concentration, as shown in Figure 24.

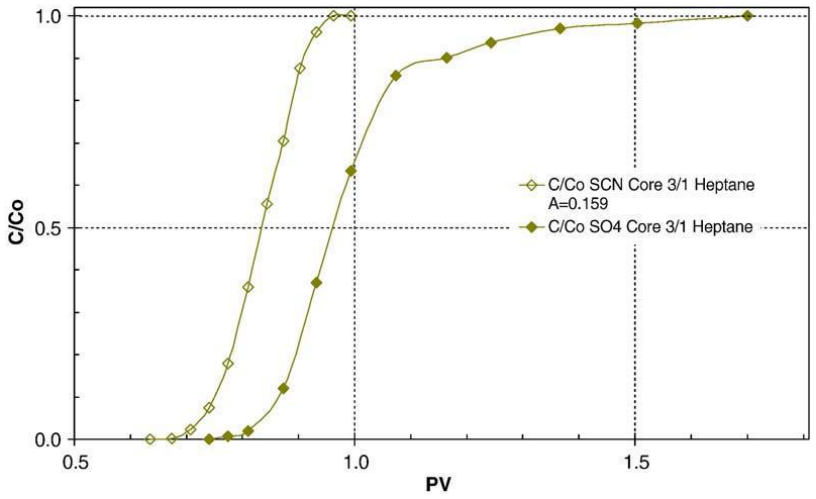

Figure 24. Illustration of the ion chromatographic wettability test. The area between two green curves of tracers SO_4^{2-} and SCN^- (Strand, Standnes, & Austad, 2006).

The affinities of these ions to the calcite surface are the reason for such an early breakthrough of tracer ions and a delay in the curves' placement. The area between these two effluent concentration curves is directly proportional to the water-wetness of the chalk surface and is schematically presented in Figure 24. Now, to acquire the correct value describing the fraction of water-wet area, the wettability index (WI) is determined according to equation (2.21):

$$WI = \frac{A_{wett}}{A_{ref}} \tag{2.21}$$

Where,

A_{wett}	the area between the SCN^- and SO_4^{2-} curves of a wetted core sample
A_{ref}	The area between the SCN^- and SO_4^{2-} curves of a completely water-wet reference core sample

To calculate areas A_{wett} and A_{ref} necessary for further determination of WI, the trapezoidal method of numerical integration was used. The obtained WI values are placed in the range of 0 to 1, where 0 is completely oil-wet, 0.5 is neutral-wet and 1 is

completely water-wet. Like the other methods, this one also has advantages and disadvantages. On one side, it is time effective since the test can be carried out in approximately 1 day, shows quite high reproducibility (an error in the range $\pm$ 2%) and has a good sensitivity close to neutral wetting condition. On the other hand, the test can be used only for quantification of wettability in carbonate rocks (Strand, Standnes, & Austad, 2006).

2.3.3 Effect of wettability on relative permeability

Wettability is given as a function of the reservoir's crucial input parameters such as relative permeability and capillary pressure (Shariatpanahi, 2012). It has a major role in the control of flow and spatial displacement, i.e. has direct impact on relative permeability. For this reason, wettability governs the process of total oil recovery by waterflooding that is absolutely dependent on the interplay between the rock surface and fluid phases in the pores (Willhite, 1986).

Experimental studies suggested that most reservoirs are water-wet (Shariatpanahi, 2012). Initially, the reservoir rock is water saturated and water occupies the small pores of the matrix and spreads as a thin film on rock's surface. When crude oil migrates into it, the large pores are occupied by resting on the water film, after overcoming the capillary threshold pressure. During displacement process, each phase will flow through a separate set of pores. Moreover, the increase in pressure leads to greater water displacement until reaching the connate water saturation, S_{wc}. As illustrated in Figure 11 (section 2.2.3.1), the k_{ro} is higher than k_{rw} and tends to decrease with increased water saturation while the k_{rw} increases. The intersection point of relative permeability curves, k_{rw} and k_{ro}, is placed more towards right, relative to water saturation axis, and the end point relative permeability of water, k_{rw}, should be less than 0.3, on relative permeability axis, for strongly water-wet system (Craig, 1971). During this fluid movement, some small globules of oil can be left behind in the pores known as residual oil. This is resulted by the driving forces that cannot overcome entry capillary pressure. When water breaks through at the producing end, the oil production decreases rapidly toward zero. For the oil-wet system, the roles of water and oil are switched but the principle of displacement is similar.

In a mixed-wet reservoir, some of the surfaces of the rock are covered with oil and some with water. This will make water and oil phase to flow easier through the matrix. In this

case, k_{ro} is a bit higher than k_{rw}. Still, the relative permeability of oil will decrease while relative permeability of water will increase with decreased oil saturation. Thus, the oil droplets will not be trapped by water phase, since the oil-wet surfaces provide a path for the oil to escape from nearly water-filled pores (Abdallah, 2007). The cross point of relative permeability curves will be placed around 0.5 on water saturation axis, determining system as mixed-wet (Craig, 1971).

Finally, wettability has an impact on relative permeability as it controls the flow and spatial distribution of fluids in a porous medium, i.e. oil recovery process.

2.4 Carbonates

This section gives a brief introduction to the carbonate rocks.

2.4.1 Carbonate rocks

Carbonates are, by definition, sedimentary rocks that contain around 50% of carbonate minerals such as calcite ($CaCO_3$), dolomite ($CaMg(CO_3)_2$), magnesite ($MgCO_3$) and many others. They are composed of anionic complex CO_3^{2-} and divalent metal ions Ca^{2+}, Mg^{2+}, Fe^{2+}, Mn^{2+}, Zn^{2+}, Ba^{2+}, Sr^{2+}, Cu^{2+} and others (Ahr, 2008).The carbonate rocks are mainly contained in limestones and dolomites, wherein limestones are the ones containing the most amount of calcite (*Table 5*).

Table 5. Some of most known carbonate minerals and their chemical formula

Name	Formula
Low-Mg calcite	$CaCO_3$ ($< 4\%\ MgCO_3$) (hexagonal)
High-Mg calcite	$(Ca, Mg)\ CO_3$(>4% $MgCO_3$) (hexagonal)
Aragonite	($CaCO_3$) (orthorhombic)
Siderite	$FeCO_3$
Magnesite	$MgCO_3$
Strontianite	$SrCO_3$
Rhodochrosite	$MnCO_3$
Smithsonite	$ZnCO_3$
Ankerite	$Ca\ (Mg, Fe)(CO_3)_2$
Dolomite	$CaMg(CO_3)_2$

The special case for limestones is chalk ($CaCO_3$) formed from gradual accumulation and sedimentation of skeletal debris of calcite shells from micro-organisms called coccolithophores (Figure 25). The information about microstructure of chalk is crucial as the organic coating on the chalk particles is responsible for wetting behavior (Andersen, 1995).

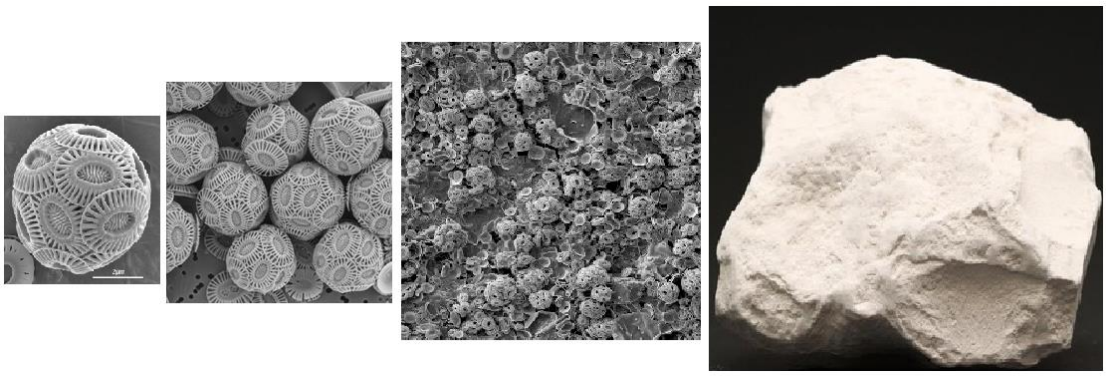

Figure 25. From Coccolithophore to Chalk material

Carbonate rocks constitutes approximately 90% of all naturally occurring carbonates (Reeder, 1983). Just a small part of them (approximately 10%) are present as semi-precious stones.

Pore size distribution in chalk

The pore size distribution (PSD) is an attribute used to characterize the pore structure. PSD quantifies the relative volumes correlated with the different pore sizes. Parameters such as variance of pore size, pore-throat size ratio (aspect ratio), cluster of pores, pore throat connectivity, and pore shape determine fluid distributions. To study pore size distribution, Milter (1996) injected mercury in SK chalk cores. The results he obtained are presented in Figure 26.

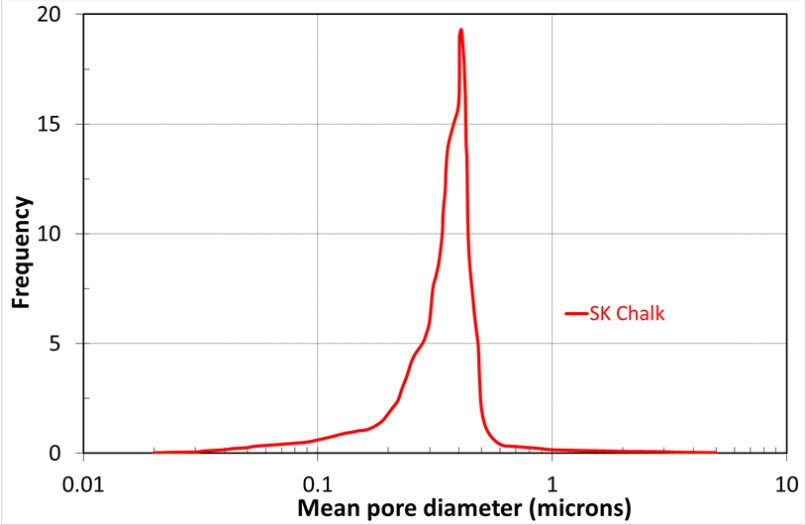

Figure 26. Pore size distribution in SK chalk determined by mercury injection. Redrawn after (Milter, 1996).

Figure 26 shows that the smallest pores are less than 100 nm, the largest pores are close to 1000 nm (1 μm) and the pore diameter is close to 500 nm. This shows that the SK chalk cores have a heterogeneous pore size distribution.

2.4.2 Carbonate reservoirs

The main reason of doing research on carbonate reservoirs is to find more ways of successfully extracting hydrocarbons, in the form of oil and gas, trapped in such reservoirs. The trapped amount of hydrocarbons comes found to be 60% of oil and 40% of gas (Schlumberger, 2015a). Two basic properties, porosity and permeability, should be considered. Carbonate reservoirs due to naturally occurring fractures, have usually high porosity and low permeability, and consequently low oil recovery which is below 30% (Treiber & Owens, 1972).

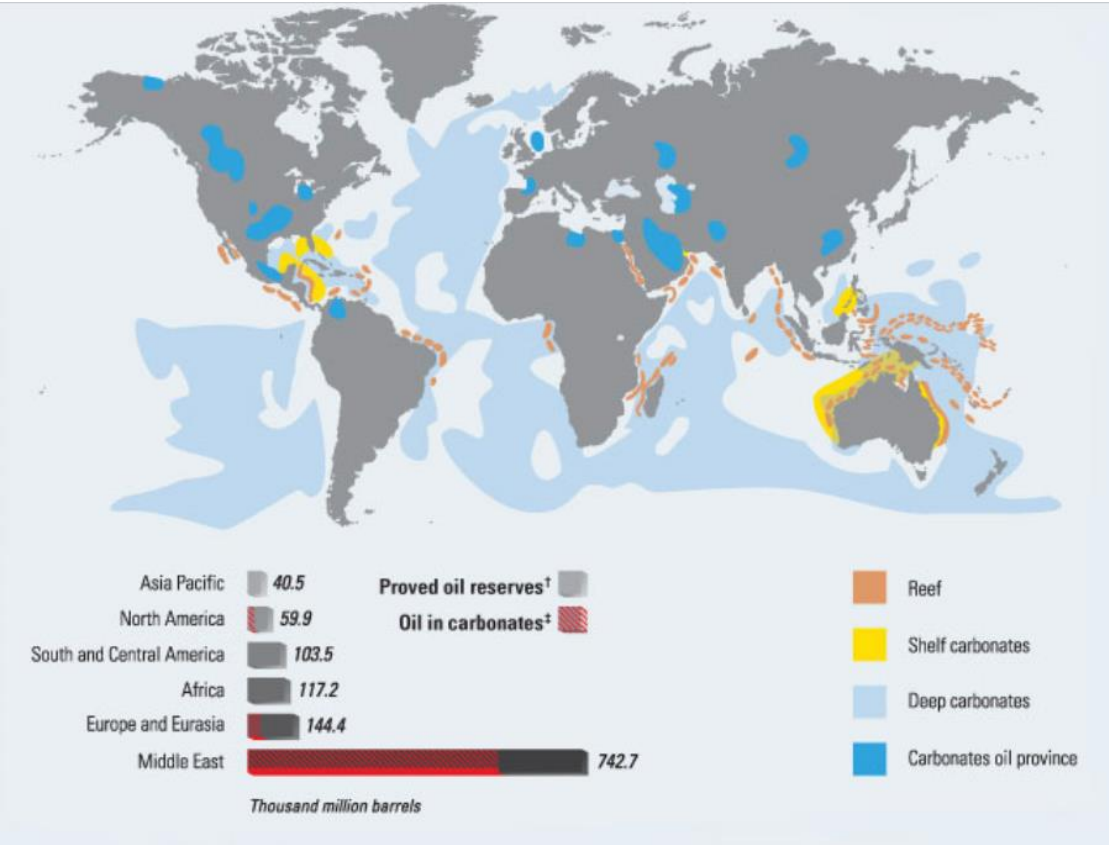

Figure 27. World Distribution of Carbonate Reserves (Schlumberger, 2015a)

Figure 27 shows the world distribution of carbonate reservoirs. The Middle East is dominated by the biggest carbonate reservoirs containing about 70% of oil and 90% of gas (Schlumberger, 2015a).The other countries that deliver smaller amount of hydrocarbons from carbonate reservoirs include West Canada, Mexico, Texas (USA), Norway (Central North Sea), Poland, Kazakhstan, Western and Southern China, Iran and Libya (Gluyas & Swarbick, 2004).

2.5 Wetting in carbonates

Improved spontaneous imbibition of water is believed to be crucial for oil production in carbonate reservoir systems, especially in fractured ones (Austad et al., 2005). To manage this, the IFT between oil and water should be decreased or the gravity contribution should be increased or apply the wettability alteration mechanisms. Spontaneous imbibition of water is the result of altering the wetting state from oil-wet to water-wet. In such cases, the capillary forces are changed from negative to positive, water imbibes, and oil can be expelled. There are several methods for altering the wettability in carbonate rock, but also a number of factors affecting initial wettability, such as pore size, pore geometry, pore structure, brine, composition, temperature,

salinity, rock mineral composition, oil composition and pH. These factors will have a certain different effect on changing the wetting state, which is not so easy to determine separately. Therefore, Buckley (1998) provided a provisional list of interactions that affect the wettability. This list includes surface precipitation, polar interactions, ion binding, and base/acid interactions. The upcoming section describes some methods for wettability alteration as well as the effects of some factors on initial wetting state of the chalk material.

2.5.1 Wettability alteration by modified Sea Water

The potential of seawater to act as a wettability modifier has been studied in a certain number of experiments. (Puntervold, Strand, & Austad, 2009) Several experimental studies have been carried out on seawater flooding and have led to the conclusion that seawater, when implemented, increases the water wetness of chalk material, especially at high temperatures (Figure 28) (Strand, Puntervold, & Austad, 2008a; Puntervold, 2008; Puntervold & Austad, 2008; Zhang, 2006). The improvement in oil recovery is observed by both spontaneous imbibition and forced displacement (Ravari, 2011).

The mechanism of wettability alteration by seawater, known as an EOR fluid in carbonates, can be presented as the symbiotic interaction between the potential determining ions in chalk Ca^{2+}, Mg^{2+}, and SO_4^{2-} (Zhang, 2006) and the adsorbed carboxylic groups on the chalk rock surface (Strand, Puntervold, & Austad, 2008a; Zhang, 2006).

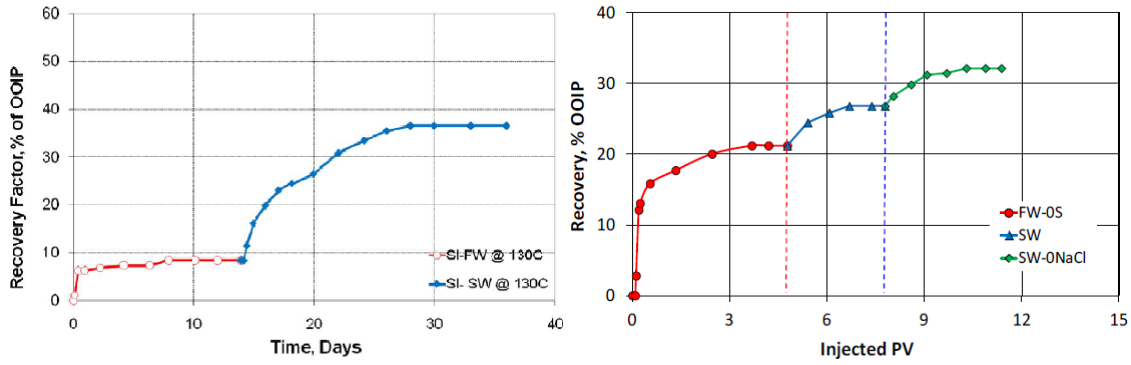

Figure 28. Spontaneous imbibition at 130°C of FW and SW into Res# 4-12 using crude oil with AN=0.50 mgKOH/g. Low perm. 0.1-1 mD.(left) and Forced displacement at 100°C from the limestone reservoir core by injection of FW, SW and SW-0NaCl (Ravari, 2011)

The mechanism for seawater-induced wettability alteration in chalk was initially suggested by Zhang et al. (2006), while Strand et al. (2006) utilized this mechanism in limestones, experimentally verifying that limestone showed similar interactions

between the determining ions as in the chalk reservoir. Accordingly, the large amount of sulfate ions present in seawater will adsorb onto the positively charged water–wet sites on the carbonate surface. The imbibing fluid with higher sulphate content showed the highest oil recovery as illustrated in Figure 29.

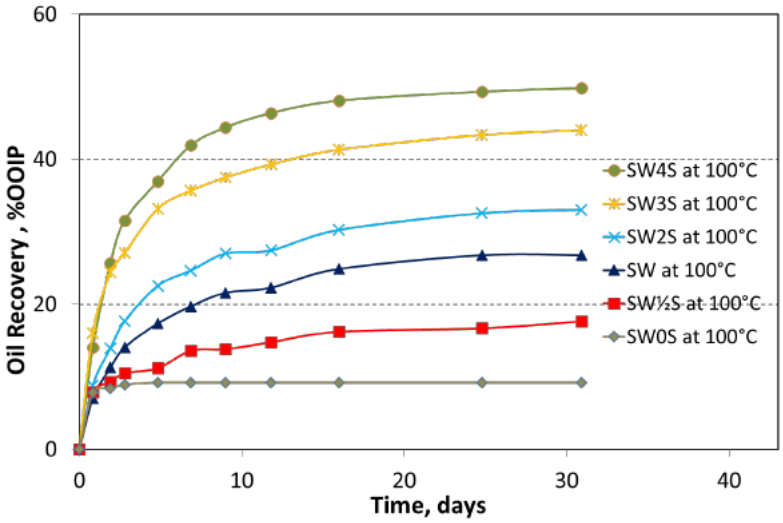

Figure 29. Spontaneous imbibition onto chalk cores at 100 °C, with various sulphate content in the imbibing brines (Zhang, 2006)

The positive $CaCO_3$(s) surface charge will be lowered. Now, close to the chalk surface, more of Ca^{2+} will be localized. This appears due to the less electrostatic repulsions. Thus, the Ca^{2+} ions react with adsorbed negatively charged carboxylic groups bonded to the calcite surface (Figure 30), but some of the carboxylic material will be desorbed from the surface.

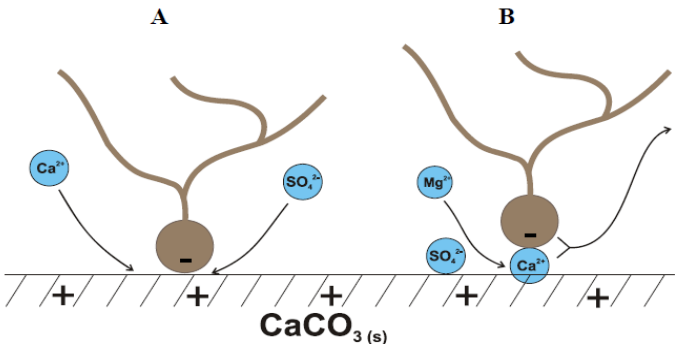

Figure 30. Mechanism for the wettability alteration induced by SW. A: Proposed mechanism when Ca^{2+} and SO_4^{2-} are active. B: Proposed mechanism when Mg^{2+}, Ca^{2+} and SO_4^{2-} are active at higher temperatures (Zhang, 2006).

Similar to sulphate ions, increased concentration of Ca^{2+} ions at temperature of $70°C$ results in increased oil recovery as illustrated in Figure 31.

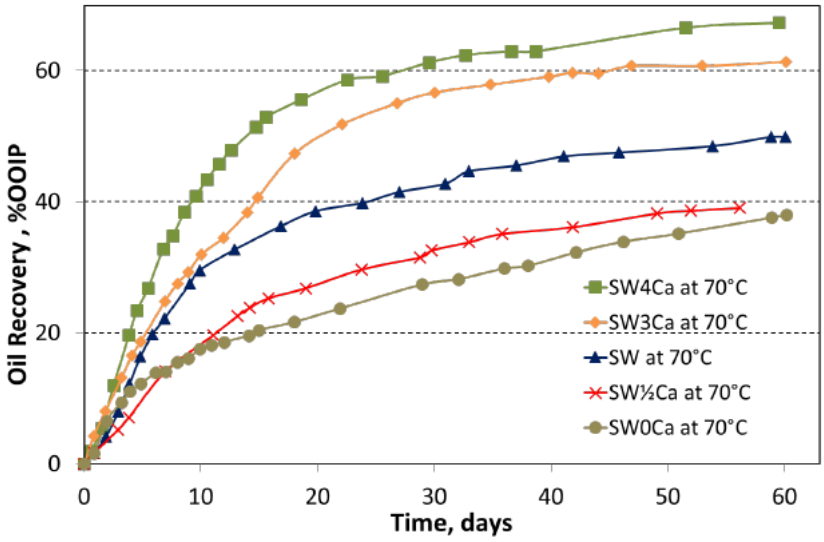

Figure 31. Spontaneous imbibition onto chalk cores at 70 ° with crude oil: AN=0.55 mgKOH/g and $S_{wi} = 0$, with different Ca^{2+} content in the imbibing brines (Zhang, 2006).

The offered mechanism was also experimentally tested at high temperatures. At high temperatures (100-130°C), Mg^{2+} is able to substitute Ca^{2+} at chalk surface (Figure 30.B) (Puntervold & Austad, 2008). The degree of substitution increases with temperature (Korsnes, 2006). The ability of Mg^{2+} ion to dislocate Ca^{2+} ion linked to carboxylic groups on the chalk surface contributed the access through the aqueous phase. The Mg^{2+} ion is small, but it has a high charge density and that makes it strongly solvated in water (Burgess, 1978). With increased temperature, the Mg^{2+} ion will become partially dehydrated and hence more reactive (Strand, Puntervold, & Austad, 2008a). The combination of mentioned effects lead to elimination of the organic material, establishing the preferentially water-wet chalk surface. In addition, as the wettability alteration is catalyzed by concentration of the potential determining ions SO_4^{2-}, its affinity increases towards chalk surface with increased temperature (Strand, Standnes, & Austad, 2006). So, this mechanism will not modify wetting state and improve oil recovery if there is an absence of Ca^{2+} or Mg^{2+} or SO_4^{2-}, meaning all of them must be present in the injected fluid (Zhang, 2006). Figure 32 illustrates the impact on oil recovery by different compositions of injected brine, as the temperature of the system is increased.

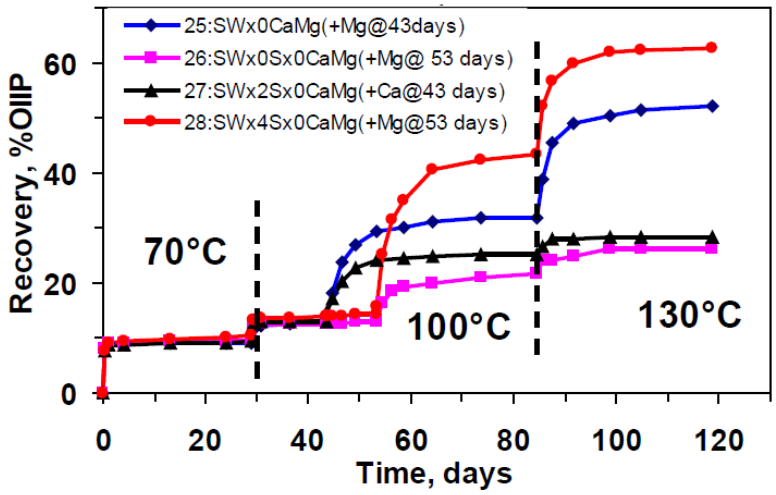

Figure 32. Spontaneous imbibition tests at different temperatures and compositions of the potential determining ions.

Furthermore, the term "Smart Water" refers to optimizing injection brine in terms of chemical compositions and salinity with purpose of EOR brine injection. By performing the Smart Water flooding, the mechanism will have different wettability change in both carbonates and sandstones due to certain distinctions in the rock properties (Yousef, 2011). Carbonates need a seawater with salinity of 33000 ppm for wettability alteration process, while in sandstones a low saline water (< 2000 ppm) is needed for wettability alteration to take place (Figure 33) (Morrow & Buckley, 2011). Figure 33 illustrates the salinity effects on oil recovery in sandstones (left) and carbonates (right), when injection brine with different salinities were introduced into the flooding process. In both case, the flooding with low salinity concentrated injection brine gave higher oil recovery (Yousef, 2011).

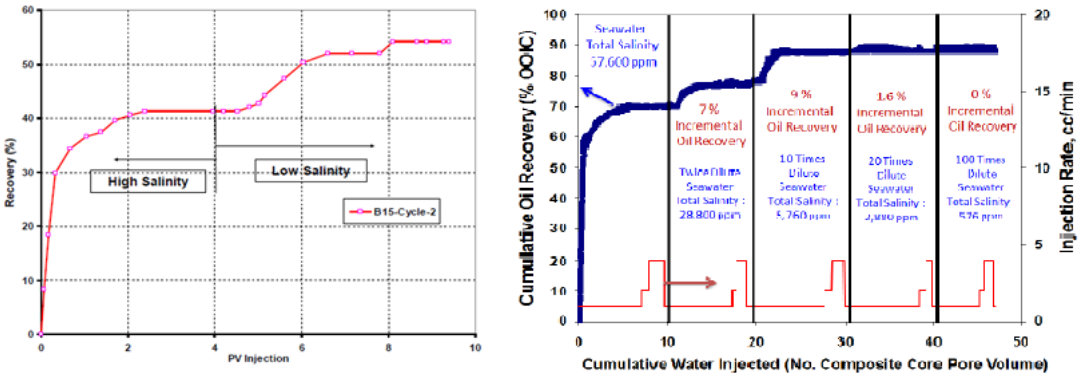

Figure 33. Low Salinity EOR-effect in sandstones (left at high salinity of 100 000 ppm and low salinity of 750 ppm) (Yousef, 2011) and carbonate/limestone (1.seawater : 57,600 ppm; 2. Twice diluted seawater:28,800ppm- 7% incremental oil recovery; 3. Ten times diluted seawater: 5,760ppm-9% incremental oil recovery; 4. Twenty times diluted seawater: 2,880

ppm-1,6% incremental oil recovery; 5. Hundred times diluted seawater: 576ppm-0% incremental oil recovery) (Group S. W., 2015)

Further studies confirmed that besides Ca^{2+}or Mg^{2+} and SO_4^{2-}ions, the concentration of non-determining ions Na^+ , Cl^- in seawater has large effects on EOR. The spontaneous imbibition test showed increased oil recovery when concentration of Na^+ and/or Cl^- in seawater was lowered or even removed as they do not alter wettability (Puntervold & Austad, 2008; Fathi, Austad, & Strand, 2011; Puntervold, Strand, Ellouz, & Austad, 2015). The access of potential determining ions to the calcite surface is affected by the concentration of non-active ions, i.e. the removal of non-determining ions results in increased relative concentrations of the active ions and hence will improve the oil recovery (Figure 34).

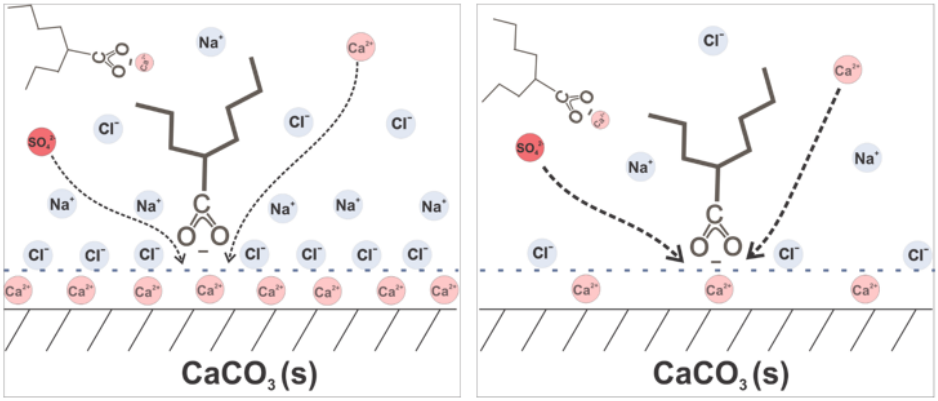

Figure 34. Effect of salinity and the access of potential determining ions to the calcite surface is affected by the concentration of non-active ions (Puntervold, Strand, Ellouz, & Austad, 2015).

Likewise, if the injection brines were spiked with a higher concentration of sulfate, the catalyst for wettability alteration, besides the reduction in Na^+ and Cl^- ions, even a further increase in oil recovery could be observed. This improvement is presented in Figure 35.

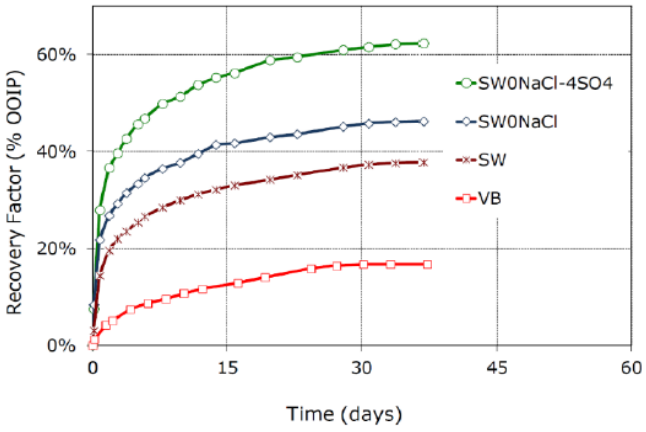

Figure 35. Spontaneous imbibition in oil saturated chalk core at Tres=90°C with AN=0.5 and S_{wi}=0.1 and using formation water-VB, seawater, seawater depleted in NaCl (SW0NaCl) and seawater depleted in NaCl and spiked with 4x sulfate (SW0NaCl-4SO_4) (Fathi, Austad, & Strand, 2011).

In summary, the key parameters in Smart Water mechanism for wettability alteration in carbonates by seawater flooding, and hence better EOR response, are the potential determining ions, non-determining ions, temperature and their interplay.

2.5.2 Initial wetting in Carbonates

As deposition and sedimentation take place in an aqueous phase, carbonate reservoirs were originally filled with water. Later on, hydrocarbons migrated into the reservoir pores and a chemical equilibrium between the crude oil, brine and rock was established over geological time (Austad, 2013; Ahr, 2008) with respect to the major parameters such as:

- Initial water saturation and thin film forces
- Brine salinity and content of divalent ions
- Rock mineral and surface charge (Jadhunandan & Morrow, 1995)
- Polar oil components, solubility and stability (Kaminsky & Radke, 1998)
- Temperature/pressure (Buckley & Liu, 1998)
- Capillary pressure (Hirasaki, 1991)

In carbonate reservoirs/naturally fractured carbonate reservoirs, the potential for oil recovery processes is driven by reservoir parameters such as the relative permeability of oil and water, fluid distributions and capillary forces. For this reason, the information about initial wetting conditions plays a major role, especially for naturally fractured carbonate reservoir systems (Shariatpanahi, Strand, & Austad, 2011). To estimate the

initial wetting state of a system, we should consider the water film stability as proposed by Hirasaki and Zhang (2004). Instability of water film caused by the various interactions in crude oil/brine/rock (COBR) system determines the initial wettability of the rock. A study from all over the world confirmed that the majority of carbonate rocks appear to be mixed-wet to oil-wet (Taber, 1997). Considering these wetting conditions, it can be concluded that they do not present ideal state as they will result in generally low oil recovery (Fathi, 2012). To acquire a higher oil recovery, the process of wettability alteration should be taken into consideration. Alteration of the wettability of carbonate rocks will change their initial wettability towards more water-wet according to Wu et al. (2008).

2.5.2.1 Effects of Crude Oil on Initial wetting

Crude oil is a complex mixture of hydrocarbon and non-hydrocarbon substances. The mixture contains important components such as Paraffins, Naphthenes, and Aromatics. The asphaltenes and resins are the components responsible for wettability alteration (Kovscek, 1993; Wolcott, 1993). These components contain a polar end (hydrocarbon) used for adsorption to the rock surface. This hydrocarbon end is oriented outwards, making the surface preferentially oil-wet (Anderson W. G., 1986a; Puntervold, 2008; Speight J. G., 2014). The asphaltenes and resins, as oil constituents, contain both acidic and basic components. The acidic components are quantified by acid number (AN). These components, found in heavier fractions, are represented as carboxylic acids (RCOOH), which can be deprotonated to negatively charged carboxylates ($RCOO^-$) The base components can, on the other hand, be positively charged and quantified by BN or base number. They are presented as R_3NH^+ ($R3NH^+$) at low pH and can be deprotonated to R_3N: at high pH. The surface of carbonates is naturally positively charged. Hence, a very strong bond will be established with the negatively charged end of the carboxylic group, ($-COO^-$), as illustrated in Figure 36.

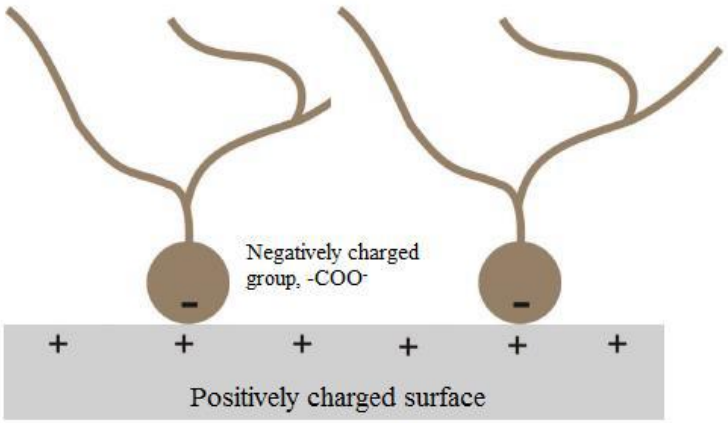

Figure 36. Adsorption of negatively charged carboxylic groups to positively charged carbonate surface.

However, when the carbonate rock surface is directly exposed to the oil phase, the polar components will tend to adsorb on its surface. As a consequence there will be a non-uniform wettability, where some areas that are covered by organic layers become oil-wet and other remain water-wet corresponding to the original wettability (Strand, Standnes, & Austad, 2006). The ability of crude oil components to change initial wetting state of carbonate rocks can be measured by API Gravity, AN or BN, combined with the mineralogy of the carbonate surface (Buckley & Liu, 1998). For the purpose of this work, we used AN and BN measurements to determine crude oil effects on chalk's initial wetting state.

Effects of AN/BN

The acid and base numbers are measuring the amount of acidic and basic components in crude oils, respectively. These measurements are expressed in milligrams of hydroxide per gram of sample, (mgKOH/g), required to neutralize one gram of crude oil (Strand, Puntervold, & Austad, 2016) and are measured by potentiometric titration according to a procedure proposed by Fan and Buckley (2007). Moreover, acid number plays a more significant role than the base number as mentioned in section 2.4.2. The base number has a much lower magnitude of influence on the initial wettability. A specific species of basic material, however, may influence the wettability in a way that it reduces water-wetness (Puntervold, Strand, & Austad, 2007b). The effects of the crude oil on wettability properties are given through Figure 37.

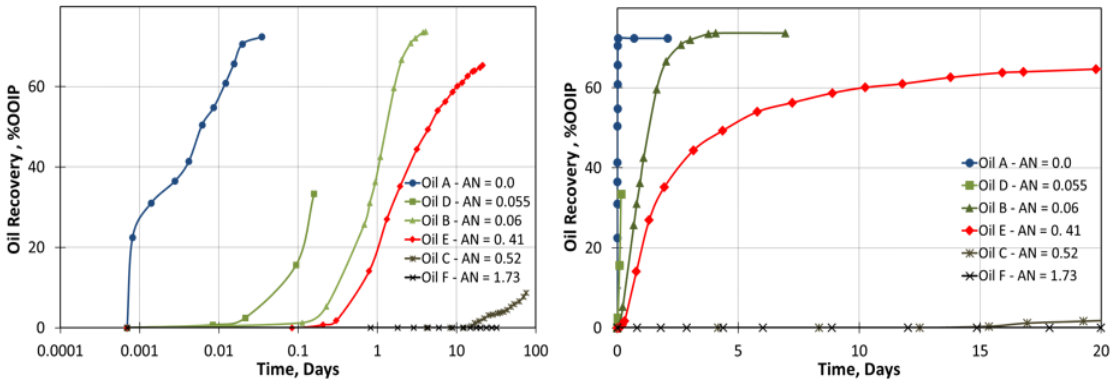

Figure 37. Initial wetting of SK Chalk- effect of different AN in crude, SI performed at 50 °C; SI (right) using 45 000ppm brine at 40 °C (Standnes & Austad, 2000)

The impact can be seen in spontaneous imbibition of water into chalk cores saturated with oil with different ANs. Water wetness decreases with increasing AN, which leads to an increase in the ultimate oil recovery as well as the imbibition rate. Puntervold (2008) tested the effects of model oil/effect of AN on initial wetting in Chalk cores. The experiment was performed on five SK chalk cores equally restored at Swi = 0.1 with FW. Model crude oil (RES40) had different AN values: 0.1, 0.5, 0.73, 1.6 (Figure 38). Spontaneous imbibition test was run with FW brine at 90°C and no chemically induced wettability alteration using FW as imbibing brine. By this experiment Puntervold (2008) proved that model oil (RES40) behaves the same way as crude oils as the water wetness decreases with increasing AN, and the same is observed for imbibition rate and ultimate oil recovery.

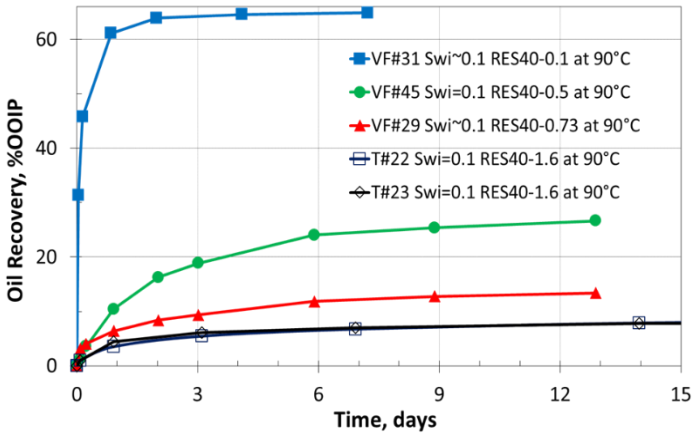

Figure 38. Spontaneous imbibition at 90 °C from SK chalk cores with Swi=0.10 and aged in Crude Oil with different AN , using formation brines as imbibing brine (Puntervold, 2008).

2.5.2.2 Effect of initially present Sulphate on initial wetting

Effect of initially present sulfate in cores prior to cleaning was studied by Puntervold (2007). Two SK chalk cores were used for experiments. One of the chalk cores was pre-flushed with DI water. The spontaneous imbibition test was performed on both cores at the temperature of 90 °C. The final results and eventual effects are illustrated in Figure 39.

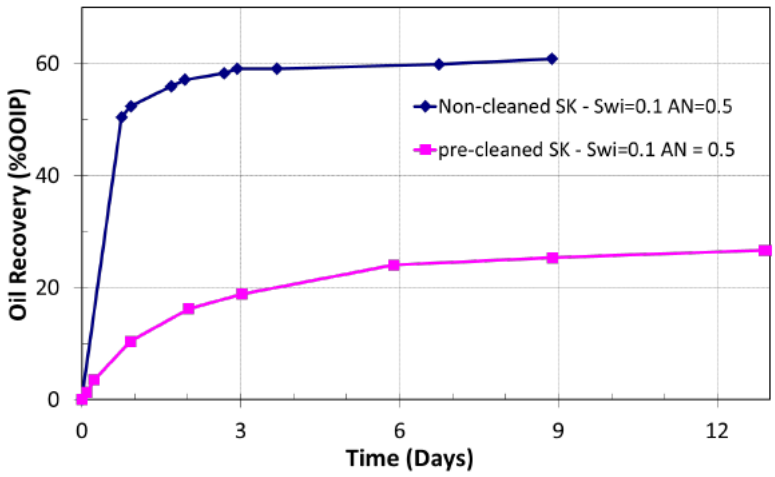

Figure 39. Spontaneous imbibition at temperature of 90 °C. Results for non-flushed and flushed chalk SK cores (Puntervold, Strand, & Austad, 2007)

It is obvious that the core which was not precleaned shows more water-wet state due to initially present sulphate material in chalk cores, that led to a higher oil recovery. The pre-cleaned chalk core showed significantly lower oil recovery (about 30%) due to absence of initial sulphates. Based on information obtained from non-cleaned core, the seawater (”Smart Water”) wettability alteration mechanism is introduced in section 2.4.1. However, several experiments confirmed that a certain amount of initially present sulphate content, either in FW or core, can increase water-wetness of chalk material, i.e. influence oil recovery at later stages (Puntervold, Strand, & Austad, 2007; Shariatpanahi, Strand, & Austad, 2011).

2.5.2.3 Effect of initial water/FW composition on initial wetting in Chalk/Limestone

The information about initial water in the reservoir is very important as it has great impact on overall fluid-rock equilibrium. To do the prediction of correct initial oil in place and mobility of present fluids it will be of crucial importance to estimate corresponding initial water saturation (S_{wi}). The information about the volume of hydrocarbons present in a porous reservoir rock is obtained from equation (2.22):

$$S_{oi} = 1 - S_{wi} - S_{gi} \qquad (2.22)$$

Where,

S_{oi} the initial oil saturation

S_{wi} the initial water saturation

S_{gi} the initial gas saturation.

The initial water in a reservoir system can exist either as formation water, injection water or a stimulation chemical mixture. Its composition will be highly dependent on the reservoir rock type and some other reservoir conditions. As an example, Figure 40 illustrates the effect of initial water saturation on adsorption of polar components. Comparing these figures, this effect was reflected in the fact that the adsorption of polar components occurred almost immediately when the initial water saturation was Swi = 10% (right) (Mjos, 2018). According to Wakwaya (2016), initial water saturation has a profound effect on the wetting condition, reduced water saturation is observed to show a more oil-wet condition as there is higher amount of available cites for adsorption within the core.

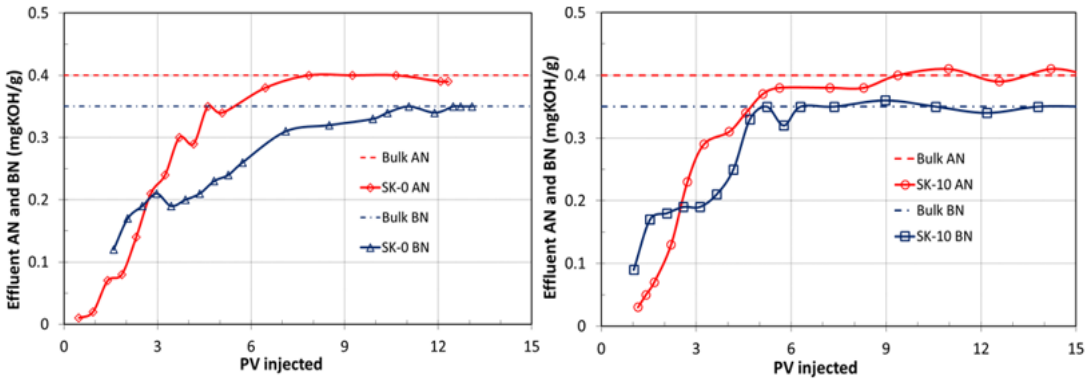

Figure 40. Effect of Swi on polar components (POC) adsorption. Formation water VB0S at Swi = 0% (left) and Swi = 10% (right) (Mjos, 2018).

Moreover, FW composition appears to have a certain influence on wetting state of reservoir rock. Formation water can contain Mg^{2+} ions in its composition. Shariatpanahi (2016) proved that the presence of these ions pushes the system towards more water-wet state. The presence of other ions did not show significant effect on wetting state of carbonate rocks. Figure 41 explains how ultimate oil recovery is changed when chalk cores are flooded with different FWs. Obviously, when DI water was used as initial brine, we see the lowest oil recovery. On the other hand, the brine containing $MgCl_2$ shows the highest oil recovery, as expected.

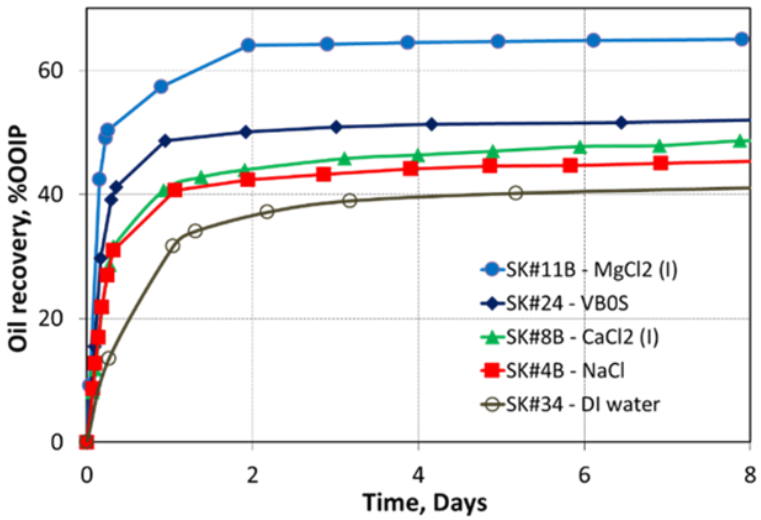

Ions	$CaCl_2$ (I) mM	NaCl mM	$MgCl_2$ (I) mM	VB0S mM	DI mM
Mg^{2+}	0	0	660	8	0
Ca^{2+}	566	0	0	29	0
Na^{+}	0	1075	0	997	0
TDS, g/l	62.83	62.83	62.83	62.83	0
IS, mole/l	1.698	1.075	1.980	1.118	0

Figure 41. Spontaneous imbibition at 25 °C from SK chalk cores with Swi=0.10. Aged in Crude Oil (AN = 0.17), using formation brines with equal salinity, 63 000 ppm, and different type of cations (Shariatpanahi S. F., 2016).

The lowest water-wetness is observed when using DI water as FW. This is due to the lack of ionic double layers outside the chalk surface, something that most likely make it easier for the carboxylic groups to break the water film and adsorb to the chalk surface (Shariatpanahi S. F., 2016). The most water-wet rock surface is obtained using FW with high Mg^{2+} concentration and reduced water wetness using FW with increasing Ca^{2+} concentration as shown in Figure 42. Increasing Ca^{2+} concentration in FW (at constant salinity), water-wetness is decreased, and adsorption of acidic components is increased.

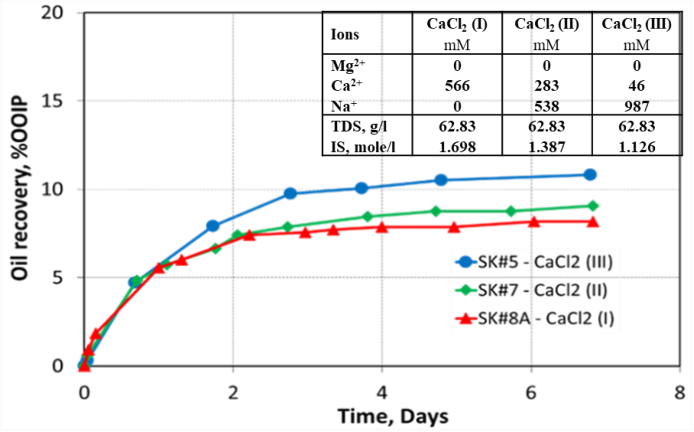

Ions	$CaCl_2$ (I) mM	$CaCl_2$ (II) mM	$CaCl_2$ (III) mM
Mg^{2+}	0	0	0
Ca^{2+}	566	283	46
Na^{+}	0	538	987
TDS, g/l	62.83	62.83	62.83
IS, mole/l	1.698	1.387	1.126

Figure 42. Spontaneous imbibition with VBOS at 25 °C from SK chalk cores with Swi=0.10 and aged in Crude Oil with AN = 0.34 and effect of Ca2+ concentration on initial wettability.

2.6 Simulation of Smart Water EOR potential

During the injection of Smart water, the wettability alteration will change the initial wetting condition of the cores from a mixed-wet to a more water-wet. The potential of flooding by "Smart Water" is change in wetting properties of not just the CBR-system, but also capillary pressure and relative permeability of oil and water phases, i.e. oil recovery. Based on this process the relative permeability curves are modelled. To model relative permeability curves for Smart water wettability alteration proses it would be necessary two sets of curves. One set of curves for mixed-wet and one set for strongly water-wet. Shift in relative permeability curves from the mixed-wet case to the more water-wet case is used to simulate the wettability alteration process during water injection. Simulations of Smart Water EOR potential must be promising for considering a pilot on Smart Water EOR. Wettability is reflected by k_{ri} and P_c and these curves do not change independently. Therefore, it is of interest to understand how relative permeability curves are affected by difference in wettability of these chalk cores.

Various methods have been proposed to determine relative permeability curves on the field and laboratory scale (Uguru, 2010). Uguru (2010) used SCAL experiments to estimate relative permeabilities from logs. On field scale, relative permeabilities can be determined from production data when the streamline simulation is used (Kulkarni, 1999). On the other hand, according to Cig (2015) to do estimation on in-situ relative permeabilities as well as capillary pressure, wireline formation testers were taken into consideration. On lab scale, there are three test methods implied for calculation of relative permeabilities on artificial chalk cores (McPhee, 2015). The methods include steady state, unsteady state and centrifuge test. Each method provides a different information required for relative permeability curves generation (Figure 43). The main focus of this project should be on core measurements and less on logs.

Steady state is mostly used when the saturation values of displacing phase are low. Test can describe the relative permeability over a wide range of saturations. If S_{or} cannot be measured, end point relative permeability cannot be measured either. It becomes estimating rather than measuring these .

Unsteady state is used after water breakthrough providing mainly late saturation values. During this test, the value of S_{or} is usually not correct. On the other hand, its value is lower than the S_{or} value obtained by steady state test. Main goal by this test is

estimation of end effective permeabilities. The unsteady state method is used in this project during forced imbibition, with an aim of determining relative permeabilities.

The centrifuge test mainly gives accurate measurement of the displaced phase if the displaced phase is much more viscous than displacing phase and high rotation speed is used so P_c is negligible (McPhee, 2015).

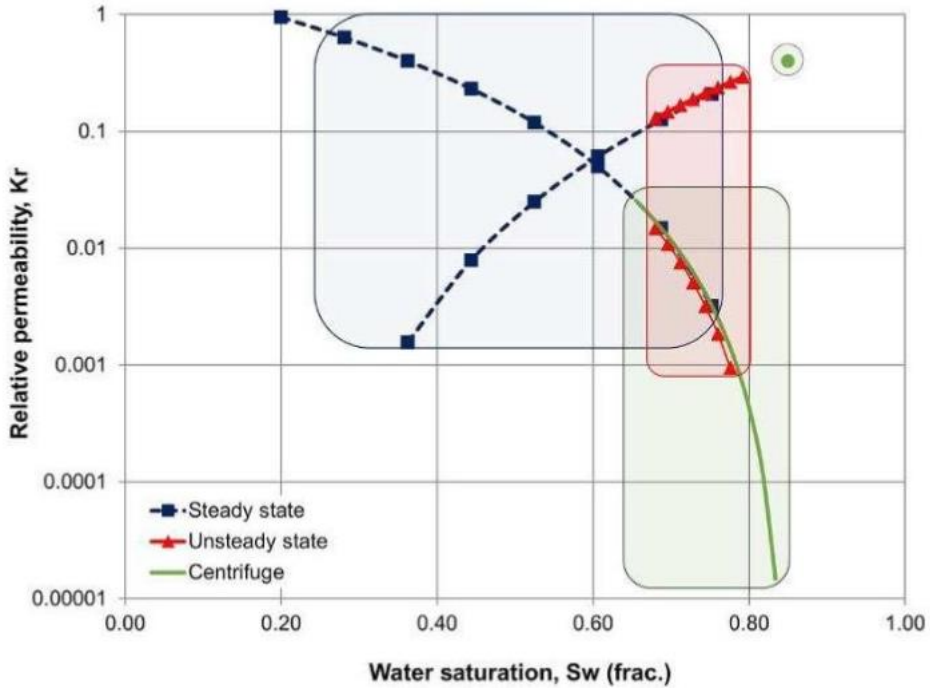

Figure 43. Relative permeabilities based on steady state (blue line), unsteady state (red line) and centrifuge test (green line).

3. Materials and methods

3.1 Materials

The following section presents rock and fluid materials that have been used in this experimental work.

3.1.1 Rock material

Outcrop chalk samples from Stevns Klint (Copenhagen, Denmark) of Maastrichtian age were used as a porous medium. The cores are characterized by their chemical and physical properties. In this study the porosity of cores is quite high, in the range 45-50%, and the permeability is low, approximately 5 mD, as reported in Table 6. Generally, the chalk material is made up of microscopic particles known as coccoliths

where the calcite is extracted from seawater. Hence, the rock material is believed to be an analogue to the North Sea chalk.

Table 6. Reservoir Chalk Core Properties

Core	SKR1	SKR2	SKC3	SKC6
Dry weight, g	109.1	107.68	106.19	105.97
Length, cm	7.06	7.07	7.10	7.08
Diameter, cm	3.78	3.79	3.79	3.79
Bulk volume, ml	79.22	79.76	80.09	79.87
Weight of saturated core, g	146.63	146.85	144.18	145.88
Density of liquid, g/ml	1	1	1	1
Pore volume (PV), ml	37.53	39.17	37.99	39.91
Porosity, %	47	49	47	50
Injection rate, PV/day	1	1	1	1
Pump Rate, ml/min	0.026	0.027	0.026	0.027
Initial water saturation (S_{wi})	0.2	0.2	0.2	0.2
Density of formation water (FW), g/ml	0.997	0.9976	0.9976	0.9976
Target dry weight, g	116.59	115.50	113.77	113.93
Permeability, mD	4.02	4.09	4.25	4.33

To calculate parameters mentioned in Table 6, following equations were used:

$$PV = \frac{(Weight\ of\ saturated\ core - Dry\ weight)}{Density\ of\ liquid} \quad (3.1)$$

$$Bulk\ volume = Length \cdot \pi \cdot Diameter^{2}/_{4} \quad (3.2)$$

$$Porosity = \frac{PV}{Bulk\ volume} \quad (3.3)$$

$$Pump\ rate = \frac{(Injection\ rate \cdot PV)}{1440} \quad (3.4)$$

$$Target\ weight = Dry\ weight + PV \cdot S_{wi} \cdot desity\ of\ FW \quad (3.5)$$

Minerology of the chalk cores used specifically in this experimental work is presented in Figure 44.

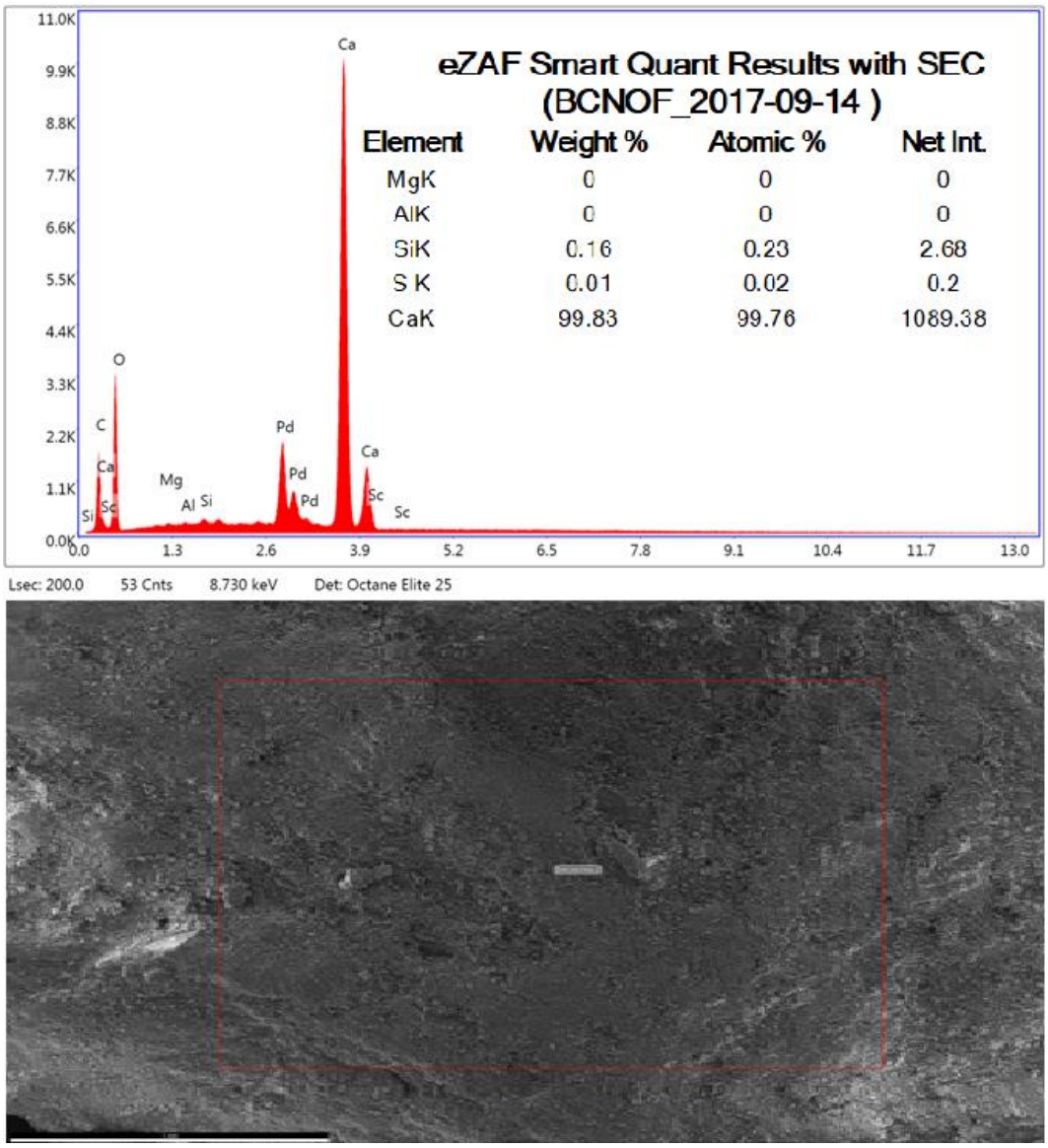

Figure 44. Minerology of chalk core (Torrijos, 2017)

A Zeiss Supra 35VP Environmental Scanning Electron Microscope (SEM) was used to analyze the chalk material structure. From Figure 44 (top figure), we observe that the core is pure calcium (99.83 wt%) with almost no sulphate (0.01 wt%) and very low silica content (0.16 wt%).

3.1.2 Oil material

For establishing desired initial wetting conditions, using correct oils was highly essential. As mentioned in section 2.4.2.1, acid number is a prime factor for changing the wetting conditions of chalk. For this purpose, AN was manipulated by diluting Heidrun oil with n-Heptane. Characteristics of oils are presented in the table.

Heidrun

Heidrun oil is the crude oil produced from the Heidrun oil field (Norwegian Continental Shelf) by water and gas injection (varies between different formations) in the Åre, Tilje, Ile and Garn Formations. The biodegraded crude oil is used as base crude oil with a high AN=2.80 mg KOH/g and a BN=0.74 mg KOH/g. The measured data for this oil are presented in Appendix B.

RES 40 (original)

The RES 40 oil was prepared by mixing Heidrun oil with n-heptane in the volume ratio of 60:40. Thereafter, the acid number of this oil mixture was measured to be equal to 1.80 mg KOH/g. The viscosity of this oil mixture was found and presented in Appendix B.

RES 40-0

To reach the desired AN value, the oil mixture was first treated with silica gel for a period of two weeks. The silica gel of 20 wt% was added in two steps during this period, so 10 wt% silica gel was added each time. The main purpose of adding silica gel was to remove surface-active components in the oil, also known as carboxylic acid and base groups. For the whole duration of two weeks, the mixture was stirred and thereafter centrifuged to separate oil from the silica gel. The crude oil was then filtered through 5 μm Millipore filter. The value of acid number was measured to be equal to zero. This oil mixture was named RES 40-0. This oil was further treated as given below to reach the desired AN values.

RES 40-0.15/RES 40-0.34/ RES 40-0.68

The oils are used to change the wetting properties of chalk cores. The crude oils of desired ANs were created by mixing the RES40-0 and the crude oil with higher acid number, RES40 (original), in appropriate ratio so that we ended up with three different crude oils with the values of AN=0.15 mg KOH/g for RES 40-0.15 oil, AN=0.34 mg KOH/g for RES 40-0.34 oil and AN=0.68 mg KOH/g for RES 40-0.68 oil.

The tests mentioned in this study are performed using the crude oil RES 40-0.15, and later compared to the tests performed by students Harestad (2019) and Wathne (2019) using RES40-0.34 and RES 40-0.68 on similar chalk samples (see sections 5 and 6). The calculated amount of RES40 and RES40-0 to be mixed can be found in Appendix B.

Synthetic Oil-Model Oil

Synthetic, model oil is used for flooding the reference cores and to replace crude oil in other two cores. This oil replaces crude oil in order to keep desired wetting state of cores. Marcol 82 (in amount of 58 wt%) and n-heptane (in amount of 42 wt%) were mixed in order to create desired properties of synthetic oil. This oil came out with an AN=0. The viscosity of this synthetic oil was estimated to be around 2.6 cP at room temperature of 23°C. All the measured properties of Marcol 82 oil, n-heptane as well as formed synthetic oil can be found in Table 7. A detailed explanation of Marcol 82 oil and n-heptane can be found in Appendix A and all obtained results in Appendix B.

Table 7. Crude oil measured properties

Crude Oil	***AN (mg KOH/g)***	***Density (g/cm3)***	***Viscosity (cp @ 23 °C)***
Heidrun	2.80		28.344
RES40	1.80	0.820	2.5872
Res 40-0	0.00	0.809	2.3922
Res 40-0.15	0.15	0.818	2.89
Res 40-0.34	0.35	0.814	3.54
Res 40-0.68	0.70	0.817	2.93
Synthetic Oil	0	0.783	2.6867

3.1.3 Brines

A brine is defined as an aqueous solution containing dissolved salts, such as seawater and saltwater (Speight, 2017). The salinity of a brine depends on the amount of salt dissolved in it (Table 8). Table 8 present types of water with different salt concentrations dissolved in it.

Table 8. Different water salinities (Speight, 2017)

Fresh water (ppt)	Brackish water (ppt)	Saline water (ppt)	Brine (ppt)
<0.5	0.5–30	30–50	>50

For this project, two seawater brines were used, SW0T and SW1/2T. The brines were prepared using deionized (DI) water and appropriate salt concentrations. The brine compositions are given in Table 9.

Table 9. Brine composition for SW, SW0T and SW1/2T

Ion composition	$\boldsymbol{SW}$		$\boldsymbol{SW0T}$		$\boldsymbol{SW\,1/2\,T}$	
	m, g/l	mole/l	m, g/l	mole/l	m, g/l	mole/l
$NaCl$	23.38	0.400	26.79	0.458	23.41	0.401
Na_2SO_4	3.41	0.024	0.00	0.000	1.71	0.012
$LiCl$	0.00	0.000	0.00	0.000	0.51	0.012
$KSCN$	0.00	0.000	0.00	0.000	1.17	0.012
$NaHCO_3$	0.17	0.002	0.17	0.002	0.17	0.002
KCl	0.75	0.010	0.75	0.010	0.75	0.010
$MgCl_2 \cdot 6H_2O$	9.05	0.045	9.05	0.045	9.05	0.045
$CaCl_2 \cdot 2H_2O$	1.91	0.013	1.91	0.013	1.91	0.013

To avoid any sort of precipitation, chloride, carbonate and sulphate salts were mixed separately with certain amount of DI water. The solutions were thereafter mixed together and diluted to 1 liter. The solution was left to stir for the next 30 minutes to 1 hour. After stirring, brines were filtered using 0.22 μm Millipore filter and bottled for further use. Short explanation of the brines is given below:

SW: Synthetic seawater.

SW0T: Synthetic seawater that does not contain any sulphate (SO_4^{2-}) or thiocyanate (SCN^-). Used for chromatography tests.

SW 1/2 T : Synthetic seawater containing equal amounts of sulphate (SO_4^{2-}) and thiocyanate (SCN^-). Also used for chromatography tests.

3.1.4 DI water

Deionized water (DI) is the one that has almost all mineral ions removed. Some of the mineral ions present in DI water are sodium, calcium, iron, copper, chloride and sulfate.[ii] At the University of Stavanger, high quality lab deionizer is used to provide nanopure water, with a total organic content T.O.C <5 ppb and resistivity of 18.2 MΩ cm, ready for our experiments. DI water is used as formation water (FW) in this project.

3.2 Methods

This section briefly describes the methods used in this project.

[ii] https://en.wikipedia.org/wiki/Purified_water#Deionization

3.2.1 Core preparation

All cores were drilled from the same carbonate block with an oversized core bit in the same direction. Thereafter, cores were cut and milled to have approximately the same diameters and lengths.

3.2.2 Set up/Hassler cell preparation

It is paramount to have set up well cleaned before starting up any flooding process. We used Hassler cells (Figure 45) for the flooding tests. The system was primarily cleansed by injection of the following chemicals precisely in this order: n-heptane, DI water and finally N_2 gas. It is also crucial to have the inlet and outlet lines precleaned to as much extent as possible, especially in cases when oil flooding had been performed through those systems before. Next stage was mounting the core into the Hassler cell, followed by applying vacuum to the system and finally building up the pressure.

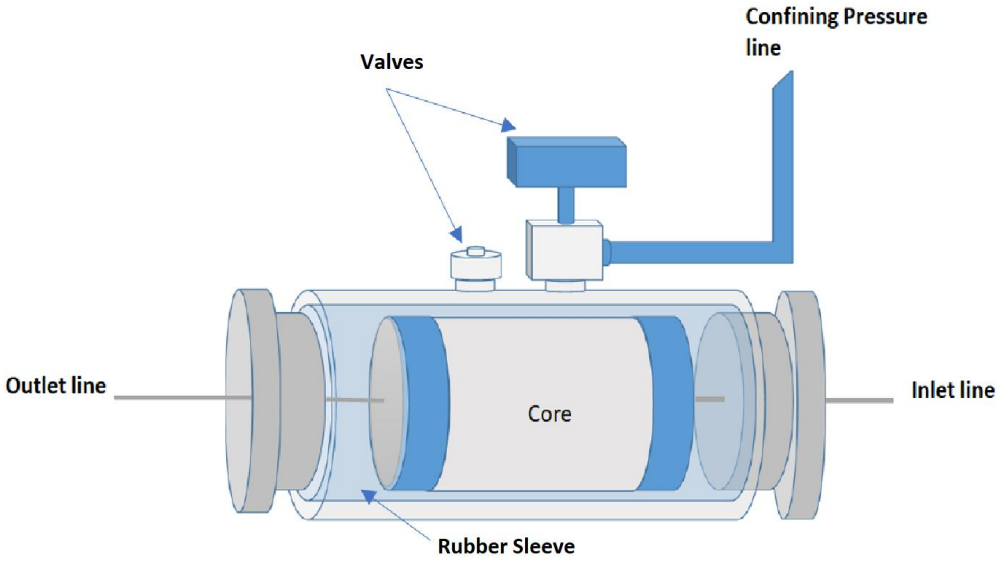

Figure 45. Hassler cell/Core holder (modified after Ingrid Omland BS, 2015)

3.2.3 Core restoration

The main goal of cleaning core material between the tests is removal of organic compounds, such as sulphates, without altering its wettability (Morrow, 1990). This procedure restores the core to initial completely water-wet conditions. Solvent used for cleaning, can have a certain influence on initial wetting of the cores (Shariatpanahi, 2012). For this reason, choosing the right cleaning solvent is of major importance.

To remove dissolvable salts present in the core from before, especially sulphates that can affect wettability, the Hassler cell is used for cleaning (Figure 46). During core

cleaning, a back pressure of 10 bars and confining pressure of 20 bars were applied. The cores were flooded by 250 ml of DI water at a rate of 0.1 ml/min and at room temperature of 23°C. To confirm that all sulphates were removed, a batch test was performed, and effluents were collected. When barium chloride was added to these effluents, no precipitation of barium sulphate ($BaSO_4$) occurred confirming that there were no more sulphates in the cores. The chemical equation for the batch test can be written as follows:

$$Ba^{2+}(aq) + SO_4^{2-}(aq) \leftrightharpoons BaSO_4(s) \tag{3.6}$$

During the flooding process, pressure drop was measured across the cores in order to determine the absolute and effective permeability of the cores. The permeability is calculated using Darcy's law (equation (3.7)), simplified as

$$k = \frac{q\mu L}{A\Delta P} \tag{3.7}$$

Where,

k	Permeability $[mD]$
q	Flow rate $[m^3/s]$
μ	Viscosity $[Pa \cdot s]$
L	core length $[m]$
A	cross sectional area $[m^2]$
ΔP	pressure drop $[Pa]$.

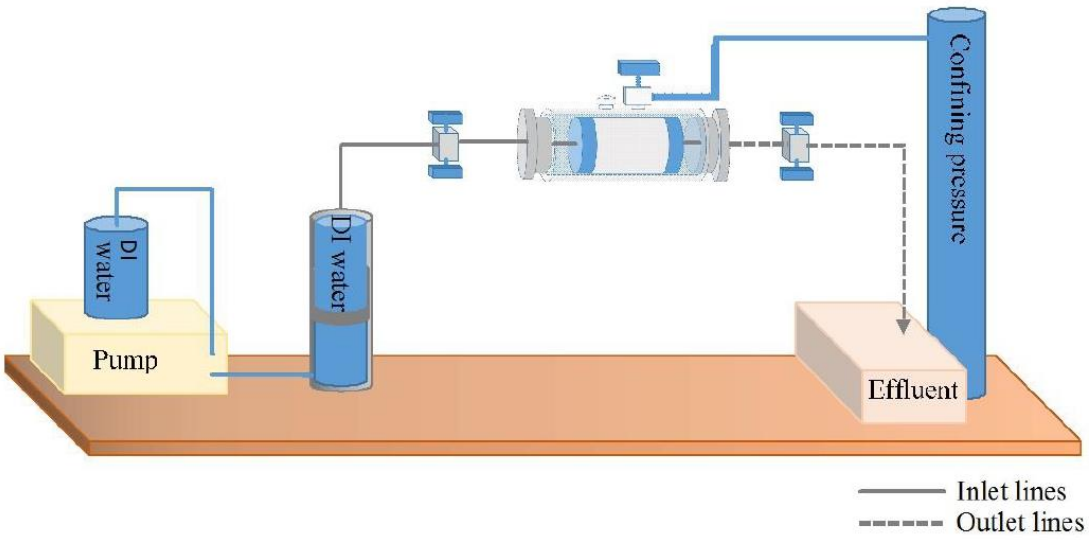

Figure 46. Set up for core cleaning (Hassler cell). (modified after (Omland, 2015))

3.2.4 *Initial water saturation (Swi)*

To establish initial water saturation, the clean and dry core was placed in a vacuum set up connected to the pump as shown in Figure 47.

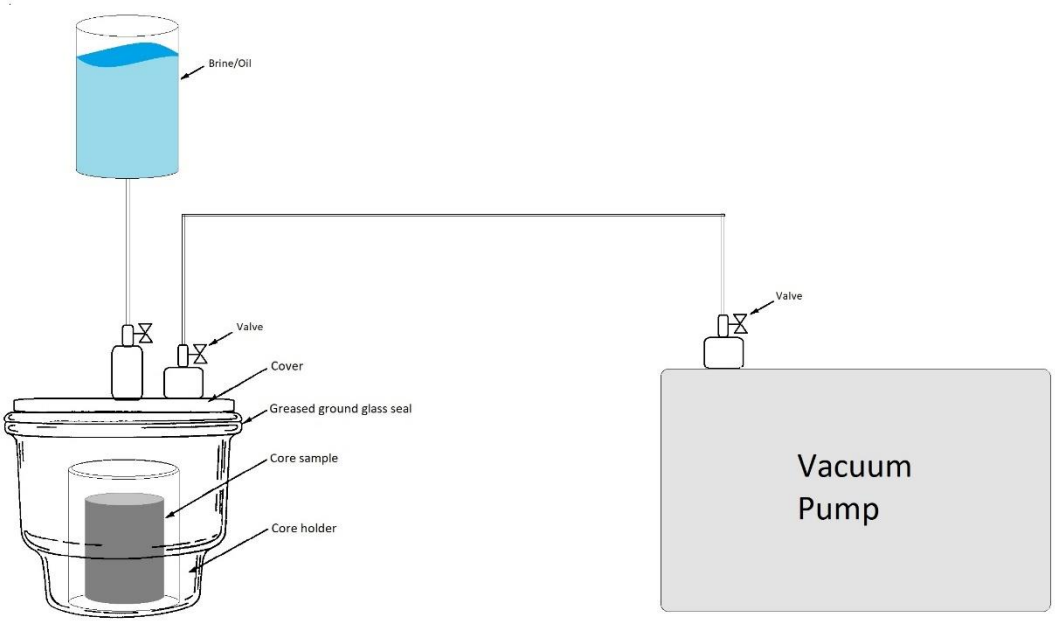

Figure 47. Typical Vacuum Pump Illustration (water/model oil saturation)

The vacuum pump generates a vacuum environment inside the chamber. This permits a complete saturation of the core by DI water. After saturation by DI water, the core was placed for drying in a desiccator (Springer, 2003), Figure 48.

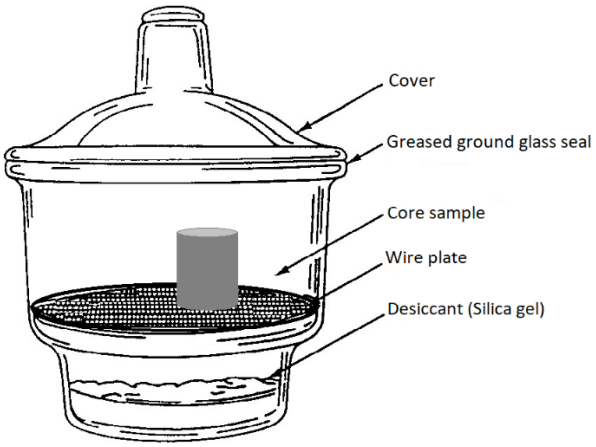

Figure 48. Typical Desiccator Illustration

A desiccator contains silica gel which absorbs water molecules. When the cores were placed in a desiccator containing silica gel, silica absorbed water from the cores and the water saturation of the cores was reduced to the pre-defined value of 20% ($S_{wi} = 20\%$),

i.e. 80% of the DI water from the cores got soaked by silica. The cores were, then, stored in a sealed container and equilibrated for 72 hours to secure an even ion distribution. This procedure is in line with the procedure described by Springer (2003).

3.2.5 Oil saturation/Oil flooding

The two reference, water-wet cores were, then, placed again in vacuum pump to be fully saturated with model oil. The two mixed-wet cores were after reaching Swi, also placed in a vacuum chamber, connected to a vacuum pump, to be fully saturated by oil *RES 40-0.15*. When saturated, each core was individually mounted in Hassler cell for further oil flooding (Figure 49). The core was, then, flooded by 2 PVs of this oil in each direction at the rate of 0.026 ml/min at room temperature, with confining and back pressures of 20 bars and 10 bars, respectively. Afterwards, the core was flooded by 1 PV of synthetic model oil and aged for 3 days in the Hassler cell at 23°C.

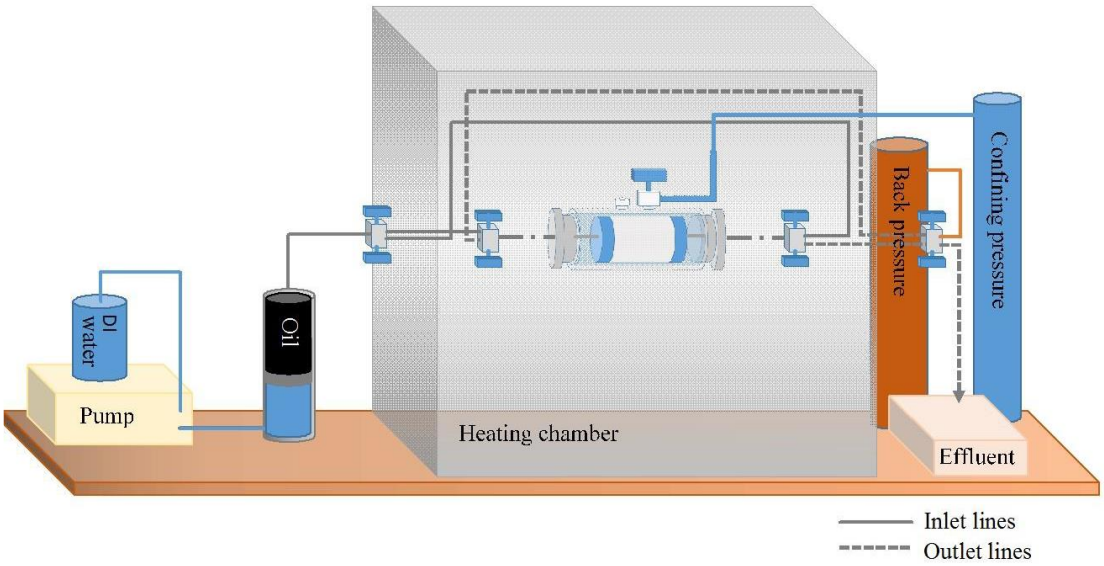

Figure 49. Oil flooding set up (modified after (Omland, 2015))

3.2.6 Core Aging

The aging process happened while the cores were placed in Hassler cells at ambient temperature of 23°C for a period of 3 days.

3.2.7 Oil recovery by forced imbibition (FI)

The forced imbibition or forced displacement was performed using Hassler cell set up illustrated in Figure 49. Test was performed at room temperature conditions (23 °C). After establishing initial conditions, the cores undergone forced imbibition test. Cores

were flooded by formation water (DI water). The amount of oil expelled from the core over the flooding period was determined based on graded burette. Obtained values can be seen in Appendix B.9. Table 10 summarizes flow rates for each core during forced imbibition flooding.

Table 10. The pore volume and injection rates for core SK-R1, SK-R2, SK-C3 and SK-C6 during the forced imbibition.

Core	*PV (ml)*	*1PV/d (ml/min)*	*4PV/d (ml/min)*
SK-R1	*37.53*	*0.0260*	*0.104*
SK-R2	*39.17*	*0.0272*	*0.109*
SK-C3	*37.99*	*0.0263*	*0.105*
SK-C6	*39.91*	*0.0277*	*0.111*

3.2.8 Oil recovery by spontaneous imbibition (SI)

The spontaneous imbibition was performed using Amott glass cells (Figure 21) at room temperatures (23 °C). The cores undergone procedure as described in section 2.3.3. The chalk core was placed in glass cell and cell was filled by imbibing brine, in this case DI water. The oil produced during the test was recorded over the time. Obtained values can be found in Appendix B.8.

3.3 Analytic methods

This section briefly describes the analytical methods performed as part of the project.

3.3.1 pH measurements

To measure pH of the brines, the pH meter seven compact™ from Mettler Toledo was used. To ensure accuracy, the measurements were repeated until three same pH values were obtained. The electrode used was semi micro-pH and all measurements were performed at room temperature of 23°C. An error in measurements was in range ± 0.02.

3.3.2 Density measurements

The densities of the brines and oils were measured using the Anton Parr DMA4500 Density Meter at room temperature of 23°C. Initially the densitometer was precleaned with White Spirit, Acetone and DI water. Thereafter, a certain amount of brine or oil sample was injected into the tube using syringe and the density was measured. To

ensure accuracy, the measurements were repeated several times. An error in measurements was in range ± 0.001 g/cm^3.

3.3.3 Viscosity measurements

The viscosity of oil was determined using the rotational rheometer Physica MCR 302 from Anton Paar. A certain amount of the oil sample was placed on a metal plate, and the rheometer was set to measuring position with the plates close to each other with the fluid sample in between the plates. To ensure accuracy, the plates were precleaned with White Spirit, Acetone and DI water before each measurement. Also, rheometer was calibrated before every measurement by using function "Zero Gap". The viscosity of oil was determined through the shear stress - shear rate relationship giving the curve with 7 points. The measurement for each sample was repeated until three matching curves were obtained. An error in measurements was in range ± 0.0005 Pa.s. Plot of viscosity measurements can be found in section 4.1.

3.3.4 Acid and Base number determination

To determine AN and BN values of oil samples we used a Mettler Toledo T55 auto titrator with an internal standard developed by Fan and Buckley (Fan & Buckley, 2007). The standards are modified versions of ASTM D2896 for base number, and ASTM D664 for acid number titration. Initially the instrument performs a blank test as a reference during potentiometric titration of oil samples, where the measurement of electrical potential is converted to equivalent acid and base numbers. Each measurement requires 1 ml of titration solvent and 1 ml of spiking solution, detailed description is given in Appendix A. To secure the test repeatability, a Mettler Toledo weight instrument with accuracy down to the fourth decimal was used. Calibration and blank measurements were made regularly to compensate for changes in electrode properties with time, when exposed to air. All measurements were repeated several times to obtain the correct value. An error in measurements was in range ± 0.02.

3.3.5 Ion Chromatography

The SW0T brine (seawater with no tracer or sulphate) was injected into the core in the same direction as FI flooding at a rate of 0.2 ml/min. After establishing dynamic equilibrium, the core was subjected to flooding by seawater brine SW1/2T, containing equal amounts of tracer (thiocyanate) and sulphate, to carry out the CWT analysis. The

effluent brine samples were collected frequently during the chromatographic wettability test. Samples were, then, diluted 1000 times with DI water using the trilution™ LH system from a Gilson GX-271 liquid handler. The diluted samples were filtered and placed into small sample glasses for further analyses. To obtain chemical composition of the effluent samples, we placed three different containers with sample bottles within the DIONEX ICS-5000+ instrument and ran the program. The software controlling the chromatograph uses retention time of 20 mins, which is the travel time through the columns. It plots a graph of conductivity versus retention time where the area under each peak, that represents an ion, corresponds to its relative concentration. The external ion method was used as a basis for the calculation of ion concentrations of the effluents. In the he external standard method, the standards are run separately, and concentrations are determined. The absolute analyte response is plotted against the analyte concentration. In such a way, the calibration curve is created.

3.3.6 Interfacial Tension (IFT) measurements

Interfacial tension measurements were performed by tensiometer as shown in Figure 50.

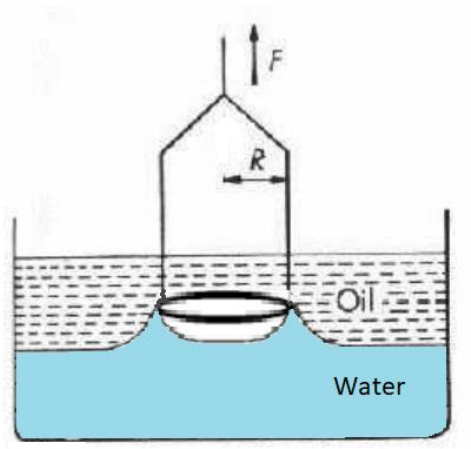

Figure 50. Interfacial tension in water/oil system[iii]

Initially there is only water in the container (step 1, figure 51) and a ring is placed on the surface of water (step 2, figure 51). There is no force acting on the ring. Then, we sink the ring which causes a small negative force (steps 3 and 4, figure 51). Afterwards, a small amount of oil is poured carefully on top of water. When the ring breaks through the surface, there is a small positive force due to the ring supporting wires (step 5, figure

[iii] http://www.mastrad.com/tsd1.htm

51). While starting to lift the ring through the surface, the force increases until it reaches its maximum (steps 6 and 7, figure 51). After the maximum there is a small decrease in the force until the lamella breaks (step 8, figure 51). The whole process is illustrated in Figure 51.

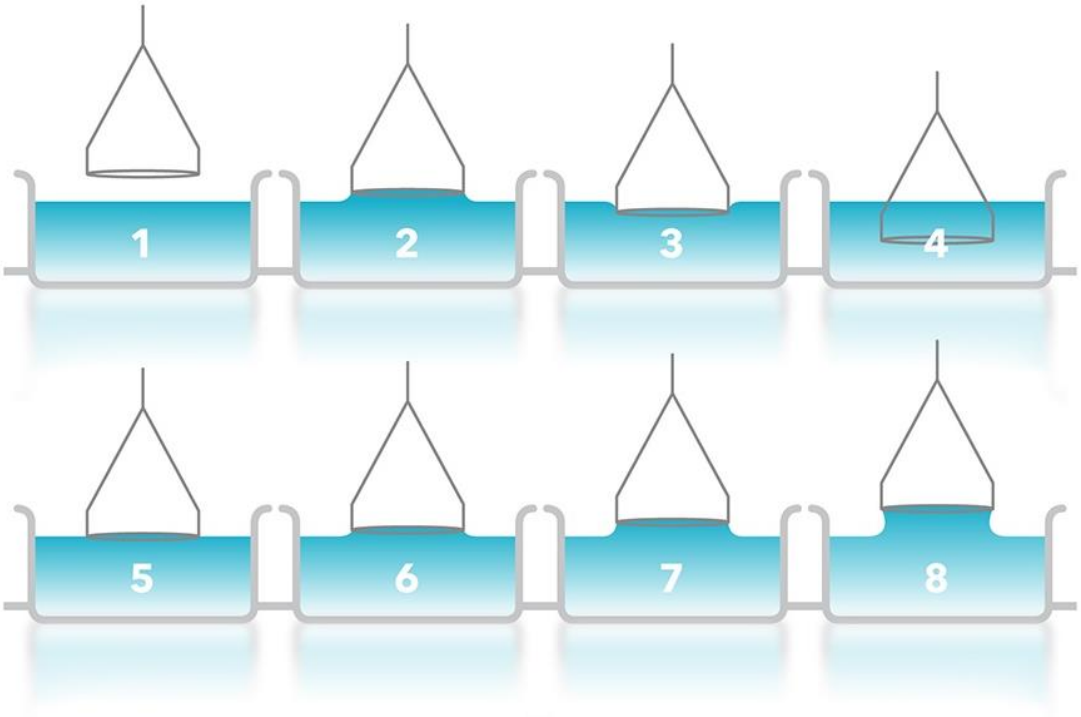

Figure 51. Step by step interfacial tension measurement in water (white)/oil (blue) system (BS, 2018)

As carried out in all previous measurements, this process was also repeated several times to obtain correct values. An error in measurements was in range ± 0.

3.4 Modeling tool

Sendra (2008) is a two-phase core flooding simulator designed to simulate a certain number of experiments. This software tool (Figure 52) covers various experiments including unsteady-state and steady-state flow, single- and multi-speed centrifuge and porous plate experiments. In this project the unsteady-state flow experiment is modeled at constant rate in the horizontal direction. This experiment includes imbibition and drainage processes as unsteady state waterflooding processes. Sendra is designed to give analysis on relative permeability, using Corey (1954) parameter and capillary pressure, using Skjæveland et al. (2000) parameter, from experimental data through history matching approach. The main input data are presented in Figure 52.

For this study we used this program to confirm the already-designed relative permeability curves and see if relative permeability curves change with change in the wetting properties of the system.

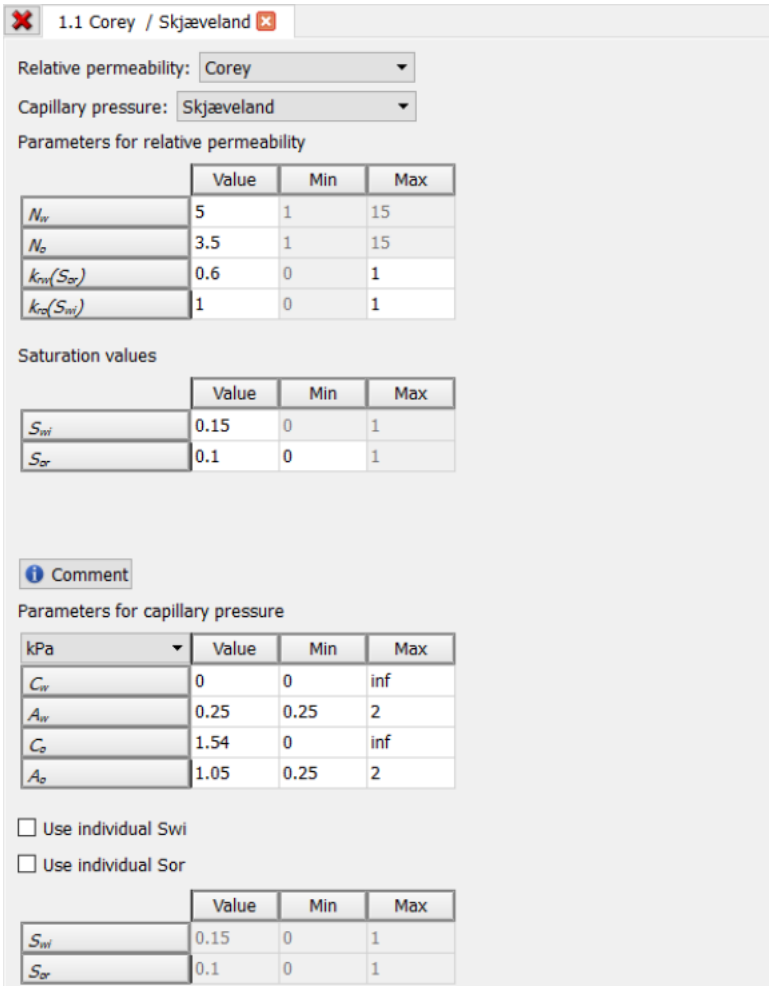

Figure 52. Sendra modeling tool. Input parameters required for simulation.

4. Obtained results and discussion

The results are based on two reference water-wet cores (SK-R1, SK-R2) and two cores with mixed wettability (SK-C3, SK-C6) with initial water saturations of S_{wi}=20%. The obtained results are, then, compared to the cores SK-C1, SK-C2, SK-C4 and SK-C5 tested by two other students from smart water group, Harestad (2019) and Wathne (2019). The results presented in the following sections are based on the effect of the wetting state of the cores on properties, such as permeability, of the reservoir system, by analyzing effluent samples. The change in water wetness of all four chalk cores was evaluated by forced displacement, spontaneous imbibition and chromatographic wettability tests.

4.1 Synthetic model oil determination

The idea was to generate a synthetic oil that does not contain polar components so that it cannot influence the wettability of the cores when the flooding process is introduced. Basically, this oil was prepared to have the same viscosity as the crude oil RES40 (0.0027 Pa.s). The results of viscosity measurements generated by Anton Paar rheometer are illustrated in Figure 53. The values are presented in Appendix B.3.

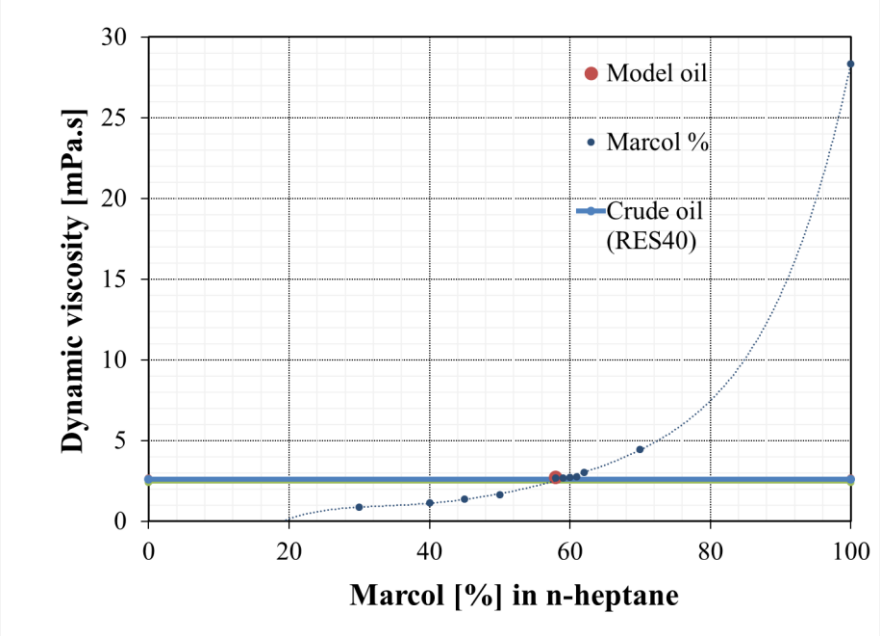

Figure 53. Determination of correct composition of model oil based on viscosity measurements. Viscosity of synthetic oil against percentage of Marcol in the synthetic oil. The dotted line represents a synthetic oil with increasing amount of Marcol.

As it is clearly observed from Figure 53, the viscosity of the model oil increased with increase in Marcol oil wt%. The viscosity of generated model oil (58 wt% Marcol 82 and 48 wt% n-Heptane) was determined to be at intersection with crude oil measurements, at 0.00269 (Pa.s) and is used in this project.

4.2 Absolute permeability determination

To remove initially present sulphate and estimate the absolute permeability of chalk cores, the cores were flooded with DI water. The water flooding process was performed at three different flow rates: 0.05, 0.15 and 0.1 ml/min. Corresponding pressure drop was recorded for absolute permeability determination. These values were used as a base for obtaining end point relative permeabilities implemented in modeling tool. To make sure that all sulphate had been removed, we did a batch test by adding barium chloride salt to the effluent. As the effluent became clear with time, it was concluded that all the sulphate had been removed. Figure 54, 55 and 56 illustrates the pressure drop over time for two reference water-wet cores and two mixed-wet cores.

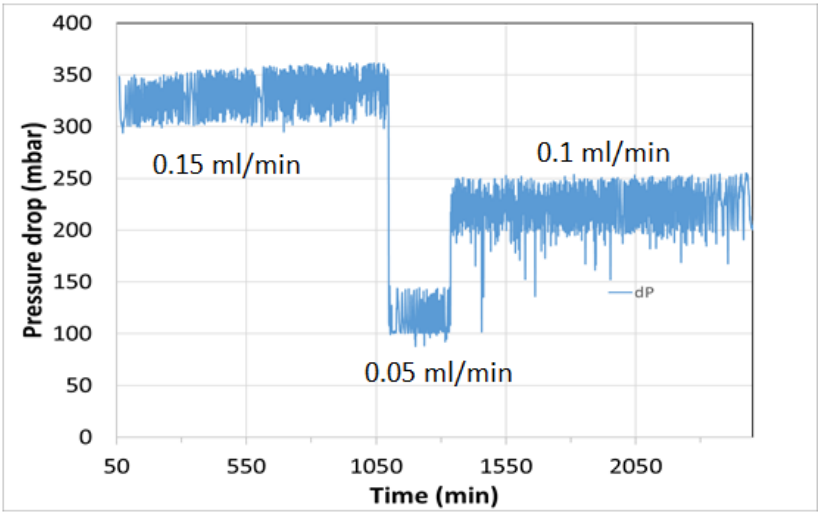

Figure 54. The pressure drop vs. time for the 100% DI saturated reference chalk core SK-R1 when flooded at different rates.

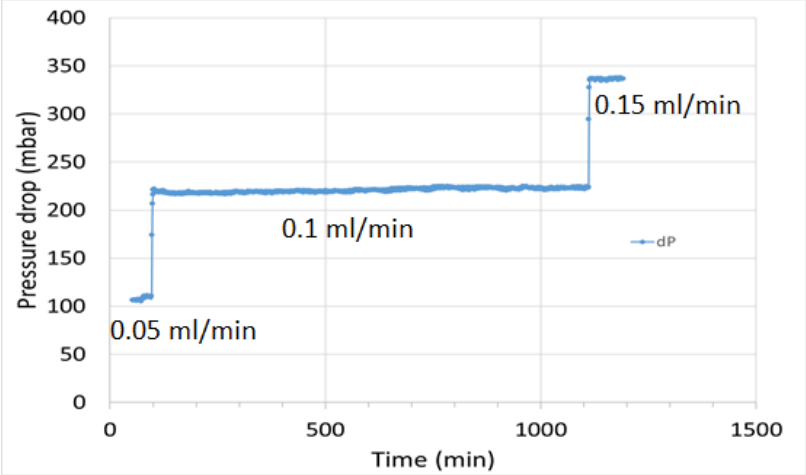

Figure 55. The pressure drop vs. time for the 100% DI saturated reference chalk core SK-R2 when flooded at different rates. Rates are 0.05, 0.1 and 0.15 ml/min.

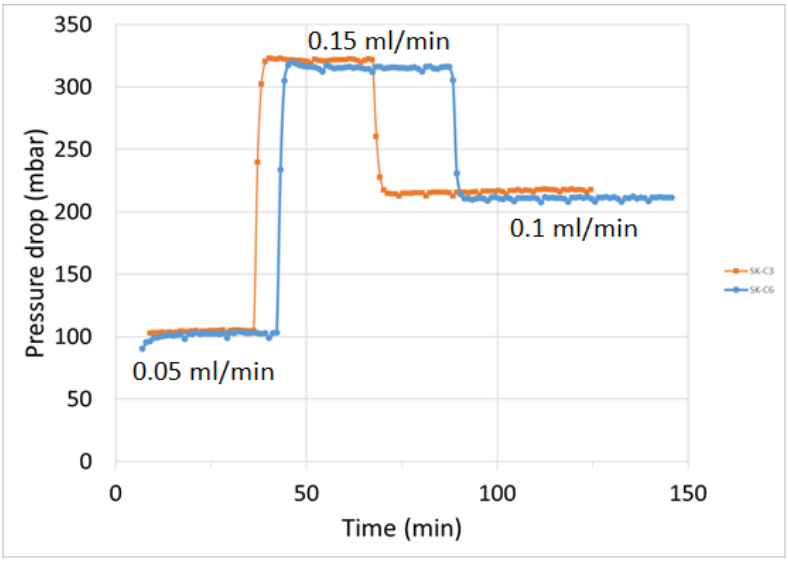

Figure 56. The pressure drop vs. time for the 100% DI saturated chalk cores SK-C3 and SK-C6 when flooded at different rates. Rates are 0.05, 0.1 and 0.15 ml/min.

As it can be observed from Figure 56, mixed-wet cores SK-C3 and SK-C6 behaved quite similar. There is no big difference between their pressure drop curves when changing the flow rates.

The absolute permeability of all four cores was calculated using a stable pressure drop (using equations (2.11), (2.12) and (2.13)). Absolute permeabilities of 4.0187 mD for core SK-R1, 4.0932 mD for SK-R2 and 4.2514 mD for SK-C3 were obtained. The exact value of absolute permeability for core SK-C6 was not calculated as we did not take it further for the simulation process. Hence, it can be easily observed that there is no significant difference between the absolute permeability values for these cores.

4.2.1 Comparation with cores tested by other two students

Figure 57 shows the pressure drop with time for the SK cores, SK-C1, SK-C2, SK-C4 and SK-C5, tested by Harestad (2019) and Wathne (2019). It can be observed that there is no major difference between these cores and the cores used in this study and discussed in section 4.2. The absolute permeability of these cores was also around 4 mD.

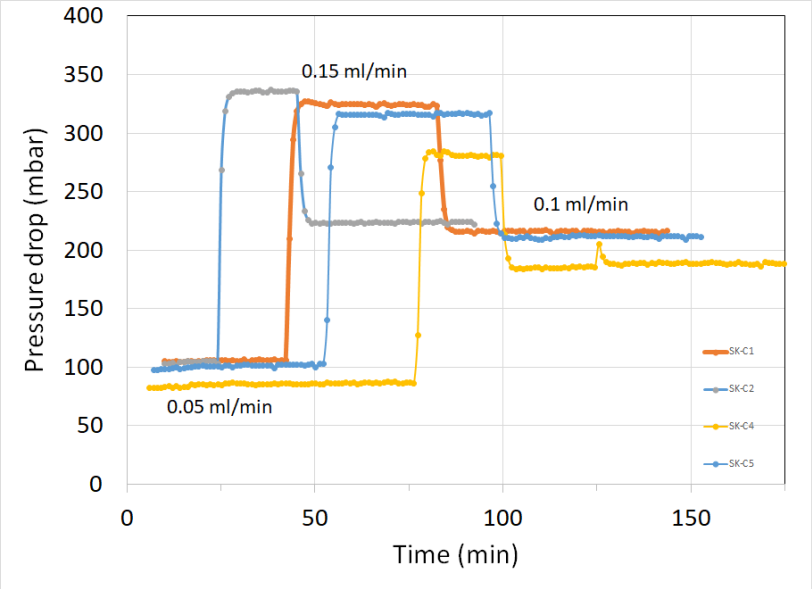

Figure 57. Pressure drop across the chalk core sample for 100% DI saturated cores SK-C1, SK-C2, SK-C4 and SK-C5 when flooded at different rates. Rates are 0.05, 0.1 and 0.15 ml/min.

4.3 Forced Displacement at 23°C for water-wet cores

The water-wet reference cores SK-R1 and SK-R2 were used to confirm the quite good reproducibility of SK chalk previously studied by Hopkins (Hopkins, 2016). Cores were restored with S_{wi}=0.2 (DI water) and saturates with model oil. The strong water-wet behavior of these reference cores was observed by performing forced displacement, i.e. viscous flooding using DI water as injection brine. Both cores were initially flooded by 1 PV of model oil, as described in section 3.2.5, and thereafter cores undergone formation water (FW) viscous flooding. During the viscous flooding cores were flooded by 1PV/d in first stage. At the end the injection rate was increased to 4 PV/d to verify the amount of mobile residual oil.

Figure 58 shows that 68% of OOIP in core SK-R1 was recovered in first seven days when flooded by 1PV/d (0.026 ml/min) and 69% of OOIP was recovered when the rate was increased four times (4PV/d). It was concluded that this reference core shows very high oil recovery. The quite high oil recovery and the piston-like shape of the recovery curve indicate strong capillary forces are present in a system. Hence, the process is controlled by capillary but not viscous forces.

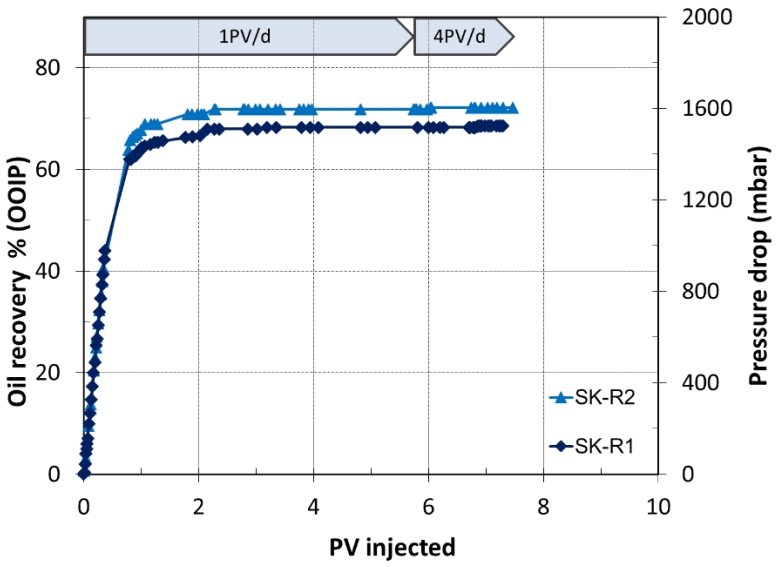

Figure 58. The oil recovery over time for the cores SK-R1 and SK-R2 during formation water flooding of 1PV/d and 4PV/d. Recovery plateau for SK-R cores reached at 2.5 PV and ΔP stabilized after 5-6 PV.

The second reference core SK-R2 behaved quite similarly, as both cores were treated in the same way. In the first stage when the core was flooded by 1PV/d (0.027 m/min), 72% of OOIP in core SK-R2 was produced while during the second stage flooded by

4PV/d the oil recovery was enhanced up to 72% of OOIP, showing noteworthy effect in oil recovery, as it can be seen from Figure 58. So, it was concluded that we obtained a quite good reproducibility from both strongly water-wet reference cores.

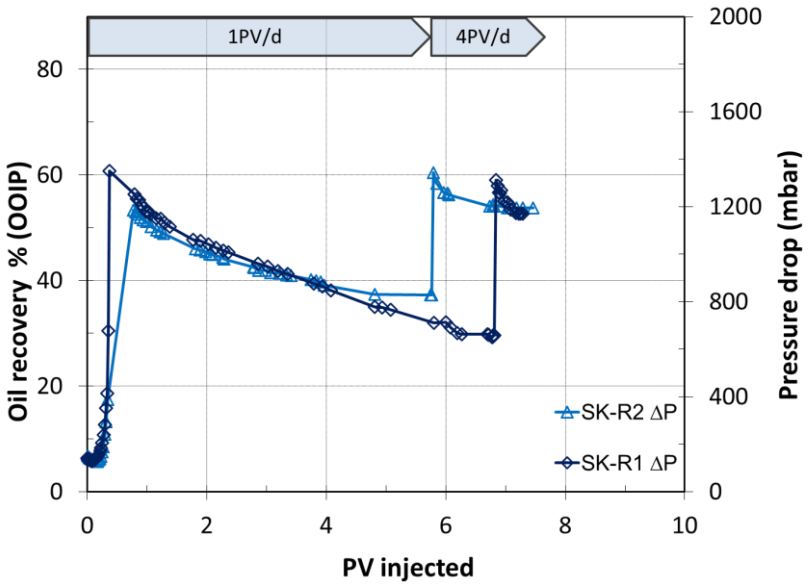

Figure 59. The pressure drop over time for the cores SK-R1 and SK-R2 during formation water flooding of 1PV/d and 4PV/d. Recovery plateau for SK-R cores reached at 2.5 PV and ΔP stabilized after 5-6 PV.

On the other hand, these two cores show slightly different pressure drop behavior (Figure 59). For SK-R1, the pressure drop increased sharply during first day of flooding as capillary forces are driving the process until the amount of formation water injected through the core was 0.4 PV. It reached its maximum at 1350 mbar and then gradually decreased to approximately 660 mbar, due to less capillary forces present, where a stable oil recovery plateau was established. After the flow rate was increased to 4 PV/d, the pressure drop again increased sharply to a maximum of 1312 mbar before decreasing again to 650 mbar where it got stabilized.

The pressure drop in SK-R2 also increased sharply during the first 0.8 PV/d to a maximum of 1186 mbar. According to Strand (2008a), if in the start of flooding process, the pressure drop curve starts decreasing immediately from its highest value, the process is driven by viscous forces. The Figure 59 shows sharp pressure drop build up when flooding has started. This information confirms that the system most likely is effected by capillary forces (Strand, Puntervold, & Austad, 2008a). Thereafter, the pressure decreased to 830 mbar and got stabilized. After increasing the flow rate to 4 PV/d, the sharp pressure build up was observed reaching the maximum of 1342 mbar,

driven by viscous forces. As can be seen from Figure 59, pressure drop curve of SK-R2 behaves similar to that of SK-R1 and decreases until it gets stabilized at 1194 mbar after 7.46 days in total. From the Figure 59 we can also conclude that pressure drop, and flow rate are dependent on each other, i.e. when increased flow rate, pressure drop increases. Additionally, the differences in pressure drop behavior can be explained by differences in tested core samples, i.e. their petrophysical properties.

4.4 Forced displacement of core with reduced water wetness

Next, we observed the effect of forced displacement on the mixed-wet cores, SK-C3 and SK-C6. The procedure for cores SK-C3 and SK-C6 was the same and was performed as follows: The cores were initially water saturated to $S_{wi} = 0.2$ and then saturated and flooded by 4 PV of a crude oil RES 40-0.15 with 2 PVs flooded in each direction. After flooding by crude oil, cores were aged in crude oil for next 3 days. During the crude oil displacement by 5 PV model oil, the effluent samples were collected to obtain the certainty that model oil "cleaned" the core from crude oil, since it was planned to have the model oil in the core at the end of this procedure shown in Figure 60.

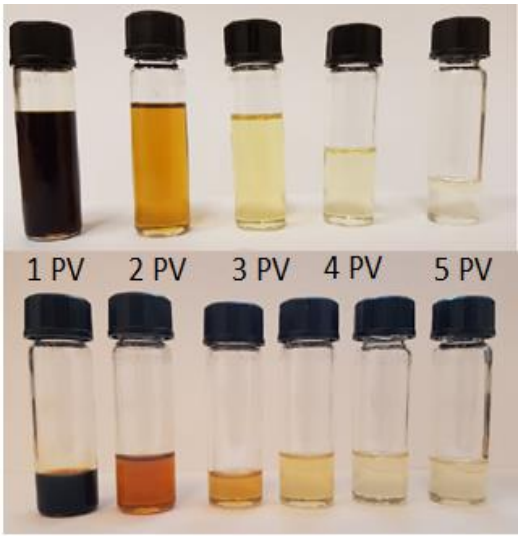

Figure 60. Core flooding samples for SK-C3 (upper) and SK-C6 (lower)

The procedure for oil recovery for these two mixed-wet cores was slightly different. The SK-C3 was flooded by DI water in the same way as reference cores by performing forced displacement. The treatment of core SK-C6 was a bit different and is discussed in section 4.6.

The first part of oil displacement by forced displacement through core SK-C3 is divided into two stages: flooding at the rates of 1PV/d (0.026 ml/min) and 4 PV/d. When the core was waterflooded by 1PV/d of formation water, we observed a recovery of 67% of OOIP after 4 days and during flooding with 4PV/d flow rate, the recovery increased to 75% of OOIP after 5 days. The results are presented in Figure 61.

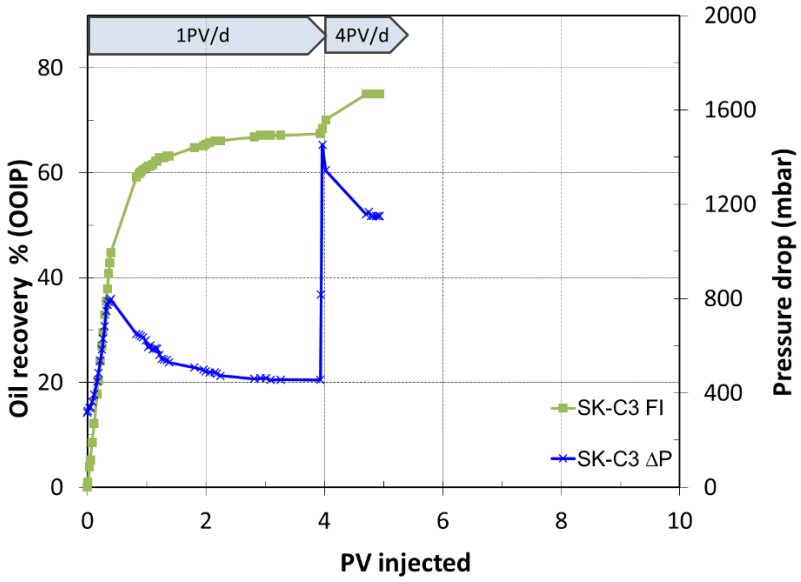

Figure 61. The pressure drop and oil recovery over time for the core SK-C3 during formation water flooding of 1PV/d and 4PV/d. Recovery plateau for SK-C3 core reached at 2.4 PV and ΔP stabilized after 4 PV.

The high recovery and the piston-like shape of the recovery curve imply the effect of strong capillary forces, but also indicate an effect similar to a water-wet core. The pressure drop curve gives the information about forces dominant in this system. From Figure 61 it is observed that when the flooding process started, a gradually increase in ΔP was observed reaching maximum at 0.4 PV injected. With the pressure drop increase, forces were being "consumed" until the pressure drop reached its maximum of 786 mbar. Thereafter, we observe a drop in ΔP curve as fewer capillary forces were now present, until it reached a stable value of 455 mbar after almost four days of waterflooding. At this point, only water was produced so we increased the flow rate expecting more oil to be produced, which should be influenced by viscous forces this time. The increase in rate lead to an increased pressure drop up to 1453 mbar, followed by a decrease again to 1150 mbar after five days where it got stabilized. Also, there were no more driving forces that would trigger further mechanisms leading to an even enhanced oil recovery, and hence, the maximum oil production had been received.

Finally, we see that all three cases have quite similar pressure drop behavior and the mixed-wet core, obtaining a good oil recovery, indicates a water-wet core-like behavior.

4.4.1 Comparison with cores of different wettability

To show the effect of polar components on wettability and oil recovery, we used results from cores SK-C1 and SK-C2, flooded by different crude oils and tests performed by

Harestad (2019) and Wathne (2019), for further comparison. As we can clearly observe from Figure 63, all cores show similar behavior. The oil recovery by forced displacement (Figure 62) appears to be the highest in the core SK-C3, as expected due to the lowest AN value of oil in this case. Although cores SK-C1 and SK-C2 are flooded by oils with higher ANs, their recovery is quite close to SK-C3 as all of them are water-wet state as claimed to be true using chromatographic wettability tests given in section 4.6. The pressure drop curves (Figure 63) match more-or-less as the driving mechanism for these cores is the same as in the previously discussed cores in section 4.3. The detailed results obtained during forced displacement can be found in Appendix B.9. Table 11 summarizes oil recovery for all cores after flooding 1PV/d and 4PV/d.

Table 11. The oil recovery for all cores after flooding 1PV/d and 4PV/d.

	SK-R1	*SK-R2*	*SK-C1*	*SK-C2*	*SK-C3*
$\%OOIP$ (1 PV)	68.45	71.80	73.03	67.80	67.45
$\%OOIP$ (4 PV)	68.61	72.12	74.33	69.40	75.02

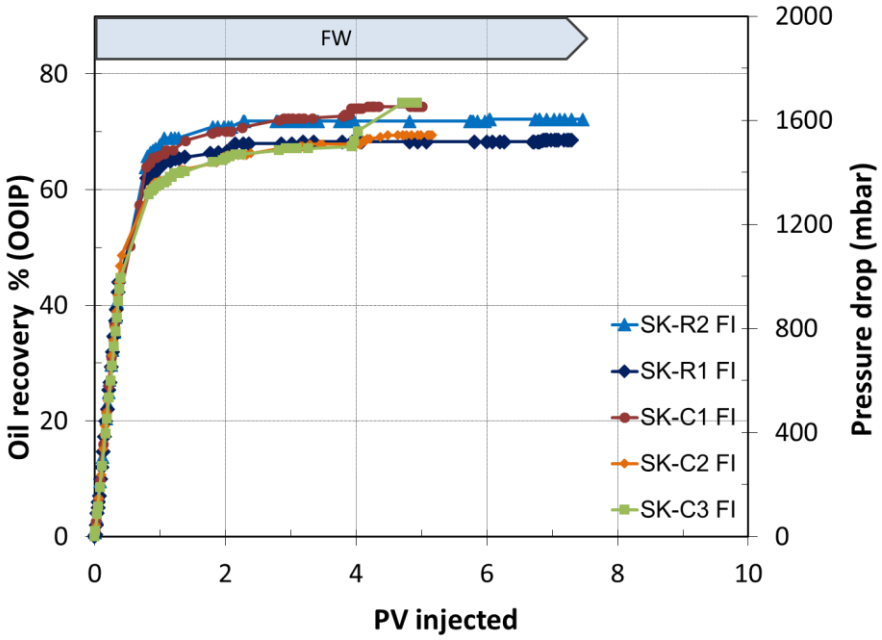

Figure 62. The oil recovery over the time for the core SK-R1, SK-R2, SK-C1 , SK-C2 and SK-C3 during formation water flooding of 1PV/d and 4PV/d. Tests on cores SK-C1 and SK-C2 are performed by Harestad (2019) and Wathne (2019) but with the same procedure as the other cores in this figure.

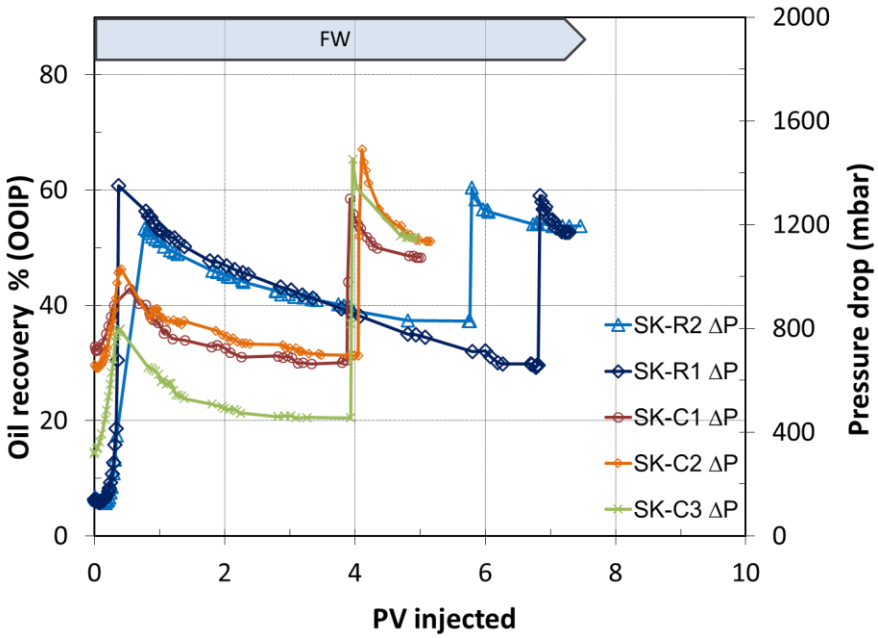

Figure 63. The pressure drop over the time for the core SK-R1, SK-R2, SK-C1, SK-C2 and SK-C3 during formation water flooding of 1PV/d and 4PV/d. Tests on cores SK-C1 and SK-C2 are performed by other students but with the same procedure as the other cores in this figure.

4.5 Spontaneous Imbibition by DI water at 23°C for water-wet cores and core with different wettability

After forced displacement process was finished, the same cores were cleaned with 4 PVs of n-heptane and 5 PVs of DI water, dried at 90°C, and saturated by formation water to S_{wi}=20%. Thereafter, cores were saturated up to 100% by model oil. Prepared cores were used in spontaneous imbibition test performed at room temperature by formation water (DI water). During this test the core SK-R1 produced 66.86% of OOIP during 2.8 days when the production had reached its plateau, as shown in Figure 64. The SK-R2 showed even higher oil recovery of 74.82% for the same time spent in the imbibition cell. Core SK-C3 showed a bit lower recovery. It took 5 days for capillary forces to push the maximum oil out of core to give a recovery of 63.44% of OOIP. Obtained results are illustrated in Figure 64.

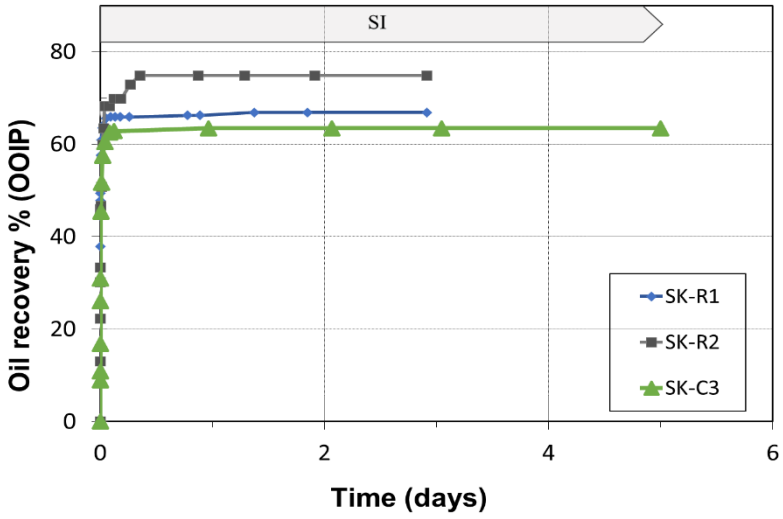

Figure 64. Oil recovery by spontaneous imbibition at room temperature of 23°C for core SK-R1, SK-R2 and SK-C3.

The oil production in SI test was driven by strong positive capillary forces. Additionally, to observe imbibition the capillary pressure, P_c, needs to have a positive value. The components that controls the P_c are interfacial tension and wettability given by the equation (2.10). Based on IFT data, discussed in section 4.9, the model oil used for flooding the core SK-R1 has a value of 41 mN/m which is quite high. Consequently, cores will show good oil recovery.

It is also important to mention that the core treated with a crude oil with AN 0.15 mgKOH/g oil behaved very water-wet, almost to the same level as the completely water-wet cores. This is according to theory saying that low AN gives small changes in wettability, and that water wetness is more reduced with higher AN (Standnes & Austad, 2000).

4.5.1 Comparison with cores of different wettability

The two cores SK-C1 and SK-C2 tested by Wathne (2019) and Harestad (2019) were also subjected to the same preparation and cleaning procedure but treated with crude oils with higher acid numbers for a variation in wettability and exposed to SI test. SK-C1 was treated with an oil with AN=0.68 mgKOH/g, and SK-C2 with an oil with AN=0.34 mgKOH/g, thus core SK-C1 is expected to behave less water-wet. For 12 days in the SI cell, the core SK-C1 produced 51.29 % of OOIP while SK-C2 produced 57.6% of OOIP during six days of spontaneous imbibition. Figure 65 illustrates the oil recovery for the five chalk cores after SI test was performed.

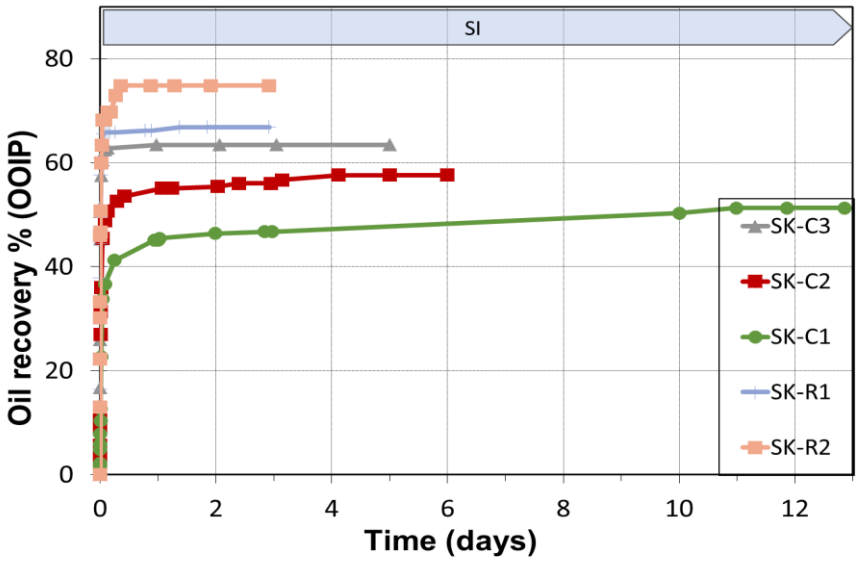

Figure 65.The spontaneous imbibition performed at room temperature of 23°C for cores SK-R1, SK-R2, SK-C1, SK-C2 and SK-C3

The reference core SK-R2 showed the highest oil recovery, while the SK-C1 had the lowest due to highest AN value of crude oil. The higher the AN, the less the capillary forces present and hence less is the water-wetness of a system. As a reminder, the cores SK-C1 and SK-C2 were, in previous steps, flooded by crude oils with AN=0.68 and AN=0.34 mgKOH/g. Consequently, the results are placed as expected according to previously published literature. Table 12 summarizes oil recovery by spontaneous imbibition for cores SK-R1, SK-R2, SK-C1, SK-C2 and SK-C3.

Table 12. The oil recovery by spontaneous imbibition for SK-R1, SK-R2, SK-C1, SK-C2 and SK-C3.

	SK-R1	*SK-R2*	*SK-C1*	*SK-C2*	*SK-C3*
%OOIP	66.86	74.82	51.29	57.61	63.43

4.6 Total recovery (SI+FI) for core the core with reduced water wetness

The only difference with SK-C6 is the order in which the procedure was performed on the core sample. Right after flooding and aging process described in section 4.3, the core was subjected to SI test. As observed in Figure 66, the SK-C6 showed a rapid and a high recovery oil.

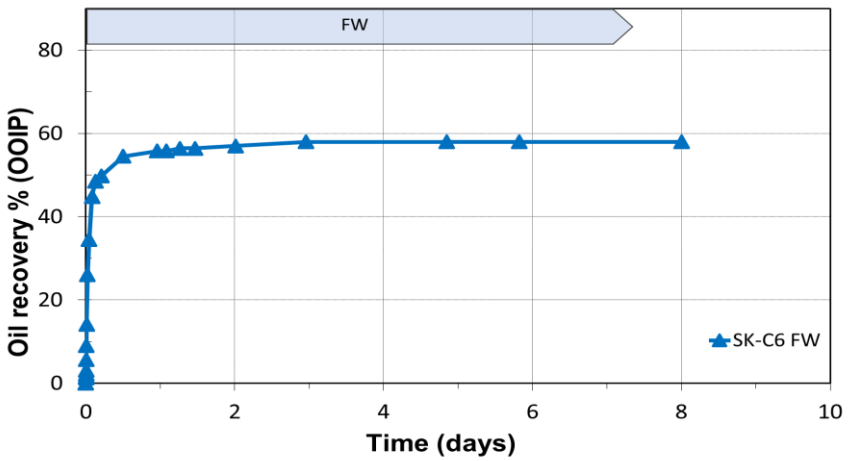

Figure 66. The spontaneous imbibition test performed at room temperature of 23°C for core SK-C6.

Evidently, the core produced 57.94% of OOIP in a duration of 8 days, where the stable plateau was established after just 3 days. Subsequently, the core was placed in a Hassler cell for upcoming waterflooding process. The results of the waterflooding are illustrated in Figure 67.

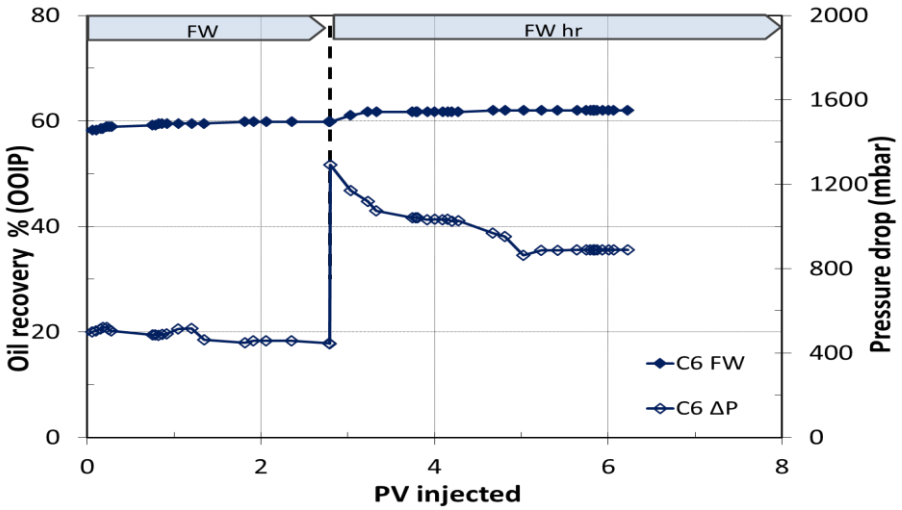

Figure 67. The forced imbibition, FI, (displacement) by formation water at room temperature of 23°C for core SK-C6 when flooded by 1PV/d and 4PV/d (FW hr).

Note that the oil recovery starts at 57.94 %OOIP recovered by spontaneous imbibition. From Figure 67, we observe that there was just a small increase in oil production during the first three days of flooding at 0.028 ml/min flow rate, giving a value of 59.82% of OOIP. Quite similar situation was observed when the pump rate was increased to 0.110 ml/min. The oil produced at a higher rate during three days was 0.7 ml.

The pressure drop data were drastically different from the previously discussed cases. ΔP curve slightly decreased with some small fluctuations in the beginning. This can be

explained as a result of “exhausted” capillary forces which have been used quite a lot during the SI test. The pressure drop was stabilized at 446 mbar after 3 days of waterflooding. Again, after increasing pump rate, the ΔP jumps to a maximum of 1292 mbar before decreasing to 888 mbar after 6 days where it stabilized, and the oil production ended. The total oil recovery for this core is presented in Figure 68.

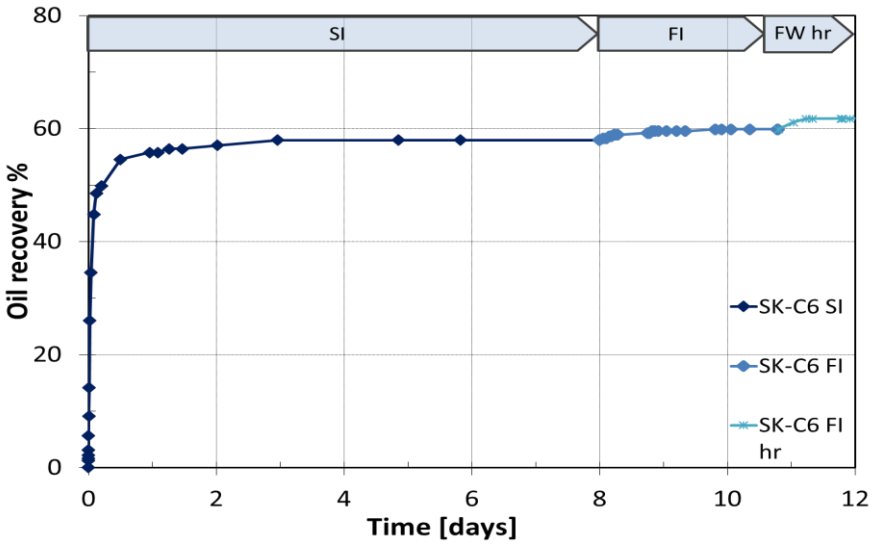

Figure 68. The total oil recovery after performed SI, FI and FW hr on chalk core SK-C6 at room temperature of 23°C.

4.6.1 Comparison with cores of different wettability

Comparing the results gathered from SI test for the cores SK-C4 and SK-C5, we can conclude that these two produced less oil than the core SK-C6 (Figure 69), especially core SK-C4 that produced 5.84% of OOIP. This test provides information about wetting state of the chalk cores. Consequently, SK-C4 is the least water-wet, SK-C5 is intermediate water-wet while SK-C6 is strongly water-wet. The Figure 69 is important because it explains differences in initial wetting state of chalk cores.

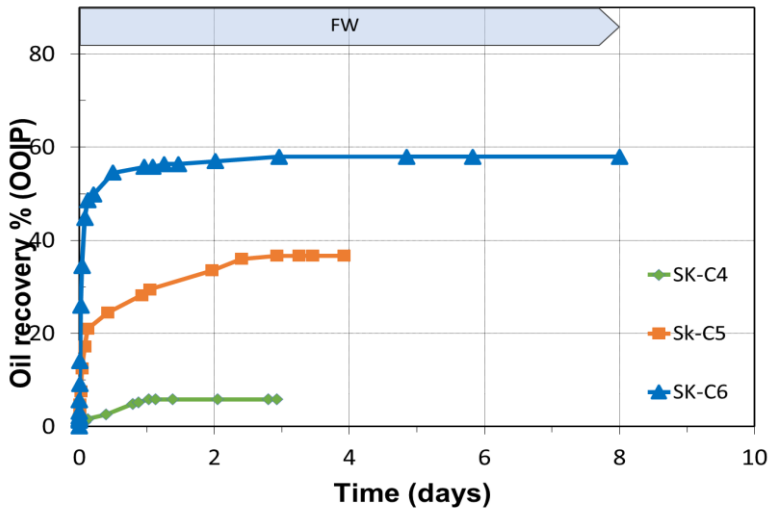

Figure 69. The spontaneous imbibition test performed at room temperature of 23°C for cores SK-C4, SK-C5 and SK-C6.

In addition, the pressure drop, and oil recovery data were compared in Figure 70 and Figure 71, respectively. The SK-C4 and SK-C5 cores have higher values for ΔP at the start of viscous flooding as expected and they stabilize rapidly. The higher values of ΔP are observed for these cores because during the SI test, not all of the capillary forces had been "consumed", so more capillary forces were "left" to drive the process. Hence, the oil recovery is greater during viscous flooding than during spontaneous imbibition for SK-C4, a bit lower for SK-C5 and the lowest for SK-C6 (Figure 71).

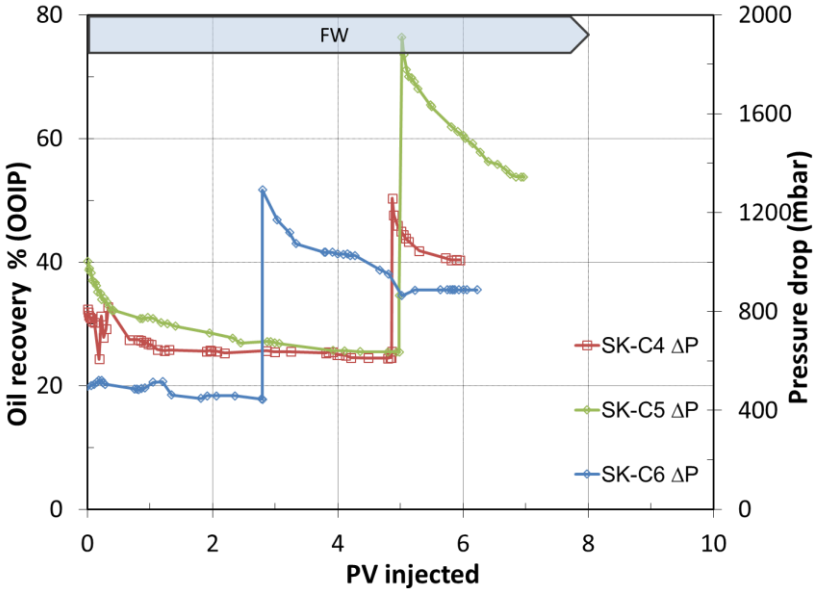

Figure 70. The pressure drop during the forced imbibition, FI, (displacement) by formation water at room temperature of 23°C for core SK-C4, SK-C5 and SK-C6 when flooded by 1PV/d and 4PV/d.

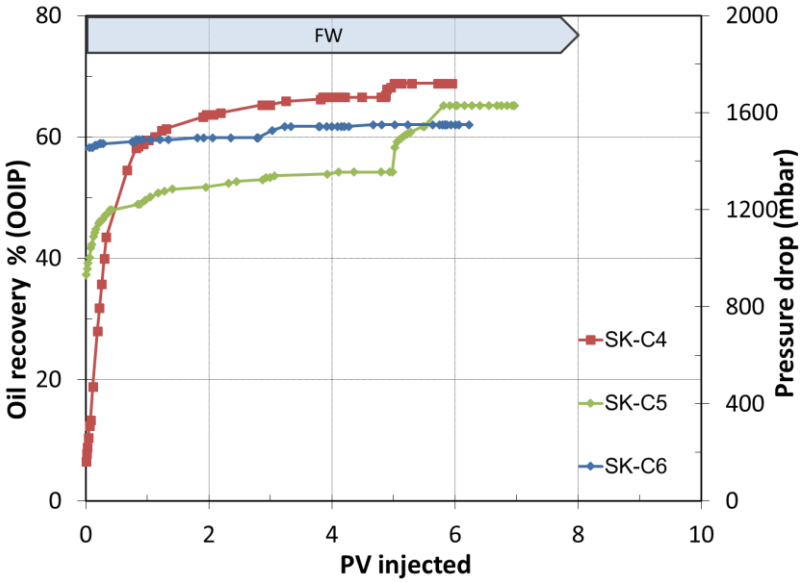

Figure 71. The oil recovery during the forced imbibition, FI, (displacement) by formation water at room temperature of 23°C for core SK-C4, SK-C5 and SK-C6 when flooded by 1PV/d and 4PV/d (FW hr)

Now, summing up the results obtained from these two processes, we end up with a total oil recovery of 66.5% of OOIP and 59.8% of OOIP for SK-C4 and SK-C5, respectively. The total recovery for all three cores, SK-C4, SK-C5 and SK-C6, is plotted in Figure 72.

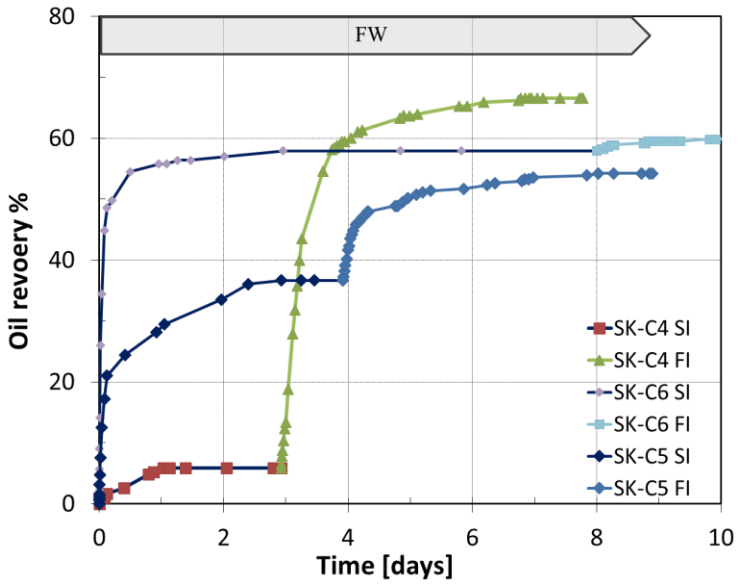

Figure 72. The total oil recovery after performed SI, FI and FI hr on chalk cores SK-C4, SK-C5 and SK-C6 at room temperature of 23°C.

The final results do not exactly follow the theory. Apparently, the least water-wet core produces the most oil, while most water-wet core shows lowest oil recovery. Explanation for such a phenomenon can eventually be given by differences in IFT for

different oils used for flooding the cores, explained in detail in section 4.8. However, the difference in the amount of recovered oil is not big as all the cores are said to be water-wet as defined by the CWT tests described in section 2.3.2.5. Thus, the obtained results are quite satisfactory. Table 13 summarizes oil recoveries after spontaneous imbibition test for cores SK-C4, SK-C5 and SK-C6.

Table 13. Summary of oil recovery by spontaneous imbibition for cores SK-C4, SK-C5 and SK-C6.

	SK-C4	*SK-C5*	*SK-C6*
$\%OOIP$	5.84	36.65	57.94

4.7 Chromatography wettability test for water-wet surface area in reference cores

In order to verify the water-wet surface area of the given reference cores it was necessary to perform chromatographic wettability tests (CWT). At the end of the previously described flooding processes, residual oil saturation, S_{or}, was established. Effluent samples, 44 in total, were collected after every 20 minutes and were further analyzed using ion chromatography. Thereafter the CWT was performed. Results obtained from ion chromatography of the effluent samples obtained during CWT tests performed on SK-R1, SK-R2, SK-C3 and SK-C6 are presented in Figure 73, Figure 74, Figure 75 and Figure 76, respectively.

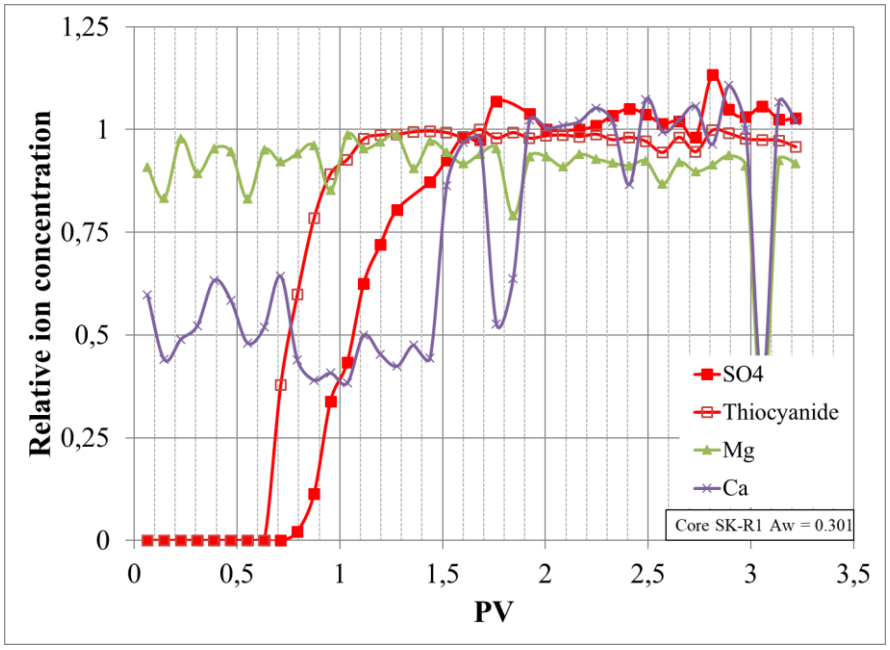

Figure 73. Chromatography wettability data plotted for core SK-R1, with an area of Aw=0.301.

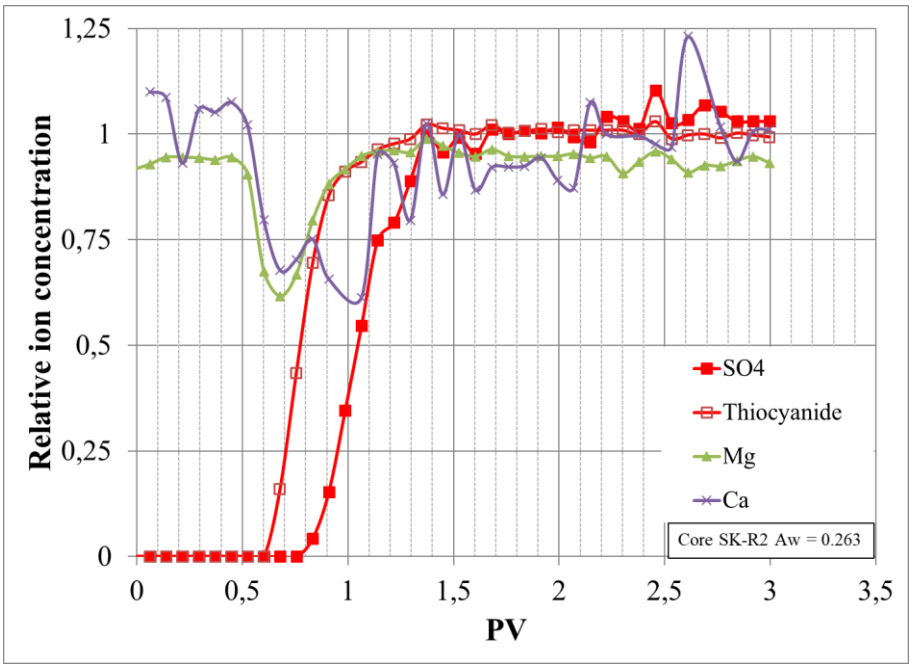

Figure 74. Chromatography wettability data plotted for core SK-R2, with an area of Aw=0.263.

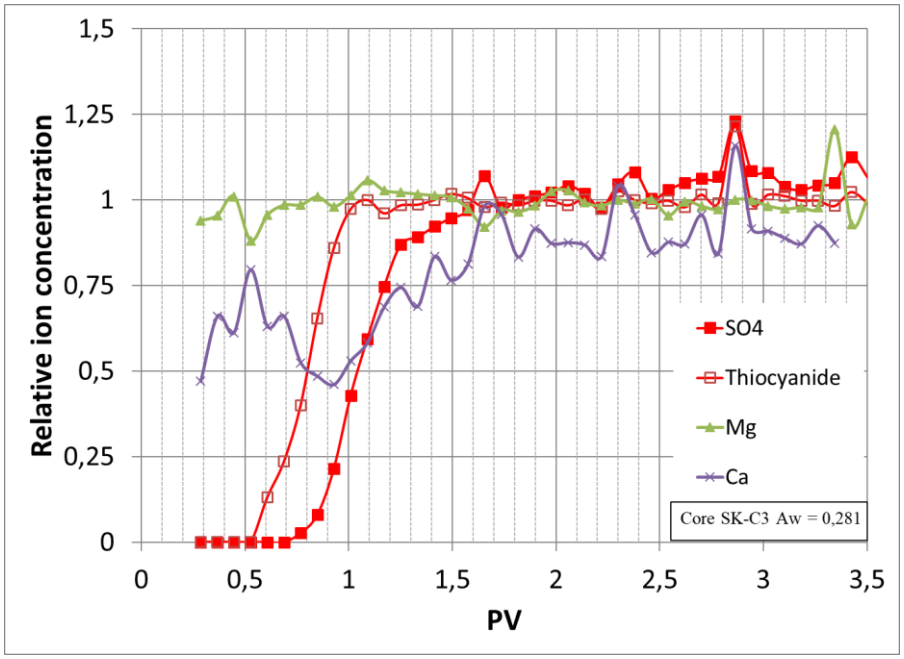

Figure 75. Chromatography wettability data plotted for core SK-C3, with an area of Aw=0.281.

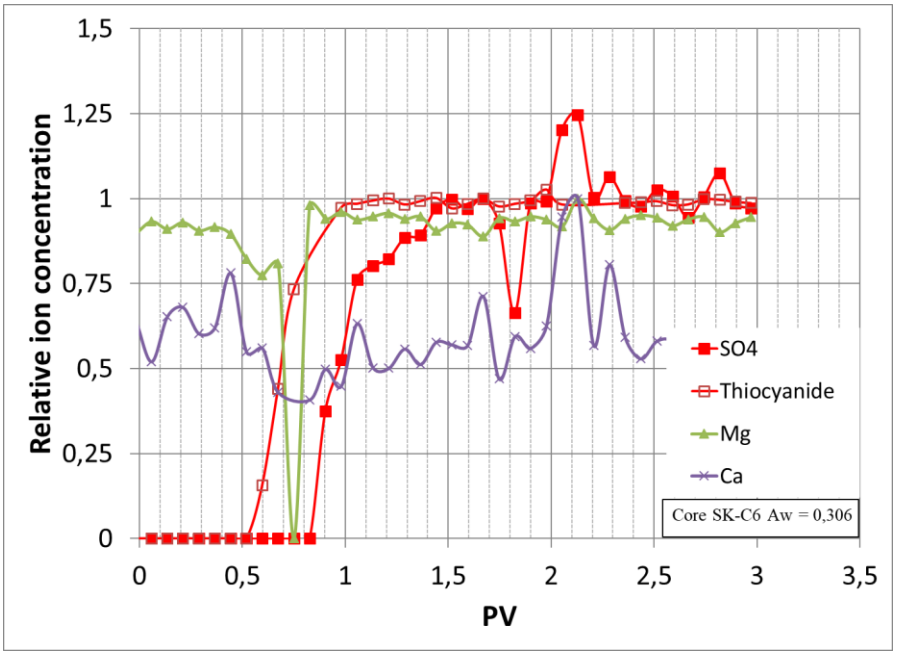

Figure 76. Chromatography wettability data plotted for core SK-C6, with an area of Aw=0.306.

That as can be seen from the figures, thiocyanate comes out first as it is non-affine to the chalk surface, followed by sulphate which gets adsorbed on the water-wet calcite surfaces. It is noticed that the dispersion front of SCN^- is quite similar for all cores, equal 0.63 PV, 0.60 PV, 0.53 PV and 0.52 PV for SK-R1, SK-R2, SK-C3 and SK-C6, respectively . Also, the eluent curves for thiocyanate passes through the points C/Co=0.5 and PV=1.0, which indicates that the injected fluid is contacting the total PV

of the core. On the other hand, the dispersion front for SO_4^{2-} is a bit wider, at it is adsorbed to the surface, equal 0.71 PV, 0.76 PV, 0.69 PV and 0.83 PV for SK-R1, SK-R2, SK-C3 and SK-C6, respectively. From the figures, the areas between the SO_4^{2-} and SCN^- curves are 0.301, 0.263, 0.281 and 0.306 for the cores SK-R1, SK-R2, SK-C3 and SK-C6, respectively. As the two reference cores are strongly water-wet and as the other two wettability-altered cores exposed to RES40-0.15 also gave almost same area values, this indicates a quite water-wet state for the SK-C3 and SK-C6 cores. The results are quite in a line with results obtained from SI test. To confirm this observation, we calculate the wettability index as discussed in section 2.3.2.4. We take the average value of two water-wet reference cores (0.282) as the reference value for calculations.

$$WI = \frac{0.281}{0.282} = 0.996$$

$$WI = \frac{0.306}{0.282} = 1.08$$

The wettability index of 0.996 for SK-C3 and 1.08 for SK-C6 confirms that the cores are strongly water-wet and that they have not been affected by high grade of adsorption.

As mentioned in section 2.3.2.5, sulphate is quite sensitive towards chalk surface. Consequently, figures clearly demonstrate variation in the Ca^{2+} concentration in the SO_4^{2-} dispersion zone. Hence, the sulphate adsorb onto charged surface as the concentration of sulfate ions increases.

On the other hand, the concentration of Mg^{2+} is less affected by the gradient in the sulfate concentration.

4.7.1 Comparation with cores of different wettability

The CWT results of other four cores, SK-C1, SK-C2, SK-C4 and SK-C5, tested by Harestad (2019) and Wathne (2019) are presented in Figure 77.

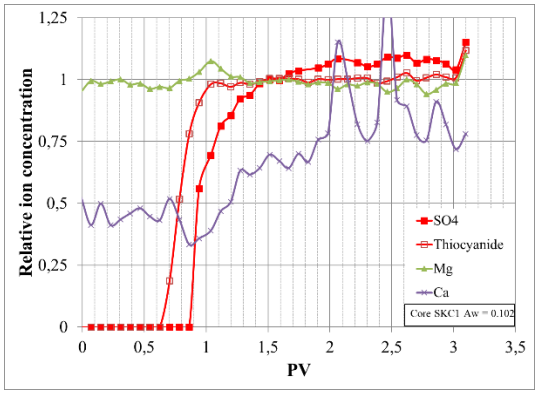

Core SK-C1; Aw=0.102

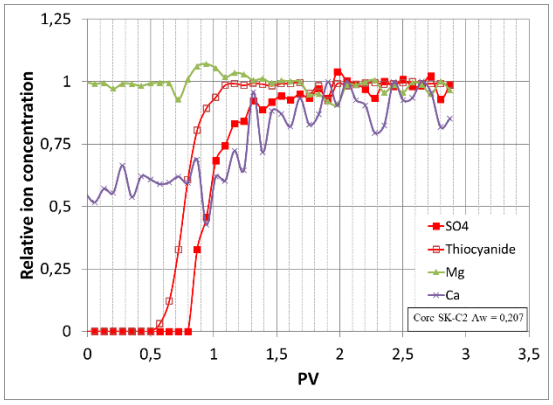

Core SK-C2; Aw=0.207

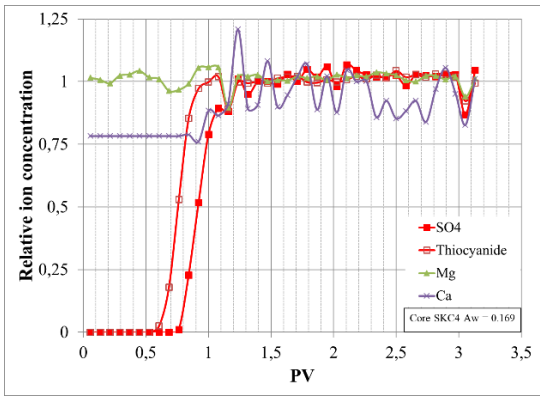

Core SK-C4; Aw=0.169

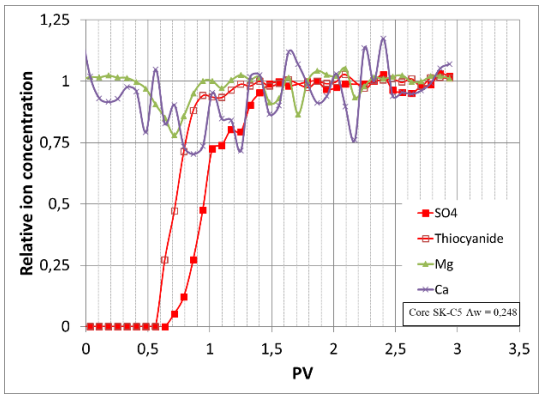

Core SK-C5; Aw=0.248

Figure 77. Chromatography wettability data for cores SK-C1, SK-C2, SK-C4 and SK-C5.

Compared to cores SK-R1, SK-R2, SK-C3 and SK-C6 tested in this study, the cores SK-C1, SK-C2, SK-C4 and SK-C5 tested by other students are less water-wet. Core SK-C1 with Aw=0.102 and SK-C4 with Aw=0.169 appears to have the smallest value for areas under curves, indicating less water wet state. Similar results are obtained with the cores SK-C2 with Aw=0.207 and SK-C5 with Aw=0.248 that shows intermediate-wet state. Table 14 summarizes the adsorption area values for all cores.

Table 14. Summary of adsorption area values for all cores

	SK-R1	*SK-R2*	*SK-C1*	*SK-C2*	*SK-C3*	*SK-C4*	*SK-C5*	*SK-C6*
A_w	0.301	0.263	0.102	0.207	0.281	0.169	0.248	0.306

4.8 pH analysis

Additionally, during flooding, the pH values were measured for randomly selected effluent samples to confirm the alkalinity of the cores. The results are plotted and

presented in Figure 78. As the pH values for all cores are above 7, it confirms that the environment is slightly alkaline, as expected due to acidic components.

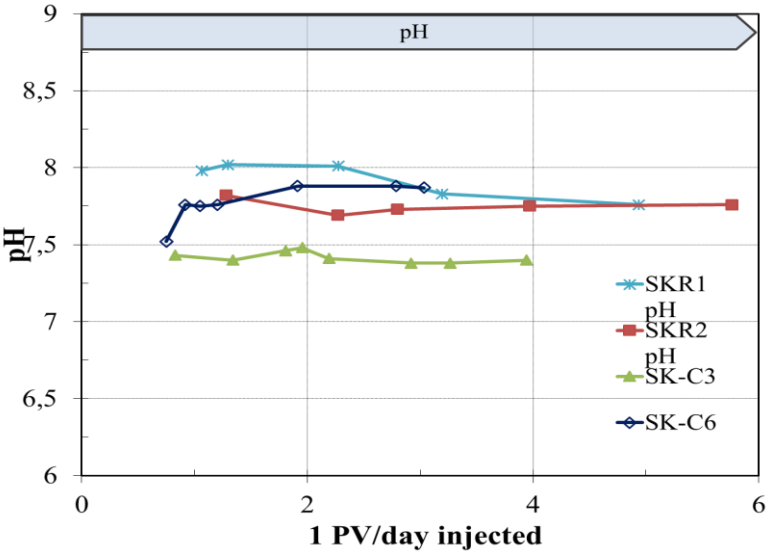

Figure 78. The pH measurement obtained for chalk cores SK-R1, SK-R2, SK-C3 and SK-C6

At alkaline conditions, the basic components in crude oil become neutrally charged. Consequently, the components active towards chalk rock surface are negatively charged acidic components.

4.9 IFT analysis

The relation between IFT and AN value in crude oils used for this project is given in Figure 79.

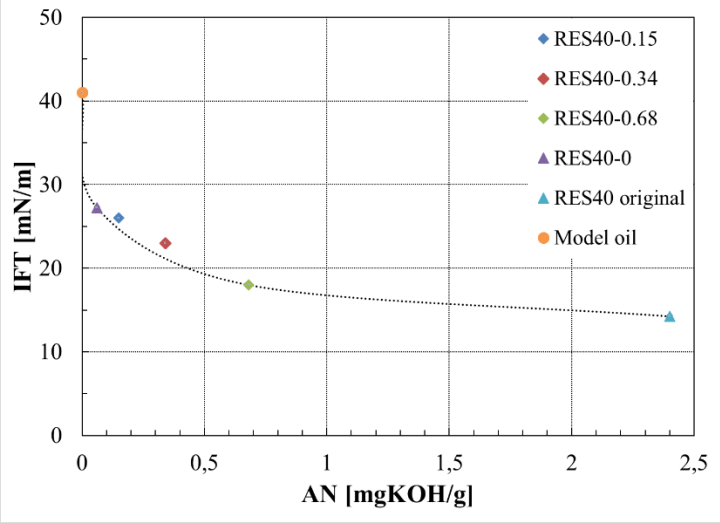

Figure 79. The Interfacial tension vs. AN number in crude oils used in this project.

As can be seen in Figure 79, the interfacial tension is decreased with increased AN in oils. Through experimental determination, the oils with acid numbers 0.15, 0.34 and 0.67 mg KOH/g were found to have interfacial tensions of 36, 23 and 18 mN/m, respectively. The IFT for model oil with AN=0 was determined to be 41 mN/m. Also, the oils RES40 and RES40-0, had IFT values of 14.25 and 27.25 mN/m, respectively, due to different amount of polar components present in these oils. Table 15 summarizes values of IFT and AN for oils discussed in this section.

Table 15. Summary of IFT and AN values for different oils

	Model oil	*RES40*	*RES40-0*	*RES40-0.15*	*RES40-0.34*	*RES40-0.68*
AN(mgKOH/g)	0	2.4	0.06	0.15	0.34	0.68
IFT (mN/m)	41	1.25	27.25	36	23	18

If the IFT observations are included in previously defined results, we conclude that if AN is higher, IFT is lower, which means less is the water-wetness of the core and less are the capillary forces present. This leads to a lower recovery with SI test and a higher recovery with FI test. This shows that the IFT plays an important role during oil recovery processes.

5.Simulated results and discussion

Parameters such as core dimensions, absolute permeabilities, porosities, fluid viscosities, initial water saturations (S_{wi}), residual oil saturations (S_{or}), injection rates, pressure drops across the cores, production histories and end point relative permeabilities obtained from experimental work were introduced to Sendra simulation program to start the simulation process. During the simulation all parameters were kept varying while Pc was assumed negligible in the matching. To obtain relative permeability curves, the Corey exponents included in the simulation process were kept varying. Simulated results during history matching of oil recovery and pressure drop, and relative permeability curves for cores SK-R1, SK-R2, SK-C1, SK-C2 and SK-C3 are presented in Figure 80, Figure 81, Figure 82, Figure 83 and Figure 84, respectively.

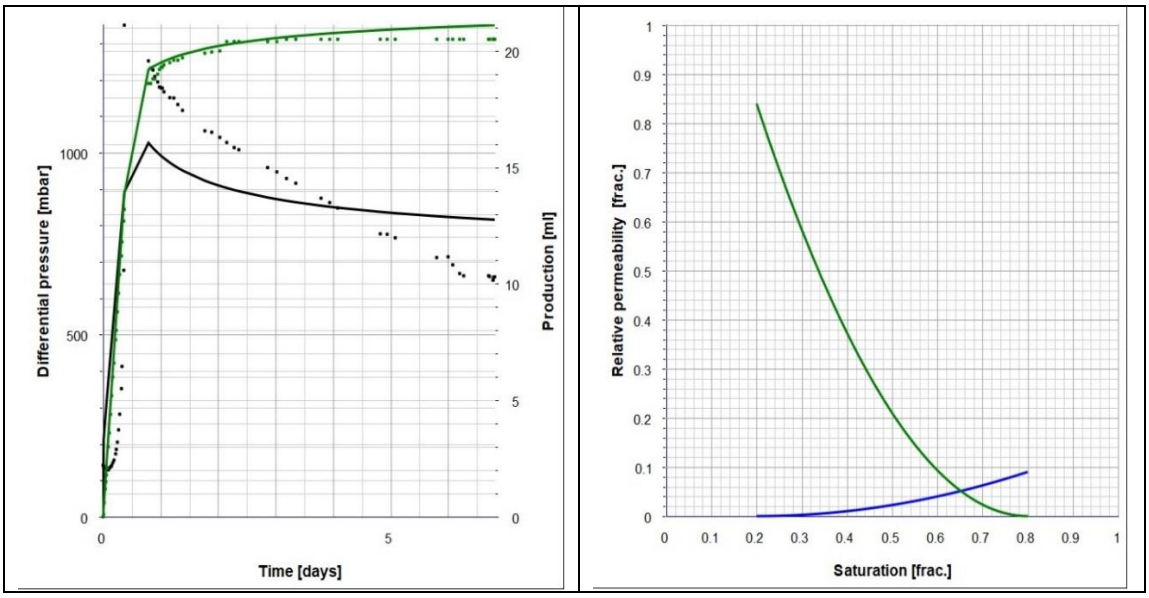

Figure 80. History matching (pressure drop and oil recovery) data (left) and relative permeability curves (right) for core SK-R1

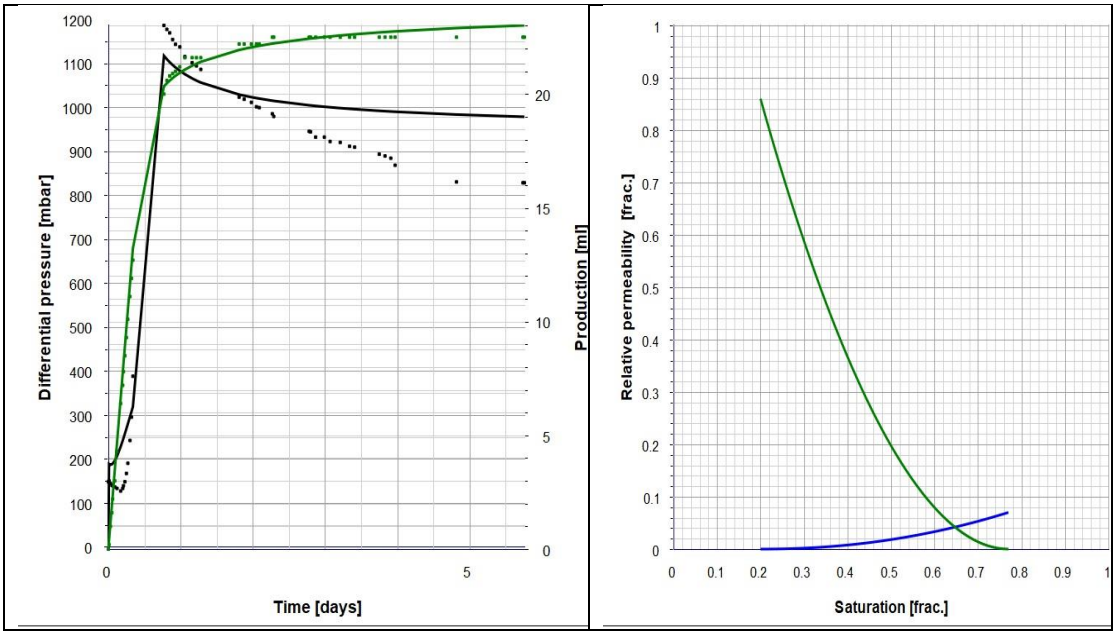

Figure 81. History matching (pressure drop and oil recovery) data and relative permeability curves for core SK-R2

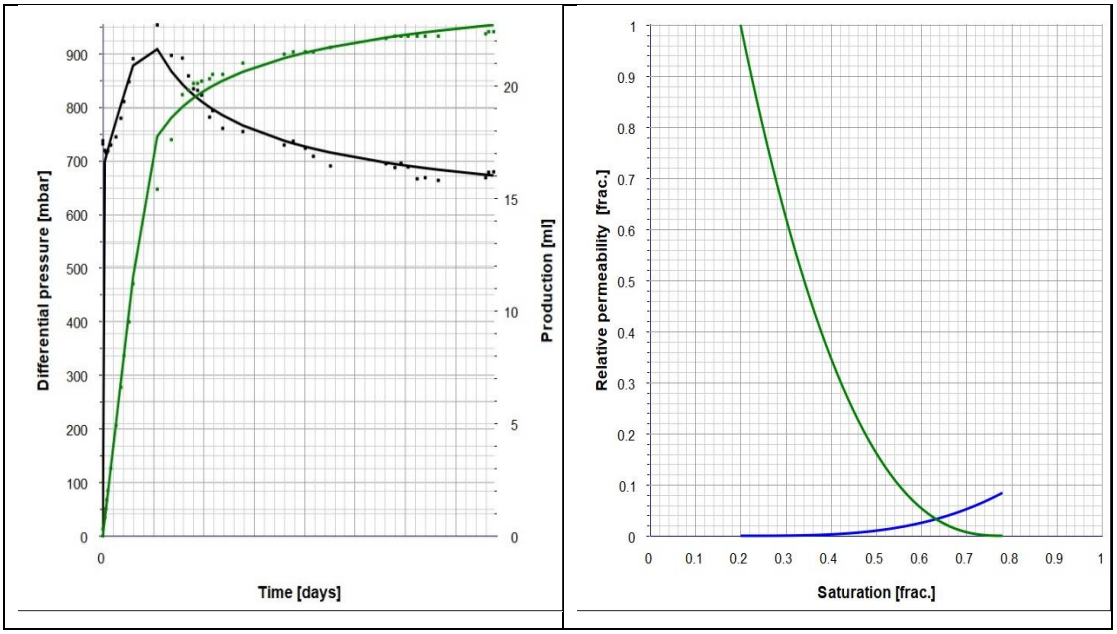

Figure 82. History matching (pressure drop and oil recovery) data and relative permeability curves for core SK-C1

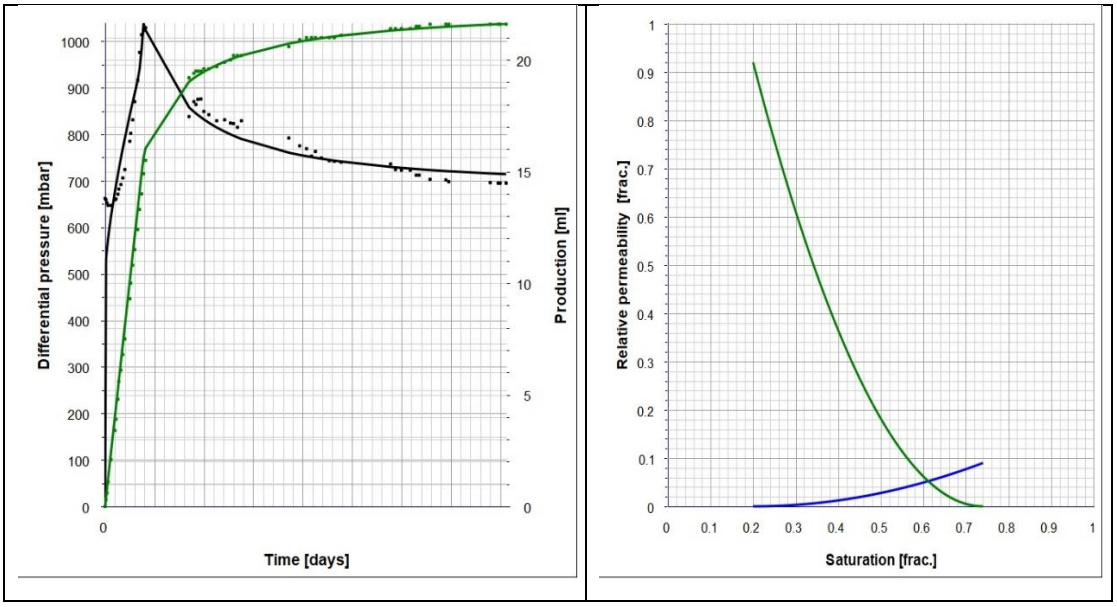

Figure 83. History matching (pressure drop and oil recovery) data and relative permeability curves for core SK-C2

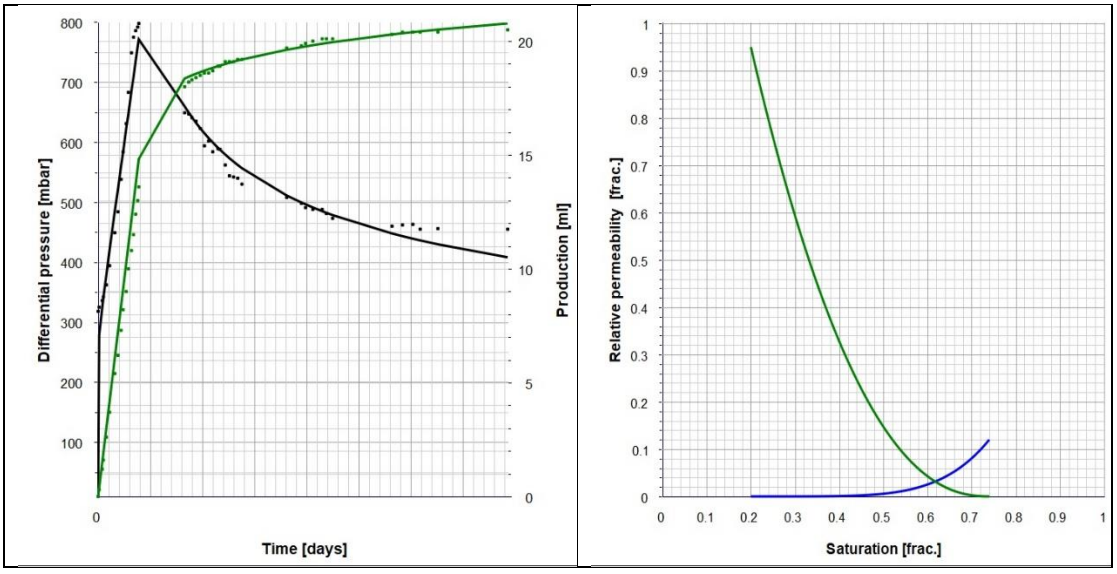

Figure 84 History matching (pressure drop and oil recovery) data (left) and relative permeability curves (right) for core SK-C3; Scatters for experimental data and smooth line for simulated data.

Figure 80 (left) and Figure 81 (left) illustrate history matching of pressure drop and oil recovery data with experimentally obtained values for cores SK-R1 and SK-R2. As can be observed from these figures, the two reference cores do not provide good matching of pressure drop data. This is especially noticeable in the beginning of pressure drop curve. The history matching of ΔP curve strongly depends on mobility of phases present in a system. In the beginning, the mobility of oil phase is high, while the mobility of water phase is low. Hence, matching of ΔP will strongly depend on mobility of oil

recovery reaches plateau, i.e. the point where water breaks through. From this point, the mobility of water phase increases and mobility of oil phase decreases until pressure drop curve stabilizes. When ΔP becomes stable, only water is produced from the system. The figures do not show pure piston like displacement since there is a peak in pressure drop curve (at water breakthrough). If there is piston like displacement, the pressure will only increase or decrease. High oil production before water breakthrough is often linked to favorable mobility ratio ($M < 1$). It means the oil phase has a higher mobility than does the water phase.

Additional manual simulations were performed on reference cores SK-R1 and SK-R2 since previous automatically driven simulation did not show good matching, Figure 85.

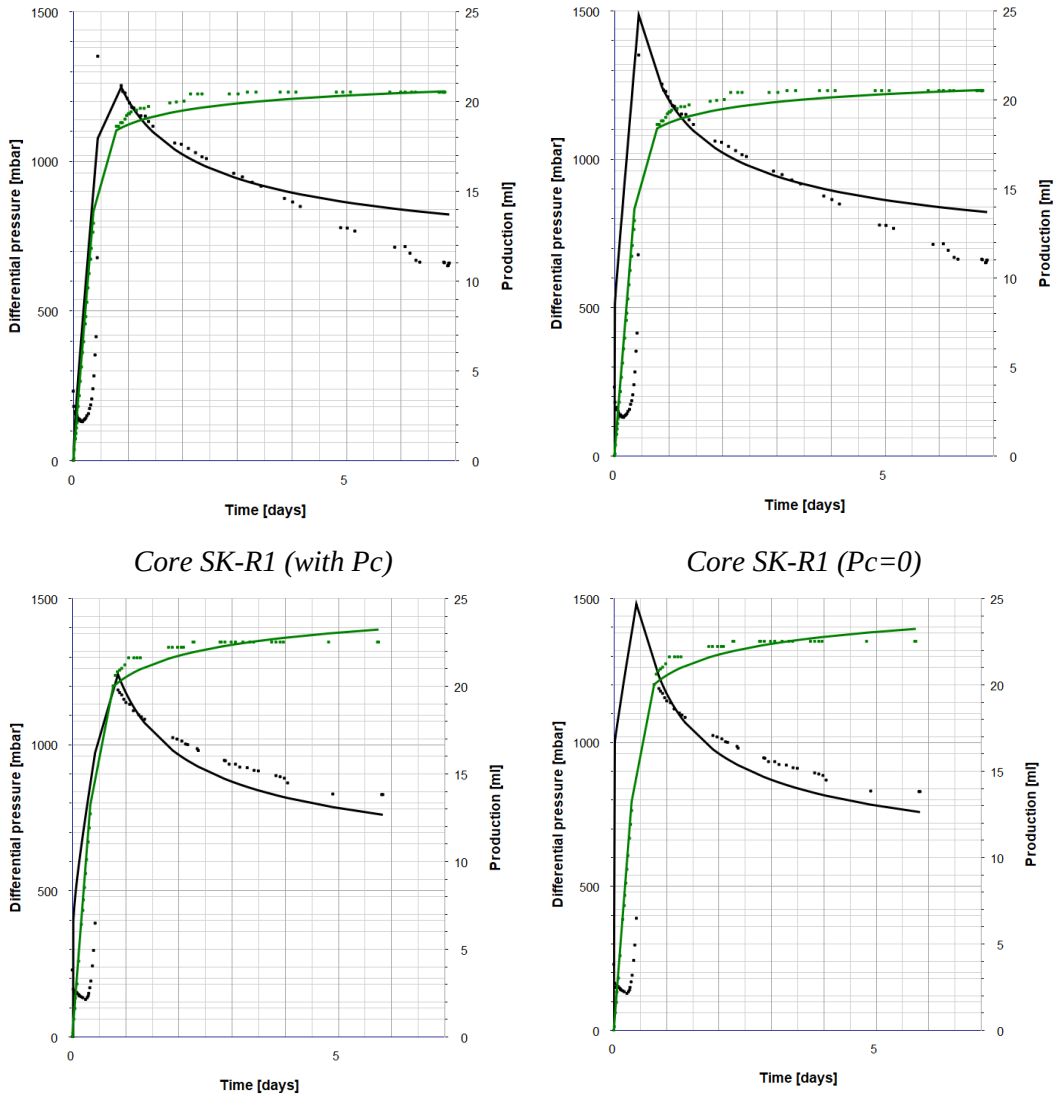

Figure 85. Manual matching of pressure drop and oil recovery data when capillary pressure (Pc) was present in simulation a) and when Pc =0 b) for reference chalk cores SK-R1 and SK-R2.

This time, Corey parameters and saturations, experimentally obtained, were step by step manually changed. Initially, c_o and c_w were set equal 0 and relative permeabilities, k_{rw} and k_{ro}, were set equal 0.2. Then, the S_{or} was set to 0.05 (low value). Next, the Corey exponents were changed until the top of the pressure curve was matched. Thereafter, the Sor is increased and consequently it was necessary to increase or decrease k_{rw} and k_{ro} values. Finally, the appropriate curve was obtained and all above mentioned parameters were set to be fixed except Skjæveland exponents that were kept varying. After doing an estimation, even better curve was generated showing a bit lower top of pressure drop curve. So, the parameters were not varying freely, but we changed them back and forth until we got a matching curve. In first case the capillary pressure was kept varying and then it was set to 0. Comparing plotted data in Figure 85 we can observe that in case of strong water-wet cores, history matching will be much better when the parameters were matched manually and capillary pressure taken into simulation.

In order to achieve the best match, we had to make corrections on relative permeability end points, k_{ro} and k_{rw}, Corey exponents, Skjæveland exponents and residual oil saturation, S_{or}. Despite attempts to get an absolute match with experimental values, the best obtained match is not considered satisfactory for the two reference cores as can be seen in Figure 80 and Figure 81.

From the results of the simulation, the pressure drop (black) and oil recovery (green) curves show quite good matching with experimental data (given by dots) for cores SK-C1, SK-C2 and SK-C3, as can be observed from Figure 82, Figure 83 and Figure 84, respectively.

The relative permeability curves for oil and water phases are presented in the same figures in the right column. As mentioned in sections 2.2.3.1 and 2.3.3, cross points of these curves should give the information about wetting state of core samples. The shape of the curves for all cores is quite similar indicating later breakthrough and quite high oil recovery. Figure 80 illustrates the results for reference core SK-R1. The end points were calculated using equation (2.2), obtaining values of $k_{rw} = 0.09$ and $k_{ro} = 0.84$. The cross point for k_{rw} and k_{ro} gave a water saturation (fraction) value of 0.65. Cuiec (1984) confirmed that such a system is quite water-wet. In Figure 81, the relative permeabilities for core SK-R2 were plotted. Calculated end point values were $k_{rw} =$

0.07 and $k_{ro} = 0.86$. The placement of crossing point was at 0.642 indicating water-wet core and high oil recovery. Figure 82 shows the results from the core SK-C1. End point values for this core were $k_{rw} = 0.08$ and $k_{ro} = 1.02$, giving a cross point of 0.625, indicating water-wet core. Similarly, for the core SK-C2 (Figure 83), the end points were calculated to be $k_{rw} = 0.09$ and $k_{ro} = 0.92$, giving a water saturation value of 0.61, also indicating water-wet state. Finally, Figure 84 shows the relative permeability curves for core SK-C3. End point relative permeabilities were estimated to be $k_{rw} = 0.12$ and $k_{ro} = 0.95$ for this core. The cross point was at 0.62, again indicating a water-wet state.

Simulation of water/oil relative permeabilities in this project shows the results to be more-or-less matching to the experimentally obtained data. Relying on the literature review, the cross point of relative permeability curves should result in setting the water saturation values in the following order: SK-R1 (0.65), SK-R2(0.642), SK-C3 (0.62), SK-C2 (0.61) and SK-C1 (0.625), i.e. from most water-wet to least water-wet states. Since the core SK-C1 shows a higher value for water saturation than the cores SK-C2 and SK-C3, the results are not as expected. The results would be satisfactory if this core showed the least water-wetness as it had been flooded with the oil containing the most polar components ($AN = 0.68$). Following relative permeabilities are the answer that there are some uncertainties about the exact values of S_{or} and the curves themselves. This case can be possibly explained by the lack of data points between the end points for relative permeability curves k_{rw} and k_{ro}. However, all cores showed same tendency for high oil recovery. Table 16 summarizes cross points for cores SK-R1, SK-R2, SK-C1, SK-C2 and SK-C3.

Table 16. Summary of cross points for cores SK-R1, SK-R2, SK-C1, SK-C2 and SK-C3.

	SK-R1	*SK-R2*	*SK-C1*	*SK-C2*	*SK-C3*
Cross point (S_w axis)	0.65	0.642	0.625	0.61	0.62

5.1 Simulated results in Excel

The data obtained from Sendra were used to plot the relative permeability curves in Excel. In addition, the fractional flow curve and capillary pressure curve was plotted in order to confirm the wetting state of chalk cores. The Corey exponents, N_w and N_o,

generated by Sendra were used for calculations. To define the shape of relative permeability curves, normalized saturation (S_n) was calculated using equation:

$$S_n = \frac{S_w - S_{wi}}{1 - S_{wi} - S_{or}} \tag{5.1}$$

Where,

S_n	Normalized saturation
S_w	Water saturation
S_{wi}	Initial water saturation
S_{or}	Residual oil saturation

Thereafter, the relative permeabilities for oil and water were calculated using the following expression:

$$k'_{rw} = k_{rw}(S_n)^{N_w} \tag{5.2}$$

$$k'_{ro} = k_{ro}(1 - S_n)^{N_o} \tag{5.3}$$

Where,

k'_{rw}	Relative permeability for water based on Corey exponent
k_{rw}	Relative permeability for water experimentally obtained
N_w	Corey exponent for water phase
k'_{ro}	Relative permeability for oil based on Corey exponent
k_{ro}	Relative permeability for oil experimentally obtained
N_o	Corey exponent for oil phase

Calculated values of relative permeabilities were used to generate Figure 86, Figure 87, Figure 88, Figure 89 and Figure 90 in Excel. These values can be found in Appendix B.

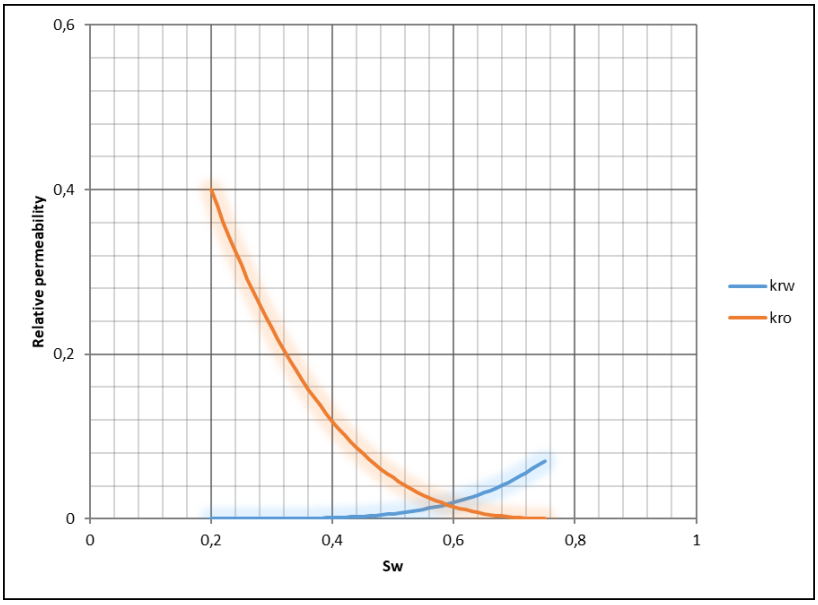

Figure 86. The relative permeability curves for core SK-R1 plotted in Excel

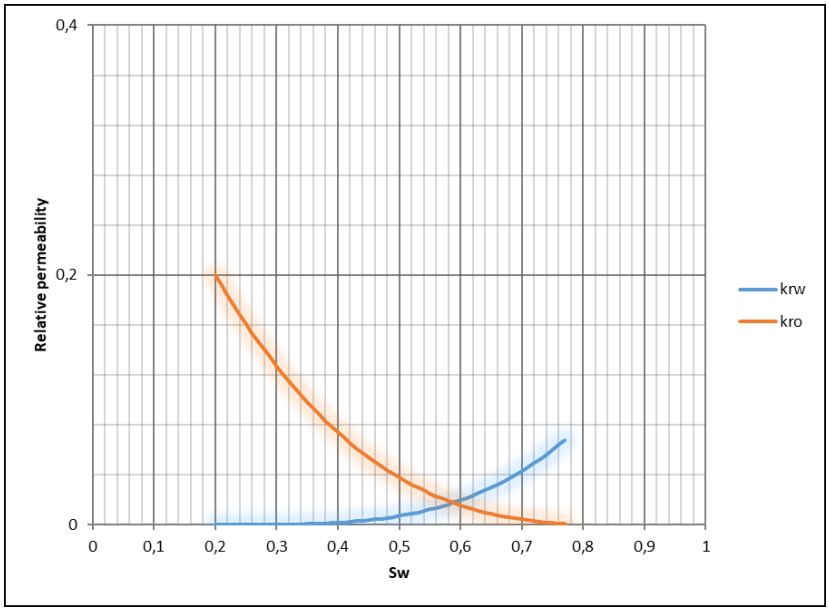

Figure 87. The relative permeability curves for core SK-R2 plotted in Excel

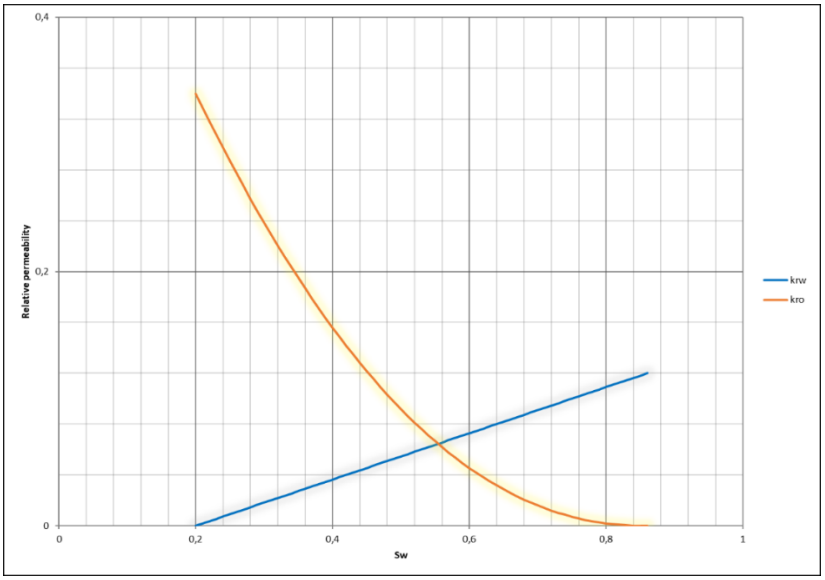

Figure 88. The relative permeability curves for core SK-C1 plotted in Excel

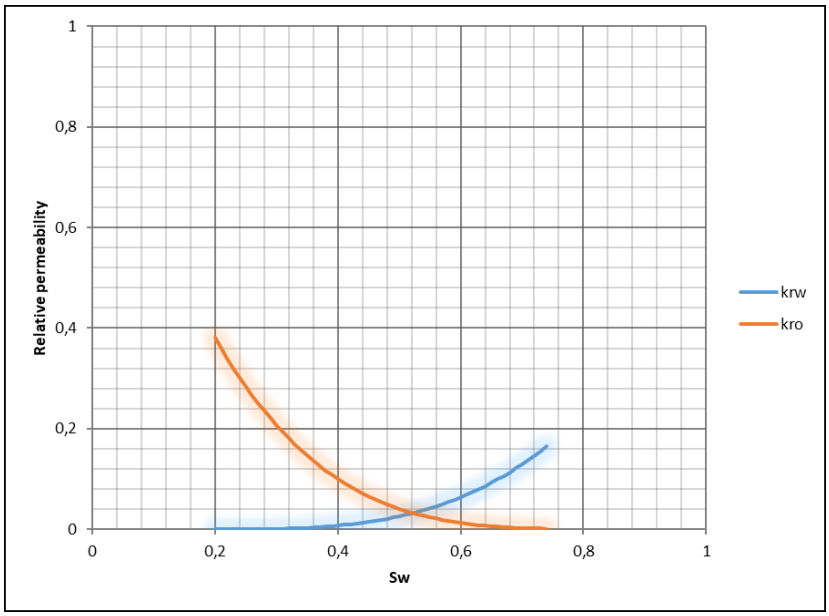

Figure 89. The relative permeability curves for core SK-C2 plotted in Excel

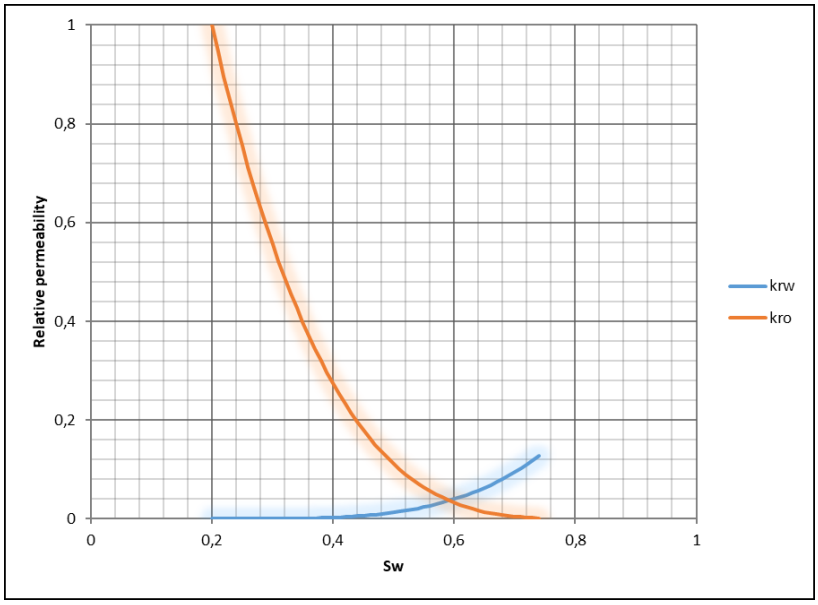

Figure 90. The relative permeability curves for core SK-C3 plotted in Excel

As can be seen from Figure 86, Figure 87, Figure 88, Figure 89 and Figure 90, the results are slightly different. Compared to modelled results, the cross point for cores SK-R1, SK-R2, SK-C1, SK-C2 and SK-C3 gave a water saturation (fraction) values of 0.595, 0.59, 0.55, 0.54 and 0.59, respectively (Table 17). It is obvious that curves generated in Excel gave better placement of intersection points. From this point of view, the wettability of chalk cores is placed in desirable and most likely correct order, from the least water-wet (SK-C2) to the most water-wet (SK-R1), except core SK-C1. Table 17 gives overview over cross points relative permeability curves generated in Excel.

Table 17. Summary of cross points obtained in Excel for cores SK-R1, SK-R2, SK-C1, SK-C2 and SK-C3.

	SK-R1	*SK-R2*	*SK-C1*	*SK-C2*	*SK-C3*
Cross point (S_w axis)	0.595	0.59	0.55	0.54	0.59

Additionally, the fractional flow (f_w) curves were plotted for all cores. The fractional flow curves can be used to say something about the behavior of the system. The equation (2.15) was used to calculate f_w. The calculated values can be found in Appendix B.

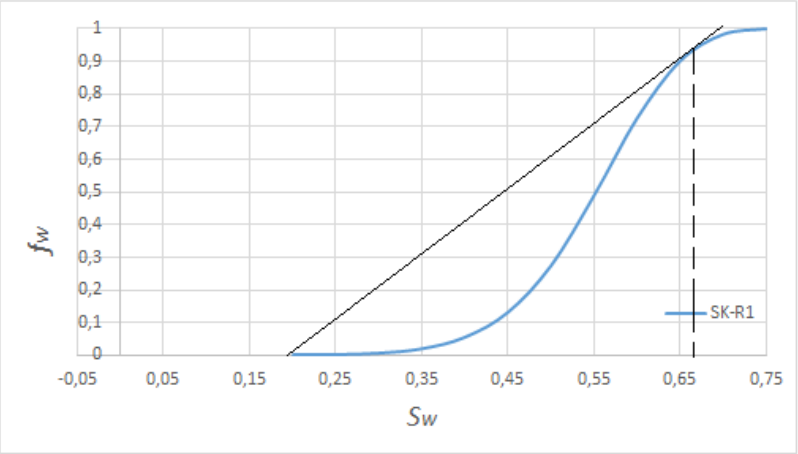

Figure 91. Fractional flow curve with tangent line for reference SK chalk core SK-R1

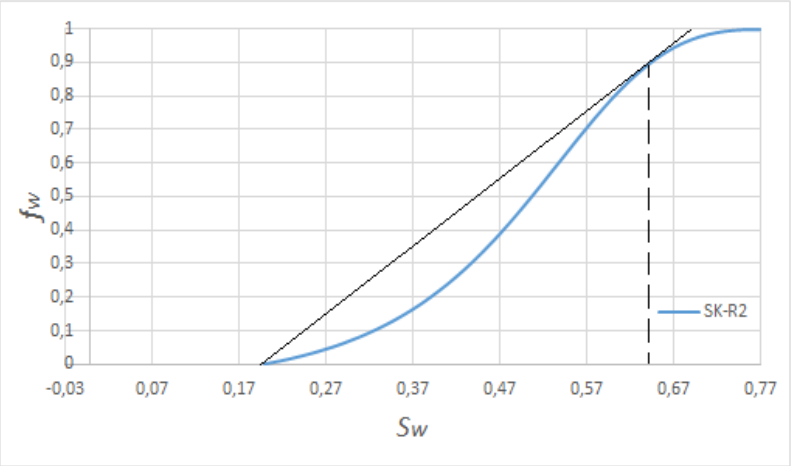

Figure 92. Fractional flow curve with tangent line for reference SK chalk core SK-R2

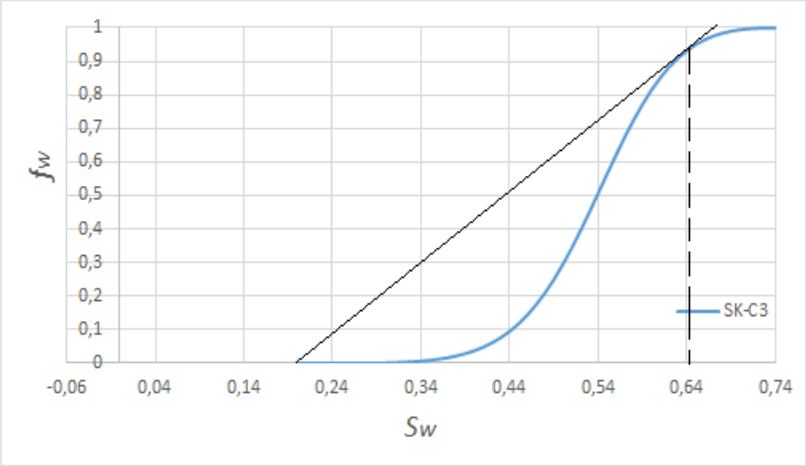

Figure 93. Fractional flow curve with tangent line for reference SK chalk core SK-C3

As mentioned in section 2.2.3.2 and based on Figure 12, the shape of curves will give information about the wetting state of chalk cores. As it can be seen from Figure 91, Figure 92 and Figure 93, cores SK-R1, SK-R2 and SK-C3 have values of front S_w higher than 0.5. This point will correspond to the cross point of relative permeability curves. Accordingly, the chalk cores are characterized as strongly water-wet .

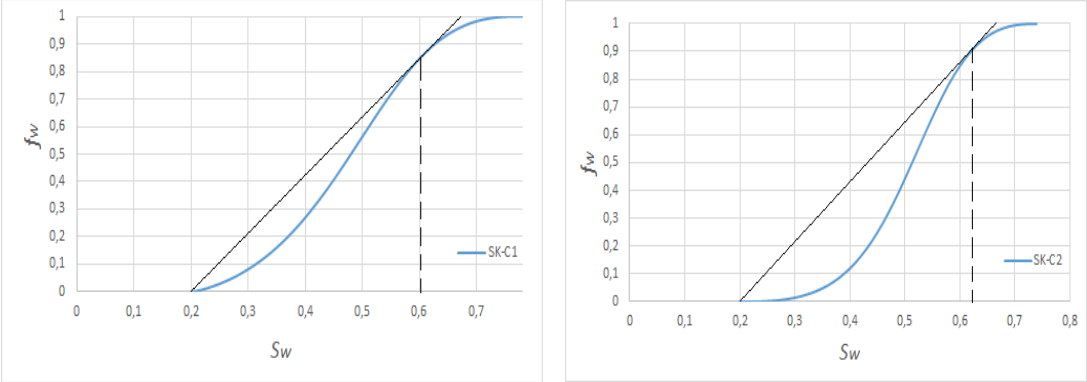

Figure 94. Fractional flow curve with tangent line for reference SK chalk core SK-C1 (left) and SK-C2 (right)

Figure 94 illustrates the fractional flow curves for the cores processed by Harestad (2019) and Wathne (2019). This figure confirms that the cores are water-wet. The values are high enough and we can state the systems are water-wet as referred in section 2.2.3.2. Basically, the front saturation values for all cores are quite similar, the difference is only in shape of fractional flow curves. The relative permeabilities are mainly valid above the front saturation (a very narrow range in this case), but it is unclear how much the estimates are affected by capillary pressure.

Capillary pressure curve can also say something about wetting state. To calculate capillary pressure, Pc, using Skjæveland constants obtained from Sendra (c_w, c_o, a_w, a_o), we should employee the equation (5.4):

$$P_c = \frac{c_w}{\left(\frac{S_w - S_{wr}}{1 - S_{wr}}\right)^{a_w}} + \frac{c_o}{\left(\frac{S_o - S_{or}}{1 - S_{or}}\right)^{a_o}} \qquad (5.4)$$

Where,

c_w Constant for the entry pressure of water phase

c_o Constant for the entry pressure of oil phase (negative number)

a_w Constant (water), dimensionless

a_o	Constant (oil), dimensionless
S_{wr}	The residual water saturation
S_{or}	The residual oil saturation

Values obtained for plotting Pc curve can be found in Appendix B. Capillary pressure curve is illustrated on Figure 95.

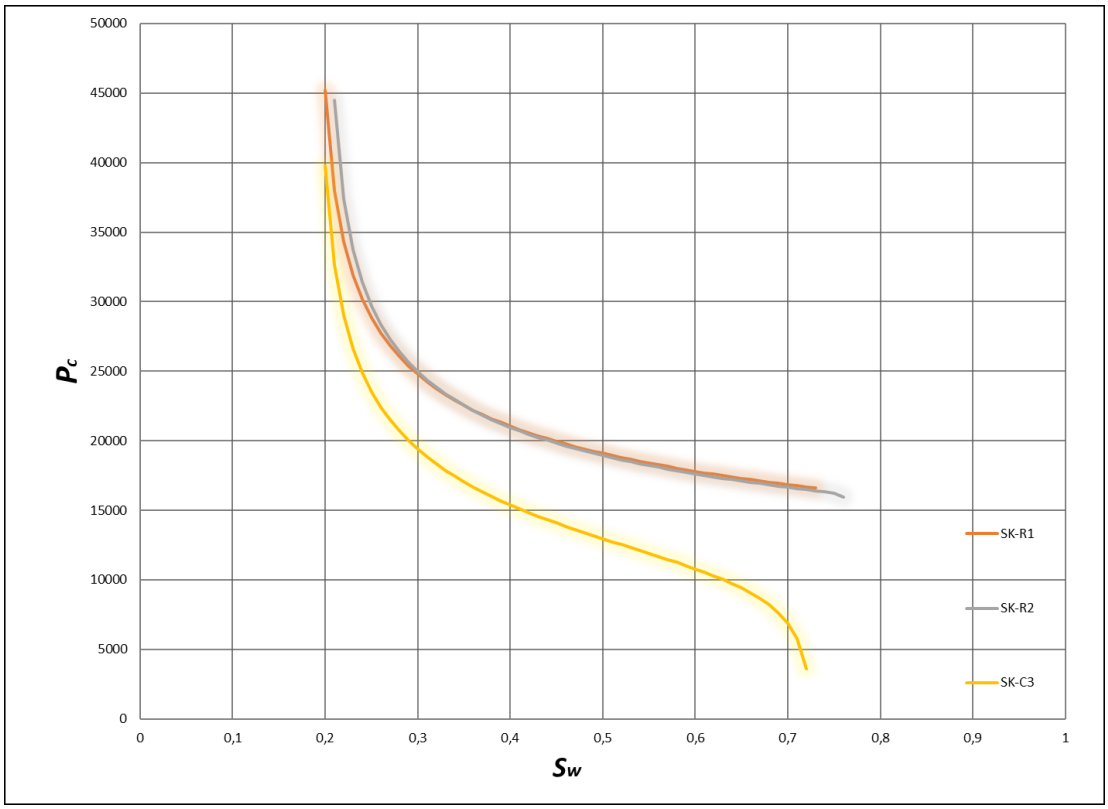

Figure 95. Capillary pressure curve for chalk cores SK-R1, SK-R2 and SK-C3 plotted in Excel

Changes in the wettability of a chalk cores have been shown a certain effect on capillary pressure curve. In order to do correct history matching for capillary pressure curves, requirement is that all the parameters of Skjæveland correlation should be different than 0. These values can be found in Appendix B. The parameters c_w, c_o and S_{or} used for estimation, were kept varying during the estimation, while the other ones remain constant. Finally, generated capillary pressure curves are suitable to define wetting state for a given SK chalk cores. As it can be observed from Figure 95, capillary pressure curves for the two reference cores (overlapping curves) shows strongly water-wet behavior where the values of Pc are all the way positive. The overall shape of capillary pressure curves represent strongly water-wet state (Skjæveland, 2000) for the cores SK-

R1, SK-R2 and mixed-wet state for core SK-C3. Among them, the chalk core SK-C3 shows lower Pc values. The results for capillary pressure curve are consider satisfactory.

6. Conclusion and further work

The main objective of the project was to understand how the adsorption of polar components change the wetting state of chalk cores. Additionally, crude oils with different amount of polar components used during core saturation, modified wettability of the cores affect relative permeability and ultimate oil recovery in strongly water-wet and fractional-wet chalk cores was studied. In order to get the answers, two reference outcrop chalk cores were flooded with synthetic oil and other two cores from the same chalk block were flooded with an oil containing a certain number of acidic components. The results showed only a small amount of adsorption of acidic components on the chalk surface and relative permeability cross points implied water-wet state for all cores. The conclusions can be summarized as follows:

- The wettability of chalk cores is affected by crude oil containing different acidic component content.
- The adsorption of acidic components is relatively small, resulting in very water-wet chalk cores when exposed to crude oil containing acidic components, AN=0.15 mgKOH/g.
- The reference cores behaved more water-wet when saturated by model synthetic oil, confirmed by forced displacement, spontaneous imbibition and chromatography wettability tests.
- Spontaneous imbibition test showed that strong water-wet cores produced most of oil, while the less water-wet cores showed lowest oil production. Also, SI test confirmed that the cores were from slightly water-wet to strongly water-wet.
- Chromatographic wettability test results confirmed less water-wet surface area in the cores treated with higher AN crude oil.
- Capillary forces are a crucial parameter for displacing the oil by SI and FI tests since they represent main driving forces for oil recovery.
- The cores SK-C3 and SK-C6 appear to be quite water-wet when flooded by an oil with smaller number of acidic components, but certainly are less water-wet than the reference cores.
- The higher injection rates did not significantly increase the oil recovery from the cores.

- The highest ultimate oil recovery was obtained for reference chalk cores, which are the most water-wet cores, while the lowest ultimate oil recovery was obtained for the cores with highest number of acidic components in oil.
- The IFT seems to have a significant effect on oil recovery, since the oil with highest IFT (synthetic oil) produced the higher amount of oil, while the oil with lowest IFT (RES40-0.68) showed the least oil production.
- The Sendra simulator estimated, by matching historical data, relative permeability curves and their cross points giving information about the wetting state from the cross-point placement relative to water saturation axis. Sendra mostly confirmed expectations and matched well with literature review. History matching of oil recovery data was good, while pressure drop data were not very well-matched using input data described in previous sections. By adjusting input data with including Skjæveland capillary pressure curves/ Corey exponents for relative permeability, the history match improved, and the generated data were satisfactory. For example, all relative permeability curves indicates water-wet systems with cross points that reflects on wetting states quite good.

Generally, the results obtained both experimentally and by simulation are considered satisfactory.

In this project the effect of wettability on relative permeability and oil recovery has been evaluated. The scope of the future work includes:

- Confirm and extend the findings from this thesis: how an increase in the initial water saturation of chalk cores influence relative permeability curves and ultimate oil recovery after waterflooding process.
- The synthetic oil should be replaced by Isopar H (C11-12 Isoparaffin) synthetic isoparaffinic oil.
- The cores should be saturated by crude oils containing high ANs, i.e. lower IFT, to evaluate new effects on a chalk cores.

Simulation work for determining relative permeability curves by unsteady state method can be improved by applying another model. Model used in future work should, besides end points, consist of some other additional experimentally obtained data, such as capillary pressure, P_c. The Johnson, Bossler, and. Naumann (JBN) method can be applied, but water production must be recorded besides the oil production. The JBN method can be used only if there is a water breakthrough in a system.

References

Abdallah, W. B. (2007). *Fundamentals of wettability*. Technology, 38, 1125-1144.

Ahmed, T. (2010). *Reservoir Engineering Handbook, Fourth Edition;*. Elsevier Science & Technology, ISBN 9780080966670.

Ahr, W. M. (2008). *Geology of carbonate reservoirs: the identification, description, and characterization of hydrocarbon reservoirs in carbonate rocks.*

Al-Hadhrami, H. S., & Blunt, M. J. (2001). *Thermally Induced Wettability Alteration To Improve Oil Recovery in Fractured Reservoirs.* doi: 10.2118/71866-PA.

Amott, E. (1959). *Observations Relating to the Wettability of Porous Rock.*

Andersen, M. A. (1995). *Petroleum Research in Chalk. Joint Chalk Research Phase IV.* Stavanger, Norway: Rogaland Research.

Anderson, W. (1986b, November). Wettability Literature Survey-Part 2: Wettability Measurement. (S. o. (U.S.), Ed.) *Journal of Petroleum Technology, 38*(11). doi:10.2118/13933-PA

Anderson, W. G. (1986a). *Wettability Literature Survey- Part 1: Rock/Oil/Brine Interactions and the Effects of Core Handling on Wettability.* doi:10.2118/13932-PA.

Anderson, W. G. (1987). *Wettability Literature Survey-Part 6: The Effects of Wettability on Waterflooding.* doi:10.2118/16471-PA.

Austad. (2013). *Water-Based EOR in Carbonates and Sandstones: New Chemical Understanding of the EOR Potential Using "Smart Water" Enhanced oil recovery field case studies.* Elsevier Science.

Austad, T. S. (2005). Seawater as IOR fluid in Fractured Chalk. SPE 93000, presented at the 2005 SPE International Symposium on Oilfield Chemistry held in Houston. *SPE 93000, Presented at the 2005 SPE International Symposium on Oilfield Chemistry held in Houston.* Texas, USA.

Baviere, M. (1991). *Preface In Critical Reports on Applied Chemistry,Vol. 33. Basic Concepts in Enhanced Oil Recovery Processes.* Ed. Baviere, M. Published for SCI by Elsevier Applied Science, London and New York, pp. V-VIII.

Brown, R.J.S. and Fatt, I. (1956). *Measurements of fractional wettability of oilfield rocks by the nuclear magnetic relaxation method.* Petroleum Transactions, AIME, Vol 207.

Brownscombe, E.R. and Dyes, A.B.,. (1952). Water imbibition Displacement.Can It Release Reluctant Spraberry Oil? *The Oil and Gas Gas Journal, November 17*, 264-267.

Buckley, J. S., & Liu, Y. (1998). *Some mechanisms of crude oil/brine/solid interactions.* Journal of Petroleum Science and Engineering, 20(3–4), 155-160. doi: http://dx.doi.org/10.1016/S0920-4105(98)00015-1.

Burgess, J. (1978). *Metal ions in solution.* John Wiley & Sons Limited, ISBN.

Castor, T. P. (1981). Recovery mechanisms of alkaline flooding. In D. O. Shah (Ed.), Surface Phenomena in Ehanced Oil Recovery . *New York and London: Plenum Press.*, 249-291.

Chilingar, G.V. and Yen, T.F. (1983). *Some notes on wettability and relative permeability of carbonate rocks. II.* Energy and Sources.

Corey, A. T. (1954). *"The Interrelation between Gas and Oil Relative Permeabilities."* . Prod. Monthly 19(1): 38-41.

Craig, F. F. (1971). *The reservoir engineering aspects of waterflooding.* Monograph Series, SPE: Richardson, TX.

Craig, F. F. (1993). *The Reservoir Engineering Aspects Of Waterflooding.* Richardson, Texas: Society of Petroleum Engineers; SPE Monograph Series Vol. 3.

Cuiec, L. (1984). Rock/crude oil interactions and wettability: an attempt to understand their interrelation. *presented at SPE Annual Technical Conference and Exhibition.* Houston, September 16-19.: SPE 13211.

Dake, L. P. (1983). *Fundamentals of reservoir engineering.* Oxford, Elsevier Science, ISBN 978-0-444-41667-4 https://books.google.no/books?id=mFqpqMA62w8C.

Donaldson, E. C. (1969). Wettability Determination and Its Effect on Recovery Efficiency. (pp. 13-14). Bartlesville, Okla: SPE 2338.

Donaldson, E. C. (2013). *Wettability.* Burlington: Elsevier Science, ISBN : 0-12-799990-6.

Donaldson, E., & Alam, W. (2008). *Wettability.* Houston, Texas: Gulf Publishing Company.

Fan, T., & Buckley, J. (2007). *Acid number measurements revisited.* SPE J., 12(4), 496-500.

Fathi, J. (2012). *Water-based enhanced oil recovery (EOR) in carbonate reservoirs : initial wetting condition and wettability alteration by "Smart Water".* Stavanger: (PhD), University of Stavanger, Faculty of Science and Technology, Department of Petroleum Engineering.

Fathi, S. J. (2011). Improved oil recovery in carbonates by modified seawater - optimal ionic composition and salinity. *Paper presented at the 16th European Symposium on Improved Oil Recovery.* Cambridge, UK, 12-14 April.

Ganesh, P. R., & Mishra, S. (2015). *Simplified physics model of CO2 plume extent in stratified aquifer-caprock systems.* Society of Chemical Industry and John Wiley & Sons, Ltd.

Gluyas, J., & Swarbick, R. (2004). *Petroleum Geoscience.* Oxford: Blackwell Publishing.

Graue, A. R. (2001). *Oil Recovery in Fractured Reservoirs.* Proceedings of 6th Nordic Symposium on Petrophysics, 15-16 May 2001, Trondheim, Norway.

Green, D., & Willhite, G. P. (1998). *Enhanced Oil Recovery.* Richardson, Texas: Henry L. Doherty Memorial Found of AIME, Society of Petroleum Engineers, ISBN 9781555630775. https://books.google.no/books?id=0cUWAAAACAAJ.

Group, S. W. (2015). *Smart Water Flooding of Carbonates.* Stavanger, Norway: University of Stavanger.

Group, S. W. (2018). Stavanger, Norway: University of Stavanger.

Hirasaki, G. (1991). *Wettability: fundamentals and surface forces.* SPE Formation Evaluation, vol. 6, no. 02.

Hirasaki, G., & Zhang, D. L. (2004). Surface chemistry of oil recovery from fractured, oil-wet carbonate formation. *SPE Journal 9(2)*, 151-162.

Hopkins, P. A. (2016). *Water-based EOR and initial wettability in carbonates. (PhD).* (Philosophiae Doctor Doctoral), University of Stavanger, Norway, University of Stavanger.

Hunter, R. J. (1996). *Introduction to Modern Colloid Science.* New York.: Oxford University Press Inc.

Høgnesen, E. J. (2005). *"Waterflooding of Preferential Oil-wet Carbonates: Oil Recovery Related to Reservoir Temperature and Brine Composition.".* Paper SPE 94166 Presented at the 14th Europec Biennial Conference held in Madrid, Spain, 13-16 June.

Jadhunandan, P., & Morrow, N. R. (1995). Effect of wettability on waterflood recovery for crude-oil/brine/rock systems. *SPE reservoir engineering, vol. 10*, 40–46.

Kaminsky, R., & Radke, C. (1998). Water films, asphaltenes, and wettability alteration. *Tech. Rep., Lawrence Berkeley Lab., CA (United States).*

Korsnes, R. I. (2006). *Does the chemical interaction between seawater and chalk affect the mechanical properties of chalk? Eurock 2006a, Multiphysics Coupling and Long Term Behaviour in Rock Mechanics.*

Kovscek, A. W. (1993). A pore-level scenario for the development of mixed wettability in oil reservoirs,. *AIChE Journal, vol. 39, no. 6*, 1072–1085.

Lake, L. W. (2010). *"Enhanced Oil Recovery".* Society of Petroleum Engineers.

Leach, R. W. (1962). A laboratory study and fleld study of wettability adjustment in waterflooding. *JPT V. 14 (Feb)*, 206-212.

Lyons, C. W. (1996). *Standard handbook of petroleum & natural gas engineering; Practical petroleum engineers' handbook [6th ed.]*. Houston, Texas: Gulf Pub. Co.

Ma, S. M. (1999). Characterization of wettability from spontaneous imbibition measurements. *Canadian Petroleum Technology, 38(13)*, 1-8.

Manrique, E., Muci, V., & Gurfinkel, M. (2007). *EOR Field Experiences in Carbonate Reservoirs in the United States.* SPE Reservoir Evaluation & Engineering, 10(6), 667-686. doi:10.2118/100063-PA.

McPhee, C. J. (2015). *Core analysis: a best practice guide.* Amsterdam, Netherlands: Amsterdam, Netherlands, Elsevier, ISBN 9780444636577.

Milter, J. (1996). *Improved oil recovery in chalk: spontaneous imbibition affected by wettability, rock framework and interfacial tension. (PhD).* Bergen, Norway: Department of Chemistry, University of Bergen.

Mjos, J. E. (2018). Effect of Initial Wetting on Smart Water Potential in Carbonates. *SPE EOR Conference at Oil and Gas West Asia, 26-28 March, .* Muscat, Oman: Society of Petroleum Engineers, SPE-190414-MS. Retrieved from https://doi-org.ezproxy.uis.no/10.2118/190414-MS

Morrow, N. R. (1979). *Interplay of Capillary, Viscous And Buoyancy Forces In the Mobilization of Residual Oil.* doi: 10.2118/79-03-03.

Morrow, N. R. (1990). Wettability and Its Effect on Oil-Recovery. *Journal of Petroleum Technology 42(12)*, 1476-1484.

Morrow, N. R., & Mason, G. (2001). Recovery of oil by spontaneous imbibition. Current Opinion in Colloid & Interface Science. *Current Opinion in Colloid & Interface Science*, pp. 6(4), 321-337. doi:10.1016/S1359-0294(01)00100-5.

Morrow, N., & Buckley, J. (2011). Improved Oil Recovery by Low-Salinity Waterflooding. *SPE Journal of Petroleum Technology, 63(05)*, 106-112.

Muggeridge, A. A. (2014). *Recovery rates, enhanced oil recovery and technological limits. Philosophical Transactions of the Royal Society A: Mathematical, Physical and Engineering Sciences* . 372(2006). http://dx.doi.org/10.1098/rsta.2012.0320.

Mørk, P. C. (2001). *Overflate og kolloidkjemi. Grunnleggende prinsipper og teorier. 7. utgave. Institutt for Industriell kjemi, Fakultet for Kjemi og Biologi.* NTNU.

Power, N. (2018). Power-law velocity profile. *https://www.nuclear-power.net/nuclear-engineering/fluid-dynamics/turbulent-flow/power-law-velocity-profile-turbulent-flow/.*

Puntervold, T. (2008). *Waterflooding of carbonate reservoirs: EOR by wettability alteration.* Stavanger, Norway: (Philosophiae Doctor Doctoral), University of Stavanger.

Puntervold, T. A. (2007b). Water flooding of carbonate reservoirs:Effects of a model base and natural crude oil bases on chalk wettability. 1606-1616. doi:10.1021/ef060624b

Puntervold, T. S. (2007a). New Method To Prepare Outcrop Chalk Cores for Wettability and Oil Recovery Studies at Low Initial Water Saturation. *Energy & Fuels, 21(6), doi:10.1021/ef700323c*, 3425-3430.

Puntervold, T. S. (2009). *Co-injection of seawater and produced water to improve oil recovery from fractured North Sea chalk oil reservoirs.* Energy & Fuels, 23(5): 2527-2536.

Puntervold, T. S. (2015). Modified seawater as a smart EOR fluid in chalk. *Journal of Petroleum Science and Engineering 133*, 440-443.

Puntervold, T., & Austad, T. (2008). Injection of seawater and mixtures with produced water into North Sea chalk formation: Impact of fluid-rock interactions on wettability and scale formation. *Journal of Petroleum Science and Engineering 2008, 63*, 23-33.

Rao, D. N. (1999). Wettability effects in thermal recovery operations. (pp. 420-430). SPE Reservoir Eval. and Eng., Vol. 2, No. 5.

Rao, D.N. and Girard, M.G. (1996). A New Technique For Reservoir Wettability Characterization. *Journal of Canadian Petroleum Technology, 35(01)*.

Ravari, R. R. (2011). *Water-Based EOR in Limestone by Smart Water : A study of surface chemistry.* Stavanger, Norway: University of Stavanger.

Reeder, R. J. (1983). *Carbonates: Minerology and Chemistry.* Mineralogical Society of America, Reviews in Mineralogy, Volume 11.

Salathiel, R. A. (1973). *Oil Recovery by Surface Film Drainage In Mixed-Wettability Rocks.* Journal of Petroleum Technology 25(10), Volume: SPE-4104.

Satter, A., & Iqbal, G. M. (2015). *Reservoir Engineering: The Fundamentals, Simulation, and Management of Conventional and Unconventional Recoveries* (1st ed.). Gulf Professional Publishing.

Schlumberger. (2015a). Carbonate Reservoirs. Retrieved 20.03.2015 from Schlumberger. *http://www.slb.com/services/technical_challenges/carbonates.aspx?entry=ad_google_cr_carbonate&gclid=CjwKEAjwiq-oBRC9gvHCsvDdn2cSJACV3DFR87888Da1AC0YTu1iWrV2BZyvRkElJU8os3dfHMP90hoCepDw_wcB* .

SENDRA. (2008).

Shariatpanahi, S. F. (2012). *Improved Waterflood Oil Recovery from Carbonate Reservoirs-A Wettability Alteration Process (PhD).* Stavanger, Norway: University of Stavanger.

Shariatpanahi, S. F. (2016). Water Based EOR by Wettability Alteration in Dolomite. *Energy and Fuels, 30(1). doi:10.1021/acs.energyfuels.5b02239*, 180-187.

Shariatpanahi, S.,F., Strand, S., & Austad, T. (2011). *Initial wetting properties of carbonate oil reservoirs: Effect of the temperature and presence of sulfate in formation water.* doi:10.1021/ef200033h

Shehata, A., M. & Nasr-El-Din, A., H. (2014). Reservoir Connate Water Chemical Composition Variations Effect on Low-Salinity Waterflooding. *Abu Dhabi International Petroleum Exhibition and Conference.* Society of Petroleum Engineers; DOI: 10.2118/171690-MS.

Skjæveland, S. M. (2000). *"Capillary Pressure Correlation for Mixed-Wet Reservoirs.".* SPE Reservoir Eval. & Eng 3(1).

SlidePlayer. (2017). Retrieved from https://slideplayer.com/slide/9964671/

Speight. (2017). *Rules of Thumb for Petroleum Engineers.* John Wiley & Sons, Incorporated, ISBN 9781119403623.

Speight, J. G. (2014). *The chemistry and technology of petroleum (5th ed. ed. Vol. 137).* Boca Raton, Fla: CRC Press.

Speight, J. G. (2017). *The Rules of Thumb for Petroleum Engineers.* doi:10.1002/9781119403647

Springer, N. U. (2003). Resistivity index measurement without the porous plate: A desaturation technique based on evaporation produces uniform water saturation profiles and more reliable results for tight North Sea chalk. *Paper presented at the International Symposium of the Society of Core Analysts Pau, France, 21-24 September*.

Standnes, D. C., & Austad, T. (2000). Wettability alteration in chalk: 1. Preparation of core material and oil properties. *Journal of Petroleum Science and Engineering, 28(3), doi: http://dx.doi.org/10.1016/S0920-4105(00)00083-8*, 111-121.

Strand. (2005). *Wettability alteration in chalk: A study of surface chemistry (PhD).* Stavanger, Norway: University of Stavanger.

Strand, S. (2008b). *"Smart Water" for oil recovery from fractured limestone - A preliminary study.* Energy & Fuels, 22(5): 3126-3133.

Strand, S. P. (2008a). Effect of temperature on enhanced oil recovery from mixed-wet chalk cores by spontaneous imbibition and forced displacement, using seawater. *Energy & Fuels 2008, 22*, 3222-3225.

Strand, S. P. (2016). Water based EOR from clastic oil reservoirs by wettability alteration: A review of chemical aspects. *Journal of Petroleum Science and Engineering, 146.*, 1079-1091. doi:10.1016/j.petrol.2016.08.012

Strand, S. S. (2006). New wettability test for chalk based on chromatographic separation of SCN- and SO4. *Journal of Petroleum Science and Engineering, 52(1-4),* 187-197. doi:10.1016/j.petrol.2006.03.021.

Taber, J. J. (1997). EOR screening criteria revisited-part1: introduction to screening criteria and enhanced recovery field projects. *SPE Reservoir Engineering 12(3),* 189-198. Retrieved from http://dx.doi.org/10.2118/35385-pa

Taugbøl, K. (1995). *Chemical flooding of oil reservoirs. Low tension polymer water flood.* Dr. Sc. Thesis. Department of Chemistry, University of Bergen, Norway.

Tong, Z. X. (2002). Spontaneous Imbibition For Mixed-Wettability States In Sandstone Induced By Adsorption From Crude Oil. *Presented at the 7th International Symposium on Reservior Wettability.* Tasmania, Australia, 12-14 March.

Torrijos, I. D. (2017). *Enhanced oil recovery from Sandstones and Carbonates with "Smart Water"; (PhD).* Stavanger, Norway: Faculty of Science and Technology, Department of Petroleum Engineering.

Torsæter, O., & Abtahi, M. (2000). *EXPERIMENTAL RESERVOIR ENGINEERING LABORATORY WORK BOOK.* Norwegian University of Science and Technology: Department of Petroleum engineering and Applied Geophysics, August, 2000.

Treiber, L. A. (1972). Laboratory Evaluation of the Wettability of 50 Oil Producing Reservoirs. *SPE J., 12,*, 531-540.

Treiber, L. E., & Owens, W. W. (1972). A Laboratory Evaluation of the Wettability of Fifty Oil-Producing Reservoirs. *Society of Petroleum Engineers Journal, 12(06), 531-540. doi: 10.2118/3526-PA.*

Wakwaya, A. (2016). *Wettability in chalk, effect of initial water saturation (MSc Thesis).* Stavanger, Norway: University of Stavanger.

Willhite, G. P. (1986). *Waterflooding.* Monograph Series, SPE: Richardson, TX.

Wolcott, J. G.-G. (1993). Investigation of crude-oil/mineral interactions: influence of oil chemistry on wettability alteration,. *SPE International Symposium on Oilfield Chemistry.* Society of Petroleum Engineers.

Wu, Y. S. (2008). *An Experimental Study of Wetting Behavior and Surfactant EOR in Carbonates With Model Compounds.* doi: 10.2118/99612-PA.

Yousef, A. S.-S.-J. (2011). Smart WaterFlooding for Carbonate Reservoirs: Salinity and Role of Ions. *SPE Middle East Oil and Gas Show and Conference.* Manama, Bahrain: Society of Petroleum Engineers.

Yousef, A., Al-Saleh, S. & Al-Jawfi, M., S. (2012). The Impact of the Injection Water Chemistry on Oil Recovery from Carbonate Reservoirs. *SPE EOR Conference at Oil and Gas West Asia,16-18 April.* Muscat, Oman: Society of Petroleum

Engineers, SPE-141082-MS. Retrieved from http://dx.doi.org/10.2118/154077-MS

Zhang, P. T. (2006). Wettability alteration and improved oil recovery by spontaneous imbibition of seawater into chalk: Impact of the potential determining ions Ca2+, Mg2+, and SO42-. *Sience Direct*.

Zhanga, R. Z. (2016). Numerical simulation of waterflooding in natural fractured reservoirsbased on control volumefinite element method. *Journal of Petroleum Science and Engineering 146*.

Zolotuchin, A. B., & Ursin, J. R. (2000). *Introduction to petroleum reservoir engineering.* Kristiansand: Høyskoleforlaget AS.

Appendix A: Chemicals

A.1 Acid number solutions

Table 18. Chemicals used for AN measurements

Solution	Chemicals	Formula	Description
Titrant	KOH (> 85%) 2-propanol	KOH $CH_3CHOHCH_3$	2.8 g KOH (>85%) dilute to 1000 ml with 2-propanol ($CH_3CHOHCH_3$)
Spiking solution	Stearic acid Acid titration solvent	$CH_3(CH_2)_{16}COOH$	0.5 g Stearic Acid – $CH_3(CH_2)_{16}COOH$ dilute to 100 ml with Acid titration solvent
Standard solution	Potassium Hydrogen Phthalate, KHP DI water	$HOOCC_6H_4COOK$	0.2 g Potassium Hydrogen Phthalate, KHP diluted to 500 ml with DI water
Titration solvent	DI water 2-propanol Toluene	$CH_3CHOHCH_3$ $C_6H_5CH_3$	6 ml DI water dilute with 494 ml 2-propanol and with 500 ml Toluene
Electrode/Electrolyte	Potassium chloride DI water	KCl	Mettler DG-114 Electrode 3 M KCl in DI water

A.2 Base number (BN) solutions

Table 19. Chemicals used for BN measurements

Solution	Chemicals	Formula	Description
Titrant	Perchloric Acid (70%) Acetic Anhydride Acetic Acid	$HClO_4$ (70%) $(CH_3CO)_2O$ CH_3COOH	5 ml 70% Perchloric Acid ($HClO_4$) 15 ml Acetic Anhydride ((CH3CO)2O) dilute to 1000 ml with Acetic Acid (CH_3COOH)
Spiking solution	Quinoline Decane	C_9H_7N $CH_3(CH_2)_8CH_3$	0.5 g Quinoline (C_9H_7N) dilute to 100 ml with Decane ($C_{10}H_{22}$)
Standard solution	Potassium Hydrogen Phthalate, KHP Acetic Acid	$HOOCC_6H_4COOK$ CH_3COOH	0.2 g Potassium Hydrogen Phthalate, KHP diluted to 250 ml with Acetic Acid CH_3COOH
Titration solvent	Methyl Isobutyl Ketone, MIKB	$(CH_3)_2CHCH_2COCH_3$	Methyl Isobutyl Ketone (MIBK), ((CH3)2CHCHCOCH3)
Electrode/Electrolyte	Sodium Perchlorate, (solid) 2-propanol	$NaClO_4(s)$ $CH_3CHOHCH_3$	Mettler DG-113 Electrode Electrolyte: Saturated Sodium Perchloride, (NaClO4 (s)), in 2-propanol

Appendix B: Experimental data

B.1: Core data

Table 20. Summary of core data

Core (SK-)	*R1*	*R2*	*C1*	*C2*	*C3*	*C4*	*C5*	*C6*	*Mean*
Dry weight [gr]	109.1	107.68	104.1	107.15	106.19	108.33	105.36	105.97	106.735
Length [cm]	7.06	7.07	6.94	7.12	7.1	7.09	7.03	7.08	7.06125
Diameter [cm]	3.78	3.79	3.79	3.79	3.79	3.79	3.79	3.79	3.78875
Pore volume [ml]	37.53	39.17	38.34	39.8	37.99	38.51	39.9	39.91	38.89375
Porosity	47%	49%	49%	50%	47%	48%	50%	50%	49%
Initial water saturation	0.2	0.2	0.2	0.2	0.2	0.2	0.2	0.2	0.2
Permeability [mD]	4.02	4.09	4.12	4.16	4.25	4.97	4.30	4.33	4.28
1 PV/day	0.026	0.027	0.027	0.028	0.026	0.027	0.028	0.028	0.027
4 PV/day	0.104	0.109	0.107	0.111	0.106	0.107	0.111	0.111	0.108

B.2 Relative permeability calculation

Table 21. Calculation of q/ΔP for core SK-R1

Average ΔP calculation (SK-R1)				
q [ml/s]	0.000433333	0.000433333	0.000433333	
ΔP [mbar]	220.714584	220.669495	219.951141	
ΔP [atm]	0.217827637	0.217783138	0.21707418	0.217561652
q/ΔP		0.001991773		

Table 22. Calculation of q/ΔP for core SK-R2

Average ΔP calculation (SK-R2)				
q [ml/s]	0.0045	0.00045	0.00045	0.00045
ΔP [mbar]	217.558624	215.923538	218.640671	217.3742777
ΔP [atm]	0.214712957	0.213099258	0.215780851	0.214531022
q/ΔP		0.002097599		

Table 23. Calculation of q/ΔP for core SK-C3

Average ΔP calculation (SK-C3)				
q [ml/s]	0.000433333	0.000433333	0.000433333	0.000433333
ΔP [mbar]	184.681641	184.396072	184.058548	184.3787537
ΔP [atm]	0.21782764	0.21778314	0.21707418	0.217561653
q/ΔP		0.001991773		

Table 24. Data for effective, absolute and relative permeability

	SK-R1	*SK-R2*	*SK-C3*
Effective permeability (mD)	3.3707	3.536110309	4.0315
Absolute permeability (mD)	4.0187	4.0932	4.2514
Relative permeability (mD)	0.8388	0.8639	0.9483

B.3: Viscosity measurement data

Table 25. Viscosity measurement data for crude oils

Res 40 0.0	0.00239	0.00239	2.3922	2.3922
Res 40 0.35	0.00260	0.00260	2.6044	2.6044
Res 40 0.5	0.00266	0.00266	2.6556	2.6556
Res 40 original	0.00270	0.00270	2.6967	2.6967
Mean	0.00259	0.00259	2.5872	2.5872
Res 40 0.15	0.00289	2.8933		
Res 40 0.35	0.00354	3.5408		
Res 40 0.7	0.00293	2.9333		

Table 26. Viscosity measurement data for model oil mixtures

Marcol oil in %	*Kinetic viscosity [Pa·s]*	*Kinetic viscosity [cP]*
0		
10		
20		
30	0.00087	0.8703
40	0.00113	1.1300
45	0.00136	1.3567
50	0.00164	1.6383
60	0.00261	2.6067
70	0.00443	4.4344
59	0.0027	2.6700
60	0.00271	2.7100
61	0.00277	2.7744
62	0.00304	3.0433
100	0.0283	28.3444
60	0.00276	2.7611
58	0.00264	2.6378
58	0.00269	2.6867

Table 27. Viscosity measurements for water types

Name	*Temperature [°C]*	*Measure points*	*Shear rate [1/s]*	*Shear stress [Pa]*	*Viscosity [Pa·s]*
DI-water	23	1	500	0.428	0.000857
DI-water	23	2	281	0.239	0.00085
DI-water	23	3	158	0.133	0.000842
Mean					0.000850
Name	*Temperature [°C]*	*Measure points*	*Shear rate [1/s]*	*Shear stress [Pa]*	*Viscosity [Pa·s]*
DI-water	23	1	500	0.426	0.000851
DI-water	23	2	281	0.237	0.000844
DI-water	23	3	158	0.132	0.000835
Mean					0.000843

Name	*Temperature [°C]*	*Measure points*	*Shear rate [1/s]*	*Shear stress [Pa]*	*Viscosity [Pa·s]*
DI-water	23	1	500	0.422	0.000845
DI-water	23	2	281	0.238	0.000845
DI-water	23	3	158	0.133	0.000839
Mean					0.000843
Name	*Temperature [°C]*	*Measure points*	*Shear rate [1/s]*	*Shear stress [Pa]*	*Viscosity [Pa·s]*
Seawater	23	1	500	0.514	0.00103
Seawater	23	2	281	0.288	0.00103
Seawater	23	3	158	0.162	0.00102
Mean					0.00103
Name	*Temperature [°C]*	*Measure points*	*Shear rate [1/s]*	*Shear stress [Pa]*	*Viscosity [Pa·s]*
Seawater	23	1	500	0.513	0.00103
Seawater	23	2	281	0.287	0.00102
Seawater	23	3	158	0.161	0.00102
Mean					0.00102
Name	*Temperature [°C]*	*Measure points*	*Shear rate [1/s]*	*Shear stress [Pa]*	*Viscosity [Pa·s]*
Seawater	23	1	500	0.51	0.00102
Seawater	23	2	281	0.286	0.00102
Seawater	23	3	158	0.161	0.00102
Mean					0.00102
DI-water		0.000845			
Seawater		0.00102			

B.4 IFT measurement data

Table 28. Interfacial tension measurements

	(mN/m)	
DI water	72	
n-Heptane	33.75	
Res 40 0.0	27.25	
Res 40 0.35	17.25	
Res 40 0.7	17.00	
Res 40	14.25	
40% Marcol	37.5	*60% n-heptane*
50% Marcol	38	*50% n-heptane*
58% Marcol	41	*42% n-heptane*
59% Marcol	42	*41% n-heptane*
60% Marcol	42.5	*40% n-heptane*
61% Marcol	42.5	*39% n-heptane*
62% Marcol	43.25	*38% n-heptane*

70% Marcol	40	*30% n-heptane*
100% Marcol	45	*0% n-heptane*
58% Marcol (RES40-0.7)	32	After forced displacement (SK-C1)
58% Marcol (RES40-0.3)	27	After forced displacement (SK-C2)
58% Marcol (RES40-0.1)	27	After forced displacement (SK-C3)
58% Marcol (RES40-0.7)	30	After forced displacement (SK-C4)
58% Marcol (RES40-0.3)	28	After forced displacement (SK-C5)
58% Marcol (RES40-0.1)	-	To small amount (SK-C6)
RES 40-0.15	26	
RES 40-0.34	23	
RES 40-0.68	18	

B.5 AN and BN data

Table 29. Crude oil fractions

Fraction-RES40	*Fraction RES40-0*	*Res40-0.15, AN*
0.030	0.970	0.146466667
Res 40 Vol (L)	*Res 40-0 Vol (L)*	*RES40-0.15 Vol (L)*
0.030	0.970	1

Table 30. Determination of AN values for crude oils used in project

	RES40-0.34	*RES40-0.15*	*RES40-0.68*	*RES 40-0*	*RES 40*
	0.34	0.12	0.65	0	2.43
	0.35	0.14	0.7	0.07	2.38
	0.35	0.16	0.67	0.08	2.4
	0.28	0.17	0.65	0.08	
	0.39				
mean	0.34	0.15	0.67	0.06	2.40

Table 31. Determination of BN values for crude oils used in project

	RES40-0.34	*RES40-0.15*	*RES40-0.68*	*RES 40-0*	*RES 40*
	0.17	0.3	0.35	0.05	0.82
	0.19	0.27	0.4	0.1	0.95
	0.19	0.22	0.39	-0.03	0.9
			0.23		
mean	0.18	0.26	0.34	0.04	0.89

B.6 pH Data

Table 32. pH measured data for different brines

DVBOS	*VBOS*	*SW*	*SW0T*	*SW1/2T*	*DI*
7.5	7.24	7.64	7.62	7.61	6.16

B.7: Density measurement data in g/cm3

Table 33. Density measured data for different brines

DVBOS	*VBOS*	*SW*	*SW0T*	*SW1/2T*	*DI*

1.00209	1.04061	1.02214	1.02148	1.02156	0.99749
1.0021	1.04133	1.02218	1.02161	1.02162	0.99759
1.0021	1.04139	1.02217	1.02161	1.02162	0.9976

Table 34. Density measured data for crude oils

	RES 40-0	*RES 40*	*RES40-0.68*	*RES40-0.34*	*RES40-0.15*
	0.80756	0.81733	0.81641	0.81323	0.81742
	0.8103	0.82015	0.81755	0.81345	0.81744
	0.81047	0.82107	0.81725	0.81367	0.81767
			0.81729	0.81368	0.81768
Mean	***0.809***	***0.820***	***0.817***	***0.814***	***0.818***

Table 35. Density measured data for model oil mixtures

n-Heptane	0.68627	0.68447	0.684
30% Marcol	0.73371	0.73406	0.73409
40% Marcol	0.75505	0.75253	0.75299
45% Marcol	0.76319	0.76163	0.76259
50% Marcol	0.76882	0.76988	0.76877
55% Marcol	0.77702	0.77754	0.77837
60% Marcol	0.78489	0.7864	0.78636
70% Marcol	0.80075	0.80189	0.80171
100% Marcol	0.84922	0.84715	0.84703
58% Marcol	0.78317	0.7832	0.7837

B.8: Spontaneous imbibition (SI) data

Table 36. Spontaneous imbibition data for chalk core SK-R1

Time (min)	*Produced oil (ml)*	*Oil recovery (%OOIP)*	*Time (days)*
0	0.00	0.00	0.0000
1	5.00	16.47	0.0007
2	11.50	37.88	0.0014
3	13.50	44.47	0.0021
4	14.50	47.76	0.0028
5	15.00	49.41	0.0035
10	17,50	57.64	0.0069
15	18.50	60.94	0.0104
30	19.30	63.57	0.0208
45	19.50	64.23	0.0313
75	19.90	65.55	0.0521
135	20.00	65.88	0.0938
195	20.00	65.88	0.1354
255	20.00	65.88	0.1771
375	20.00	65.88	0.2604
1125	20.10	66.21	0.7813
1281	20.10	66.21	0.8896
1981	20.30	66.86	1.3757
2663	20.30	66.86	1.8493

Table 37. Spontaneous imbibition data for chalk core SK-R2

Time (min)	*Produced oil (ml)*	*Oil recovery (%OOIP)*	*time (days)*
0	0.00	0.00	0.0000
1	4.10	13.00	0.0007
2	7.00	22.19	0.0014
3	9.50	30.12	0.0021
4	10.50	33.29	0.0028
5	14.50	45.97	0.0035
10	14.70	46.60	0.0069
15	16.00	50.72	0.0104
30	18.90	59.92	0.0208
45	20.00	63.40	0.0313
60	21.50	68.16	0.0417
120	21.50	68.16	0.0833
180	22.00	69.74	0.1250
268	22.00	69.74	0.1861
388	23.00	72.91	0.2694
508	23.60	74.82	0.3528
1258	23.60	74.82	0.8736
1858	23.60	74.82	1.2903
2760	23.60	74.82	1.9167

Table 38. Spontaneous imbibition data for chalk core SK-C3

Time (min)	*Produced oil (ml)*	*Oil recovery (%OOIP)*	*Time (days)*
0	0	0	0
1	2.7	8.874572706	0.000694444
2	3.3	10.84669997	0.001388889
3	5.1	16.76308178	0.002083333
4	7.9	25.96634236	0.002777778
5	9.4	30.89666053	0.003472222
10	13.8	45.35892716	0.006944444
15	15.7	51.60399684	0.010416667
30	17.5	57.52037865	0.020833333
60	18.4	60.47856955	0.041666667
120	19	62.45069682	0.083333333
180	19.1	62.7793847	0.125
1392	19.3	63.43676045	0.966666667
2976	19.3	63.43676045	2.066666667
4383	19.3	63.43676045	3.04375
7200	19.3	63.43676045	5

Table 39. Spontaneous imbibition data for chalk core SK-C6

Time (min)	*Produced oil (ml)*	*Oil recovery (%OOIP)*	*Time (days)*
0	0	0	0
1	0.4	1.252818842	0.000694444
2	0.5	1.566023553	0.001388889
3	0.7	2.192432974	0.002083333
4	1	3.132047106	0.002777778

5	1.8	5.637684791	0.003472222
10	2.9	9.082936607	0.006944444
15	4.5	14.09421198	0.010416667
30	8.3	25.99599098	0.020833333
60	11	34.45251817	0.041666667
120	14.3	44.78827362	0.083333333
180	15.5	48.54673014	0.125
300	15.9	49.79954899	0.208333333
720	17.4	54.49761964	0.5
1380	17.8	55.75043849	0.958333333
1560	17.8	55.75043849	1.083333333
1813	18	56.37684791	1.259027778
2115	18	56.37684791	1.46875
2900	18.2	57.00325733	2.013888889
4260	18.5	57.94287146	2.958333333
6979	18.5	57.94287146	4.846527778
8386	18.5	57.94287146	5.823611111
11520	18.5	57.94287146	8

B.9: Forced imbibition (FI) data

Table 40. Forced imbibition data for chalk core SK-R1

Date	Time	Brine inj. (ml)	PV corr	pH	Oil produced (ml) 1PV	Oil produced (ml)4PV	%OOIP	ΔP (mBar)
7-Feb-19	11:20	0.00	-0.08		0.00		0.00	231.0
7-Feb-19	11:35	0.39	-0.07		0.00		0.00	180.0
7-Feb-19	12:00	1.04	-0.06		0.00		0.00	163.0
7-Feb-19	12:15	1.43	-0.05		0.00		0.00	155.0
7-Feb-19	13:00	2.60	-0.01		0.00		0.00	149.0
7-Feb-19	13:20	3.12	0.00		0.00		0.00	142.0
7-Feb-19	13:36	3.54	0.01		0.10		0.33	135.0
7-Feb-19	13:54	4.00	0.02		0.60		2.00	138.0
7-Feb-19	14:15	4.55	0.04		1.20		4.00	133.0
7-Feb-19	14:32	4.99	0.05		1.50		5.00	134.0
7-Feb-19	14:43	5.28	0.06		1.80		6.00	131.0
7-Feb-19	15:00	5.72	0.07		2.10		6.99	130.0
7-Feb-19	15:30	6.50	0.09		3.00		9.99	129.0
7-Feb-19	15:58	7.23	0.11		3.60		11.99	134.0
7-Feb-19	16:29	8.03	0.13		4.40		14.65	137.0
7-Feb-19	16:58	8.79	0.15		5.20		17.32	141.0
7-Feb-19	17:27	9.54	0.17		6.00		19.98	149.0
7-Feb-19	18:00	10.40	0.19		6.60		21.98	156.0
7-Feb-19	18:36	11.34	0.22		7.60		25.31	173.0
7-Feb-19	18:55	11.83	0.23		8.00		26.65	185.0
7-Feb-19	19:24	12.58	0.25		8.80		29.31	205.0
7-Feb-19	19:54	13.36	0.27		9.60		31.97	239.0
7-Feb-19	20:25	14.17	0.29		10.40		34.64	282.0
7-Feb-19	20:59	15.05	0.32		11.20		37.30	352.0
7-Feb-19	21:20	15.60	0.33		11.80		39.30	413.0
7-Feb-19	21:54	16.48	0.36		12.70		42.30	677.0
8-Feb-19	22:15	17.03	0.37		13.20		43.96	1350.0

8-Feb-19	08:24	32.86	0.79		18.60		61.95	1252.0
8-Feb-19	09:15	34.19	0.83		18.60		61.95	1232.0
8-Feb-19	10:10	35.62	0.87		18.80		62.62	1227.0
8-Feb-19	11:02	36.97	0.90		18.80		62.62	1209.0
8-Feb-19	12:10	38.74	0.95		19.00		63.28	1194.0
8-Feb-19	13:00	40.04	0.98		19.20		63.95	1180.0
8-Feb-19	13:37	41.00	1.01		19.30		64.28	1178.0
8-Feb-19	14:05	41.73	1.03		19.30		64.28	1177.0
8-Feb-19	14:55	43.03	1.06	7,98	19.40		64.61	1167.0
8-Feb-19	17:09	46.51	1.16		19.50		64.95	1151.0
8-Feb-19	19:00	49.40	1.23		19.60		65.28	1150.0
8-Feb-19	20:30	51.74	1.30	8,02	19.60		65.28	1132.0
8-Feb-19	22:30	54.86	1.38		19.70		65.61	1116.0
9-Feb-19	07:59	69.65	1.77	8,01	19.90		66.28	1060.0
9-Feb-19	10:53	74.18	1.89		19.95		66.45	1056.0
9-Feb-19	14:10	79.30	2.03		20.00		66.61	1042
9-Feb-19	17:08	83.93	2.15		20.40		67.95	1028
9-Feb-19	20:04	88.50	2.28	7,83	20.40		67.95	1014
9-Feb-19	22:06	91.68	2.36		20.40		67.95	1008
10-Feb-19	10:04	110.34	2.86		20.40		67.95	959
10-Feb-19	13:57	116.40	3.02		20.40		67.95	947
10-Feb-19	18:08	122.93	3.19	7,76	20.50		68.28	929
10-Feb-19	22:00	128.96	3.35		20.50		68.28	916
11-Feb-19	08:29	145.31	3.79		20.50		68.28	875
11-Feb-19	12:05	150.93	3.94		20.50		68.28	863
11-Feb-19	15:30	156.26	4.08		20.50		68.28	848
12-Feb-19	09:13	183,90	4.82		20.50		68.28	777
12-Feb-19	12:06	188.40	4.94		20.50		68.28	776
12-Feb-19	15:31	193.73	5.08		20.50		68.28	766
13-Feb-19	08:59	220.97	5.80		20.50		68.28	712
13-Feb-19	13:40	228.28	6.00		20.50		68.28	714
13-Feb-19	15:41	231.43	6.08		20.50		68.28	692
13-Feb-19	18:23	235.64	6.20		20.50		68.28	668
13-Feb-19	20:10	238.42	6.27		20.50		68.28	662
14-Feb-19	06:35	254.67	6.70		20.50		68.28	662
14-Feb-19	06:59	255.29	6.72		20.50		68.28	660
14-Feb-19	08:26	257.56	6.78		20.50		68.28	650
14-Feb-19	08:31	257.69	6.78		20.50		68.28	651
14-Feb-19	08:45	258.05	6.79		20.50		68.28	658
14-Feb-19	09:09	258.67	6.81		20.50		68.28	659
14-Feb-19	09:59	259.97	6.84		20.50	0.05	68.45	1312
14-Feb-19	10:32	260.83	6.87		20.50	0.1	68.61	1288
14-Feb-19	11:06	261.72	6.89		20.50	0.1	68.61	1258
14-Feb-19	11:32	262.39	6.91		20.50	0.1	68.61	1257
14-Feb-19	11:57	263.04	6.93		20.50	0.1	68.61	1269
14-Feb-19	13:15	265.07	6.98		20.50	0.1	68.61	1223
14-Feb-19	14:33	267.10	7.03		20.50	0.1	68.61	1219
14-Feb-19	15:17	268.24	7.06		20.50	0.1	68.61	1208
14-Feb-19	15:58	269.31	7.09		20.50	0.1	68.61	1187
14-Feb-19	17:59	272.45	7.18		20.50	0.1	68.61	1172
14-Feb-19	19:08	274.25	7.22		20.50	0.1	68.61	1170
14-Feb-19	19:49	275.31	7.25		20.50	0.1	68.61	1171
14-Feb-19	20:43	276.72	7.29		20.50	0.1	68.61	1170

Table 41. Forced imbibition data for chalk core SK-R2

Date	*Time*	*Brine inj. (ml)*	*PV corr*	*pH*	*Oil produced (ml) 1PV*	*Oil produced (ml)4PV*	*%OOIP*	*ΔP (mBar)*
19-Feb-19	11:28	0.00	-0.08		0.00		0.00	397.0
19-Feb-19	12:00	0.86	-0.06		0.00		0.00	162.0
19-Feb-19	12:30	1.67	-0.04		0.00		0.00	148.0
19-Feb-19	13:00	2.48	-0.02		0.00		0.00	155.0
19-Feb-19	13:26	3.19	0.00		0.00		0.00	148.0
19-Feb-19	13:39	3.54	0.01		0.20		0.64	150.0
19-Feb-19	14:15	4.51	0.03		1.00		3.19	144.0
19-Feb-19	14:33	4.99	0.05		1.60		5.11	140.0
19-Feb-19	14:55	5.59	0.06		2.20		7.02	139.0
19-Feb-19	15:30	6.53	0.09		3.00		9.57	136.0
19-Feb-19	16:16	7.78	0.12		4.30		13.72	133.0
19-Feb-19	17:37	9.96	0.17		6.40		20.42	127.0
19-Feb-19	18:10	1.85	0.20		7.20		22.98	133.0
19-Feb-19	18:36	1.56	0.21		7.80		24.89	139.0
19-Feb-19	18:59	12.18	0.23		8.50		27.13	148.0
19-Feb-19	19:30	13.01	0.25		9.30		29.68	167.0
19-Feb-19	20:00	13.82	0.27		10.10		32.23	190.0
19-Feb-19	20:42	14.96	0.30		11.10		35.42	242.0
19-Feb-19	21:10	15.71	0.32		11.90		37.98	295.0
19-Feb-19	21:45	16.66	0.34	7.43	12.70		40.53	388.0
20-Feb-19	08:10	33.53	0.77		20.00		63.82	1186.0
20-Feb-19	08:59	34.86	0.81		20.60		65.74	1177.0
20-Feb-19	10:02	36.56	0.85		20.80		66.38	1169.0
20-Feb-19	10:57	38.04	0.89		20.90		66.70	1154.0
20-Feb-19	12:00	39.74	0.93		21.00		67.02	1143.0
20-Feb-19	13:28	42.12	0.99		21.20		67.65	1137.0
20-Feb-19	15:11	44.90	1.06		21.60		68.93	1115.0
20-Feb-19	17:35	48.79	1.16		21.60		68.93	1101.0
20-Feb-19	19:00	51.08	1.22		21.60		68.93	1094.0
20-Feb-19	20:21	53.27	1.28	7.82	21.60		68.93	1086.0
21-Feb-19	09:14	74.14	1.81		22.20		70.85	1023.0
21-Feb-19	11:00	77.00	1.88		22.20		70.85	1018.0
21-Feb-19	13:18	80.73	1.98		22.20		70.85	1011.0
21-Feb-19	14:58	83.43	2.05		22.20		70.85	1001.0
21-Feb-19	15:58	85.05	2.09		22.20		70.85	999.0
21-Feb-19	20:22	92.18	2.27	7.69	22.50		71.80	985.0
21-Feb-19	20:47	92.85	2.29		22.50		71.80	979.0
22-Feb-19	08:37	112.02	2.78		22.50		71.80	945.0
22-Feb-19	09:02	112.70	2.80	7.73	22.50		71.80	944.0
22-Feb-19	10:45	115.48	2.87		22.50		71.80	932.0
22-Feb-19	13:37	120.12	2.99		22.50		71.80	932.0
22-Feb-19	15:35	123.31	3.07		22.50		71.80	922.0
22-Feb-19	19:00	128.84	3.21		22.50		71.80	920
22-Feb-19	22:10	133.97	3.34		22.50		71.80	911
23-Feb-19	00:00	136.94	3.41		22.50		71.80	909
23-Feb-19	08:00	149.90	3.75		22.50		71.80	893
23-Feb-19	10:00	153.14	3.83		22.50		71.80	889

23-Feb-19	12:00	156.38	3.91		22.50		71.80	884
23-Feb-19	13:22	158.60	3.97	7.75	22.50		71.80	868
24-Feb-19	09:53	191.84	4.82		22.50		71.80	830
25-Feb-19	08:18	228.15	5.74		22.50		71.80	828
25-Feb-19	08:44	228.85	5.76	7.76	22.50		71.80	828
25-Feb-19	09:27	230.01	5.79		22.50	0.0	71.80	1342
25-Feb-19	10:56	232.42	5.85		22.50	0.0	71.80	1297
25-Feb-19	13:43	236.93	5.97		22.50	0.0	71.80	1258
25-Feb-19	15:20	239.54	6.03		22.50	0.1	72.12	1256
25-Feb-19	15:38	240.03	6.05	8.28	22.50	0.1	72.12	1250
26-Feb-19	08:25	267.22	6.74		22.50	0.1	72.12	1202
26-Feb-19	09:46	269.41	6.80		22.50	0.1	72.12	1208
26-Feb-19	10:10	270.05	6.81	8.24	22.50	0.1	72.12	1202
26-Feb-19	12:39	274.08	6.92		22.50	0.1	72.12	1202
26-Feb-19	15:22	278.48	7.03		22.50	0.1	72.12	1195
26-Feb-19	17:21	281.69	7.11		22.50	0.1	72.12	1194
26-Feb-19	19:15	284.77	7.19		22.50	0.1	72.12	1195
26-Feb-19	21:45	288.82	7.29		22.50	0.1	72.12	1195

Table 42. Forced imbibition data for chalk core SK-C3

Date	*Time*	*Brine inj. (ml)*	*PV corr*	*pH*	*Oil produced (ml) 1PV*	*Oil produced (ml)4PV*	*%OOIP*	*ΔP (mBar)*
19-Mar-19	10:27	0.00	-0.08		0.00		0,00	388
19-Mar-19	11:00	0.86	-0.06		0.00		0,00	368
19-Mar-19	11:59	2.39	-0.02		0.00		0,00	300
19-Mar-19	12:22	2.99	0.00		0.00		0.00	318
19-Mar-19	12:32	3.25	0.01		0.30		0.99	325
19-Mar-19	13:17	4.42	0.04		1.20		3.95	336
19-Mar-19	13:37	4.94	0.05		1.60		5.26	342
19-Mar-19	14:20	6.06	0.08		2.60		8.55	362
19-Mar-19	15:07	7.28	0.11		3.70		12.17	394
19-Mar-19	16:22	9.23	0,.16		5.40		17.77	449
19-Mar-19	16:55	10.09	0.19		6.20		20.40	484
19-Mar-19	17:40	11.26	0.22		7.30		24.02	538
19-Mar-19	18:19	12.27	0.24		8.20		26.98	584
19-Mar-19	18:51	13.10	0.27		9.00		29.61	631
19-Mar-19	19:30	14.12	0.29		10.00		32.90	683
19-Mar-19	20:05	15.03	0.32		10.80		35.54	749
19-Mar-19	20:34	15.78	0.34		11.50		37.84	775
19-Mar-19	21:09	16.69	0.36		12.40		40.80	786
19-Mar-19	21:30	17.24	0.38		13.00		42.77	792
19-Mar-19	21:58	17.97	0.39	7.43	13.60		44.75	798
20-Mar-19	08:32	34.45	0.83		18.00		59.23	649
20-Mar-19	09:35	36.09	0.87		18.20		59.88	647
20-Mar-19	10:23	37.34	0.90		18.30		60.21	641
20-Mar-19	11:20	38.82	0.94		18.40		60.54	635
20-Mar-19	12:19	40.35	0.98		18.50		60.87	623
20-Mar-19	13:15	41.81	1.02		18.60		61.20	594
20-Mar-19	14:11	43.26	1.06		18.60		61.20	602
20-Mar-19	15:09	44.77	1.10		18.70		61.53	584
20-Mar-19	16:28	46.83	1.15		18.90		62.19	589

20-Mar-19	16:58	47.61	1.17		18.90		62.19	588
20-Mar-19	18:00	49.22	1.22		19.10		62.85	562
20-Mar-19	18:59	50.75	1.26		19.10		62.85	544
20-Mar-19	19:56	52.23	1.30	7.40	19.10		62.85	542
20-Mar-19	21:00	53.90	1.34		19.20		63.17	540
20-Mar-19	21:58	55.41	1.38	7.46	19.20		63.17	530
21-Mar-19	08:27	71.76	1.81	7.48	19.70		64.82	508
21-Mar-19	11:58	77.25	1.95		19.80		65.15	498
21-Mar-19	12:55	78.73	1.99		19.90		65.48	491
21-Mar-19	14:37	81.38	2.06		20.00		65.81	488
21-Mar-19	16:43	84.66	2.15	7.41	20.10		66.14	488
21-Mar-19	17:44	86.24	2.19		20.10		66.14	481
21-Mar-19	19:03	88.30	2.25		20.10		66.14	473
22-Mar-19	09:00	110.06	2.82	7.38	20.30		66.79	460
22-Mar-19	11:27	113.88	2.92		20.40		67.12	462
22-Mar-19	13:53	117.68	3.02		20.40		67.12	463
22-Mar-19	15:42	120.51	3.09	7.38	20.40		67.12	455
22-Mar-19	19:50	126.96	3.26		20.40		67.12	456
23-Mar-19	12:07	152.36	3.93	7.40	20.50		67.45	455
23-Mar-19	12:25	152.83	3.94	7.43	20.50	0,0	67.45	818
23-Mar-19	13:00	153.74	3.97		20.50	0,3	68.44	1453
23-Mar-19	14:21	155.84	4.02		20.50	0,8	70.08	1343
24-Mar-19	07:00	181.82	4.71		20.50	2,3	75.02	1157
24-Mar-19	08:00	183.38	4.75		20.50	2,3	75.02	1168
24-Mar-19	09:00	184.94	4.79		20.50	2,3	75.02	1149
24-Mar-19	10:00	186.50	4.83		20.50	2,3	75.02	1150
24-Mar-19	11:00	188.06	4.87		20.50	2,3	75.02	1150
24-Mar-19	11:58	189.57	4.91		20.50	2,3	75.02	1150
24-Mar-19	12:08	189.83	4.92		20.50	2,3	75.02	1150
24-Mar-19	12:31	190.42	4.93		20.50	2,3	75.02	1150

Table 43. Forced imbibition data for chalk core SK-C6

Date	*Time*	*Brine inj. (ml)*	*PV corr*	*pH*	*Oil produced (ml) 1PV*	*Oil produced (ml)4PV*	*%OOIP*	*ΔP (mBar)*
19-Mar-19	08:52	0.00	-0.26		0.00		57.94	353
19-Mar-19	09:21	0.81	-0.24		0.00		57.94	426
19-Mar-19	09:48	1.57	-0.22		0.00		57.94	440
19-Mar-19	10:25	2.60	-0.20		0.00		57.94	474
19-Mar-19	10:53	3.39	-0.18		0.00		57.94	468
19-Mar-19	11:15	4.00	-0.16		0.00		57.94	474
19-Mar-19	11:52	5.04	-0.13		0.00		57.94	491
19-Mar-19	12:26	5.99	-0.11		0.00		57.94	503
19-Mar-19	12:43	6.47	-0.10		0.00		57.94	507
19-Mar-19	13:18	7.45	-0.07		0.00		57.94	513
19-Mar-19	14:23	9.27	-0.03		0.00		57.94	519
19-Mar-19	15:04	10.42	0.00		0.00		57.94	486
19-Mar-19	16:27	12.74	0.06		0.10		58.26	501
19-Mar-19	17:32	14.56	0.10		0.10		58.26	505
19-Mar-19	18:41	16.49	0.15		0.20		58.57	514
19-Mar-19	19:20	17.58	0.18		0.20		58.57	521
19-Mar-19	20:22	19.32	0.22		0.30		58.88	521

19-Mar-19	20:58	20.33	0.25		0.30		58.88	512
19-Mar-19	21:41	21.53	0.28		0.30		58.88	506
19-Mar-19	08:54	40.38	0.75	7.52	0.40		59.20	487
20-Mar-19	09:44	41.78	0.79		0.40		59.20	486
20-Mar-19	10:34	43.18	0.82		0.50		59.51	484
20-Mar-19	11:31	44.77	0.86		0.50		59.51	488
20-Mar-19	12:51	47.01	0.92	7.75	0.50		59.51	491
20-Mar-19	16:00	52.30	1.05	7.76	0.50		59.51	514
20-Mar-19	19:40	58.46	1.20	7.88	0.50		59.51	516
20-Mar-19	23:02	64.12	1.35		0.50		59.51	462
20-Mar-19	10:11	82.85	1.81		0.60		59.82	449
20-Mar-19	12:30	86.74	1.91	7.88	0.60		59.82	459
20-Mar-19	16:01	92.65	2.06		0.60		59.82	459
20-Mar-19	22:59	104.36	2.35		0.60		59.82	459
20-Mar-19	09:13	121.55	2.78	7.87	0.60		59.82	446
20-Mar-19	09:28	121.97	2.79		0.60	0.0	59.82	445
20-Mar-19	09:31	122.05	2.80		0.60	0.0	59.82	1292
20-Mar-19	15:07	131.46	3.03	8.17	0.60	0.4	61.07	1170
21-Mar-19	19:48	139.33	3.23		0.60	0.6	61.70	1119
21-Mar-19	22:12	143.36	3.33		0.60	0.6	61.70	1074
21-Mar-19	08:01	159.85	3.74		0.60	0.6	61.70	1040
21-Mar-19	09:00	161.50	3.79		0.60	0.6	61.70	1040
21-Mar-19	09:24	162.18	3.80		0.60	0.6	61.70	1040
21-Mar-19	12:07	166.74	3.92		0.60	0.6	61.70	1031
21-Mar-19	14:07	170.10	4.00		0.60	0.6	61.70	1033
22-Mar-19	16:15	173.68	4.09		0.60	0.6	61.70	1031
22-Mar-19	17:42	176.12	4.15		0.60	0.6	61.70	1033
22-Mar-19	18:47	177.94	4.20		0.60	0.6	61.70	1025
22-Mar-19	20:33	180.91	4.27		0.60	0.6	61.70	1026
22-Mar-19	06:00	196.78	4.67		0.60	0.7	62.01	968
23-Mar-19	09:23	202.47	4.81		0.60	0.7	62.01	952
23-Mar-19	14:23	210.87	5.02		0.60	0.7	62.01	864
23-Mar-19	19:18	219.13	5.23		0.60	0.7	62.01	886
23-Mar-19	23:44	226.58	5.42		0.60	0.7	62.01	886
24-Mar-19	05:04	235.54	5.64		0.60	0.7	62.01	888
24-Mar-19	07:35	239.76	5.75		0.60	0.7	62.01	888
24-Mar-19	08:41	241.61	5.79		0.60	0.7	62.01	888
24-Mar-19	09:30	242.98	5.83		0.60	0.7	62.01	888
24-Mar-19	09:51	243.57	5.84		0.60	0.7	62.01	888
24-Mar-19	10:30	244.66	5.87		0.60	0.7	62.01	888
24-Mar-19	12:00	247.18	5.93		0.60	0.7	62.01	888
24-Mar-19	13:42	250.04	6.00		0.60	0.7	62.01	888
24-Mar-19	15:05	252.36	6.06		0.60	0.7	62.01	888
24-Mar-19	18:54	258.78	6.22		0.60	0.7	62.01	888
Oil produced from SI=18,5 ml								

B.10: CWT data

Table 44. CWT flooding data for core SK-R1

	Weight of Glass [g]	*Weight of Glass [g]*	*Volume Injected [ml]*	*PV per sample*	*PV injected*	*PV corrected for midpoints*
Sample #	*Before Test*	*After Test*				
1	9.05	12.12	3.08	0.08	0.08	0.04
2	8.4	11.45	3.06	0.08	0.16	0.12
3	8.98	12	3.03	0.08	0.24	0.20
4	9.03	12.05	3.03	0.08	0.32	0.28
5	8.47	11.51	3.05	0.08	0.41	0.36
6	8.46	11.49	3.04	0.08	0.49	0.45
7	9.05	12.05	3.01	0.08	0.57	0.53
8	8.95	12	3.06	0.08	0.65	0.61
9	8.42	11.48	3.07	0.08	0.73	0.69
10	8.4	11.42	3.03	0.08	0.81	0.77
11	8.39	11.43	3.05	0.08	0.89	0.85
12	9.07	12.09	3.03	0.08	0.97	0.93
13	8.35	11.37	3.03	0.08	1.05	1.01
14	8.52	11.55	3.04	0.08	1.13	1.09
15	8.38	11.39	3.02	0.08	1.21	1.17
16	8.95	11.99	3.05	0.08	1.30	1.25
17	9.15	12.15	3.01	0.08	1.38	1.34
18	8.81	11.84	3.04	0.08	1.46	1.42
19	8.47	11.49	3.03	0.08	1.54	1.50
20	8.92	11.95	3.04	0.08	1.62	1.58
21	8.48	11.49	3.02	0.08	1.70	1.66
22	9.08	12.08	3.01	0.08	1.78	1.74
23	9.52	12.56	3.05	0.08	1.86	1.82
24	8.41	11.45	3.05	0.08	1.94	1.90
25	9.08	12.08	3.01	0.08	2.02	1.98
26	8.97	12.01	3.05	0.08	2.10	2.06
27	8.42	11.43	3.02	0.08	2.18	2.14
28	8.34	11.36	3.03	0.08	2.26	2.22
29	8.44	11.48	3.05	0.08	2.35	2.30
30	8.39	11.42	3.04	0.08	2.43	2.39
31	8.89	11.93	3.05	0.08	2.51	2.47
32	8.38	11.37	3.00	0.08	2.59	2.55
33	9.62	12.65	3.04	0.08	2.67	2.63
34	8.95	11.97	3.03	0.08	2.75	2.71
35	8.4	11.44	3.05	0.08	2.83	2.79
36	8.49	11.5	3.02	0.08	2.91	2.87
37	8.95	11.96	3.02	0.08	2.99	2.95
38	8.42	11.47	3.06	0.08	3.07	3.03
39	8.38	11.39	3.02	0.08	3.15	3.11
40	8.41	11.45	3.05	0.08	3.23	3.19
41	8.42	11.46	3.05	0.08	3.31	3.27
42	9.09	12.12	3.04	0.08	3.40	3.35
43	8.96	12.02	3.07	0.08	3.48	3.44
44	9.09	12.1	3.02	0.08	3.56	3.52

Table 45. CWT flooding data for core SK-R2

	Weight of Glass [g]	*Weight of Glass [g]*	*Volume Injected [ml]*	*PV per sample*	*PV injected*	*PV corrected for midpoints*
Sample #	*Before Test*	*After Test*				
1	8.93	11.97	3.05	0.08	0.08	0.04
2	8.44	11.36	2.93	0.07	0.15	0.11
3	8.44	11.43	3.00	0.08	0.23	0.19
4	8.38	11.39	3.02	0.08	0.31	0.27
5	8.4	11.39	3.00	0.08	0.38	0.34
6	9.01	12.04	3.04	0.08	0.46	0.42
7	8.98	11.98	3.01	0.08	0.54	0.50
8	8.44	11.47	3.04	0.08	0.61	0.58
9	9.09	12.09	3.01	0.08	0.69	0.65
10	8.48	11.49	3.02	0.08	0.77	0.73
11	9	11.99	3.00	0.08	0.84	0.81
12	8.42	11.44	3.03	0.08	0.92	0.88
13	9.08	12.06	2.99	0.08	1.00	0.96
14	8.99	12	3.02	0.08	1.08	1.04
15	9.15	12.18	3.04	0.08	1.15	1.11
16	8.46	11.46	3.01	0.08	1.23	1.19
17	8.45	11.46	3.02	0.08	1.31	1.27
18	8.36	11.39	3.04	0.08	1.38	1.35
19	9.02	12.02	3.01	0.08	1.46	1.42
20	8.43	11.45	3.03	0.08	1.54	1.50
21	8.42	11.44	3.03	0.08	1.62	1.58
22	8.45	11.47	3.03	0.08	1.69	1.65
23	9.09	12.08	3.00	0.08	1.77	1.73
24	8.43	11.45	3.03	0.08	1.85	1.81
25	8.43	11.45	3.03	0.08	1.92	1.89
26	8.38	11.4	3.03	0.08	2.00	1.96
27	8.53	11.58	3.06	0.08	2.08	2.04
28	8.4	11.42	3.03	0.08	2.16	2.12
29	8.49	11.59	3.11	0.08	2.24	2.20
30	9.11	12.13	3.03	0.08	2.31	2.27
31	8.49	11.48	3.00	0.08	2.39	2.35
32	8.35	11.4	3.06	0.08	2.47	2.43
33	8.44	11.46	3.03	0.08	2.55	2.51
34	8.39	11.4	3.02	0.08	2.62	2.58
35	8.41	11.42	3.02	0.08	2.70	2.66
36	8.41	11.43	3.03	0.08	2.78	2.74
37	9.02	12.01	3.00	0.08	2.85	2.81
38	8.5	11.54	3.05	0.08	2.93	2.89
39	8.54	11.57	3.04	0.08	3.01	2.97
40	8.48	11.47	3.00	0.08	3.08	3.05
41	9.02	12.02	3.01	0.08	3.16	3.12
42	9.04	12.03	3.00	0.08	3.24	3.20
43	8.49	11.52	3.04	0.08	3.32	3.28
44	8.41	11.43	3.03	0.08	3.39	3.35

Table 46. CWT flooding data for core SK-C3

	Weight of Glass [g]	*Weight of Glass [g]*	*Volume Injected [ml]*	*PV per sample*	*PV injected*	*PV corrected for midpoints*
Sample #	*Before Test*	*After Test*				
1	8.40	17.72	9.34	0.25	0.25	0.12
2	8.46	11.35	2.90	0.08	0.08	0.04
3	8.45	11.49	3.05	0.08	0.16	0.12
4	9.10	12.15	3.06	0.08	0.24	0.20
5	9.09	12.12	3.04	0.08	0.32	0.28
6	8.42	11.47	3.06	0.08	0.40	0.36
7	8.41	11.46	3.06	0.08	0.48	0.44
8	9.04	12.09	3.06	0.08	0.56	0.52
9	9.05	12.10	3.06	0.08	0.64	0.60
10	8.41	11.47	3.07	0.08	0.72	0.68
11	8.48	11.52	3.05	0.08	0.80	0.76
12	8.46	11.49	3.04	0.08	0.88	0.84
13	8.40	11.45	3.06	0.08	0.96	0.92
14	8.44	11.50	3.07	0.08	1.04	1.00
15	9.01	12.07	3.07	0.08	1.12	1.08
16	9.08	12.13	3.06	0.08	1.20	1.16
17	8.50	11.57	3.08	0.08	1.28	1.25
18	8.47	11.53	3.07	0.08	1.36	1.33
19	8.42	11.48	3.07	0.08	1.44	1.41
20	8.46	11.50	3.05	0.08	1.52	1.49
21	8.42	11.46	3.05	0.08	1.61	1.57
22	8.95	12.05	3.11	0.08	1.69	1.65
23	8.42	11.48	3.07	0.08	1.77	1.73
24	8.36	11.40	3.05	0.08	1.85	1.81
25	9.03	12.07	3.05	0.08	1.93	1.89
26	8.46	11.50	3.05	0.08	2.01	1.97
27	8.42	11.47	3.06	0.08	2.09	2.05
28	9.61	12.67	3.07	0.08	2.17	2.13
29	8.36	11.40	3.05	0.08	2.25	2.21
30	8.45	11.50	3.06	0.08	2.33	2.29
31	9.00	12.05	3.06	0.08	2.41	2.37
32	8.98	12.04	3.07	0.08	2.49	2.45
33	8.99	12.03	3.05	0.08	2.57	2.53
34	9.04	12.10	3.07	0.08	2.65	2.61
35	9.38	12.43	3.06	0.08	2.73	2.69
36	8.41	11.47	3.07	0.08	2.81	2.78
37	8.42	11.44	3.03	0.08	2.89	2.86
38	8.40	11.40	3.01	0.08	2.97	2.93
39	9.09	12.14	3.06	0.08	3.05	3.01
40	8.49	11.53	3.05	0.08	3.13	3.09
41	8.36	11.40	3.05	0.08	3.21	3.18
42	8.52	11.57	3.06	0.08	3.29	3.26
43	8.43	11.48	3.06	0.08	3.37	3.34
44	7.99	11.03	3.05	0.08	3.45	3.42

Table 47. CWT flooding data for core SK-C6

	Weight of Glass [g]	*Weight of Glass [g]*	*Volume Injected [ml]*	*PV per sample*	*PV injected*	*PV corrected for midpoints*
Sample #	*Before Test*	*After Test*				
1	8.92	11.85	2.94	0.07	0.07	0.04
2	9.59	12.61	3.03	0.08	0.15	0.11
3	8.48	11.52	3.05	0.08	0.23	0.19
4	8.46	11.51	3.06	0.08	0.30	0.27
5	9.04	12.07	3.04	0.08	0.38	0.34
6	8.4	11.45	3.06	0.08	0.46	0.42
7	8.95	11.98	3.04	0.08	0.53	0.49
8	8.91	11.98	3.08	0.08	0.61	0.57
9	9.05	12.12	3.08	0.08	0.69	0.65
10	8.96	12.04	3.09	0.08	0.76	0.73
11	8.4	11.46	3.07	0.08	0.84	0.80
12	8.38	11.44	3.07	0.08	0.92	0.88
13	9.04	12.1	3.07	0.08	0.99	0.96
14	9.52	12.58	3.07	0.08	1.07	1.03
15	8.36	11.4	3.05	0.08	1.15	1.11
16	8.47	11.52	3.06	0.08	1.22	1.19
17	8.43	11.48	3.06	0.08	1.30	1.26
18	9	12.06	3.07	0.08	1.38	1.34
19	8.94	12.03	3.10	0.08	1.45	1.42
20	8.4	11.46	3.07	0.08	1.53	1.49
21	8.36	11.43	3.08	0.08	1.61	1.57
22	9.05	12.09	3.05	0.08	1.68	1.65
23	8.47	11.53	3.07	0.08	1.76	1.72
24	8.45	11.5	3.06	0.08	1.84	1.80
25	8.4	11.43	3.04	0.08	1.91	1.88
26	8.48	11.51	3.04	0.08	1.99	1.95
27	8.38	11.43	3.06	0.08	2.07	2.03
28	9.12	12.17	3.06	0.08	2.14	2.11
29	9.14	12.18	3.05	0.08	2.22	2.18
30	8.96	12.01	3.06	0.08	2.30	2.26
31	8.44	11.49	3.06	0.08	2.37	2.34
32	8.51	11.57	3.07	0.08	2.45	2.41
33	8.42	11.47	3.06	0.08	2.53	2.49
34	9.05	12.09	3.05	0.08	2.60	2.57
35	8.49	11.53	3.05	0.08	2.68	2.64
36	8.98	12.04	3.07	0.08	2.76	2.72
37	8.37	11.44	3.08	0.08	2.83	2.80
38	8.44	11.46	3.03	0.08	2.91	2.87
39	8.39	11.45	3.07	0.08	2.99	2.95
40	9.16	12.2	3.05	0.08	3.06	3.03
41	8.96	12.01	3.06	0.08	3.14	3.10
42	8.38	11.43	3.06	0.08	3.22	3.18
43	8.39	11.42	3.04	0.08	3.29	3.25
44	8.93	11.96	3.04	0.08	3.37	3.33

Table 48. Area calculation for chalk core SK-R1

Thiocyanate		
PV	*C/C0*	*Area under curve*
0.63	0.00000	0.00000
0.71	0.37838	0.01526
0.79	0.59846	0.03940
0.87	0.78378	0.05593
0.95	0.89189	0.06736
1.04	0.92664	0.07383
1.12	0.97683	0.07626
1.20	0.98649	0.07945
1.28	0.98842	0.07965
1.36	0.99421	0.08023
1.44	0.99614	0.08001
1.52	0.99228	0.07966
1.60	0.98263	0.08018
Sulphate		
PV	*C/C0*	*Area under curve*
0.71	0.00000	0.00000
0.79	0.02218	0.00089
0.87	0.11290	0.00547
0.95	0.33871	0.01815
1.04	0.43347	0.03135
1.12	0.62500	0.04241
1.20	0.71976	0.05442
1.28	0.80444	0.06147
1.36	0.92944	0.07016
1.44	0.87298	0.07245
1.52	0.92540	0.07205
1.60	0.98185	0.07743
Total area thiocyanate	*Total area sulphate*	*Area between curves*
0.80721	***0.50625***	***0.301***

Table 49. Area calculation for chalk core SK-R2

Thiocyanate		
PV	*C/C0*	*Area under curve*
0.60	0	0
0.68	0.15909091	0.00606627
0.76	0.43409091	0.02284622
0.83	0.69545455	0.04379316
0.91	0.85454545	0.05949945
0.99	0.91136364	0.06801345
1.06	0.93409091	0.0715494
1.14	0.96363636	0.07284757
1.22	0.97727273	0.07500188
1.30	0.98863636	0.07596794
1.37	1.02272727	0.07772443
Sulphate		
PV	*C/C0*	*Area under curve*

0.76	0	0
0.83	0.04319654	0.00167476
0.91	0.15334773	0.00754469
0.99	0.34557235	0.01921576
1.06	0.54643629	0.03458372
1.14	0.74946004	0.04974524
1.22	0.79049676	0.05950802
1.30	0.88984881	0.06493301
1.37	0.99784017	0.07294531
Total area thiocyanate	*Total area sulphate*	*Area between curves*
0.57330976	***0.3101505***	***0.263***

Table 50. Area calculation for chalk core SK-C3

Thiocyanate		
PV	*C/C0*	*Area under curve*
0.53	0	0
0.61	0.13009709	0.00523494
0.69	0.23495146	0.014689085
0.77	0.4	0.0256334
0.85	0.65436893	0.042287348
0.93	0.86019417	0.060544441
1.01	0.97281553	0.073757956
1.09	1	0.079643837
1.17	0.96116505	0.0791735
1.25	0.98446602	0.078289695
1.33	0.98640777	0.079825465
1.41	1	0.080192564
1.49	1	0.080741292
1.57	1	0.080213571
1.66	1	0.080213571
Sulphate		
PV	*C/C0*	*Area under curve*
0.69	0	0
0.77	0.02657005	0.00107265
0.85	0.07971014	0.004262557
0.93	0.21497585	0.01178003
1.01	0.42753623	0.025853861
1.09	0.5942029	0.041248269
1.17	0.74637681	0.054120069
1.25	0.86956522	0.065023432
1.33	0.89130435	0.071319753
1.41	0.92270531	0.073232742
1.49	0.9468599	0.075475555
1.57	0.97101449	0.076919777
1.66	1	0.079051055
Total area thiocyanate	*Total area sulphate*	*Area between curves*
0.86044066	***0.579359748***	***0.281***

Table 51. Area calculation for chalk core SK-C6

Thiocyanate		
PV	*C/C0*	*Area under curve*
0.52	0	0
0.60	0.15648855	0.006013618
0.67	0.44083969	0.022954419
0.75	0.73282443	0.045102134
0.83	0.94795539	0.064167666
0.90	0.95910781	0.073046054
0.98	0.96840149	0.073829199
1.06	0.9739777	0.074642689
1.13	0.95724907	0.074941708
1.21	0.96654275	0.073928405
1.29	0.97583643	0.07488662
1.36	0.97583643	0.074509636
1.44	0.97583643	0.074999831
1.52	0.97583643	0.074754734
Sulphate		
PV	*C/C0*	*Area under curve*
0.83	0	0
0.90	0.374358974	0.014339035
0.98	0.525641026	0.034472611
1.06	0.761538462	0.049464358
1.13	0.802564103	0.060695367
1.21	0.823076923	0.062470922
1.29	0.884615385	0.065838486
1.36	0.892307692	0.067838158
1.44	0.971794872	0.071634637
1.52	0.997435897	0.075427252
Total area thiocyanate	*Total area sulphate*	*Area between curves*
0.80777671	***0.502180827***	***0.306***

B.11: Relative permeability-Excel data

Table 52. Relative permeability-Excel data for core SK-R1

N_w	2.81		4		
N_o	2.23		3		
k_{rw}	0.09		0.1		
k_{ro}	0.8		0.4		
S_{wi}	0.2		0.2		
S_{or}	0.25		0.2		
μ_o	2.69		2.69		
μ_w	0.851		0.851		
S_w	S	k_{rw}	k_{ro}		fw
0.2	0	0	0.4		0

0.21	0.016666667	7.71605E-09	0.380331481		6.41291E-08
0.22	0.033333333	1.23457E-07	0.361318519		1.08006E-06
0.23	0.05	6.25E-07	0.34295		5.76062E-06
0.24	0.066666667	1.97531E-06	0.325214815		1.9199E-05
0.25	0.083333333	4.82253E-06	0.308101852		4.94746E-05
0.26	0.1	0.00001	0.2916		0.00010839
0.27	0.116666667	1.85262E-05	0.275698148		0.000212365
0.28	0.133333333	3.16049E-05	0.260385185		0.000383526
0.29	0.15	5.0625E-05	0.24565		0.000651011
0.3	0.166666667	7.71605E-05	0.231481481		0.001052553
0.31	0.183333333	0.000112971	0.217868519		0.001636375
0.32	0.2	0.00016	0.2048		0.002463438
0.33	0.216666667	0.000220378	0.192264815		0.003610112
0.34	0.233333333	0.00029642	0.180251852		0.005171285
0.35	0.25	0.000390625	0.16875		0.007263949
0.36	0.266666667	0.000505679	0.157748148		0.010031246
0.37	0.283333333	0.000644452	0.147235185		0.013646906
0.38	0.3	0.00081	0.1372		0.018319921
0.39	0.316666667	0.001005563	0.127631481		0.024299145
0.4	0.333333333	0.001234568	0.118518519		0.031877326
0.41	0.35	0.001500625	0.10985		0.041393779
0.42	0.366666667	0.001807531	0.101614815		0.053234576
0.43	0.383333333	0.002159267	0.093801852		0.067828683
0.44	0.4	0.00256	0.0864		0.085638107
0.45	0.416666667	0.003014082	0.079398148		0.107139803
0.46	0.433333333	0.003526049	0.072785185		0.132797166
0.47	0.45	0.004100625	0.06655		0.163019657
0.48	0.466666667	0.004742716	0.060681481		0.198110757
0.49	0.483333333	0.005457415	0.055168519		0.238207354
0.5	0.5	0.00625	0.05		0.283217519
0.51	0.516666667	0.007125934	0.045164815		0.33276778
0.52	0.533333333	0.008090864	0.040651852		0.386173753
0.53	0.55	0.009150625	0.03645		0.442447481
0.54	0.566666667	0.010311235	0.032548148		0.500349476
0.55	0.583333333	0.011578897	0.028935185		0.558483626
0.56	0.6	0.01296	0.0256		0.615421551
0.57	0.616666667	0.014461119	0.022531481		0.669834014
0.58	0.633333333	0.016089012	0.019718519		0.72060462
0.59	0.65	0.017850625	0.01715		0.766906404
0.6	0.666666667	0.019753086	0.014814815		0.808232555
0.61	0.683333333	0.021803711	0.012701852		0.844384107
0.62	0.7	0.02401	0.0108		0.875425772
0.63	0.716666667	0.026379637	0.009098148		0.901624456
0.64	0.733333333	0.028920494	0.007585185		0.923383897
0.65	0.75	0.031640625	0.00625		0.94118511
0.66	0.766666667	0.034548272	0.005081481		0.955537974
0.67	0.783333333	0.03765186	0.004068519		0.966945607
0.68	0.8	0.04096	0.0032		0.975880736
0.69	0.816666667	0.044481489	0.002464815		0.982771993
0.7	0.833333333	0.048225309	0.001851852		0.987997701
0.71	0.85	0.052200625	0.00135		0.991884849
0.72	0.866666667	0.05641679	0.000948148		0.994711382
0.73	0.883333333	0.060883341	0.000635185		0.996710362

0.74	0.9	0.06561	0.0004		0.998075001
0.75	0.916666667	0.070606674	0.000231481		0.99896391
0.76	0.93333333	0.07588346	0.00011852		0.99950614
0.77	0.95	0.08145063	5E-05		0.99980584
0.78	0.96666667	0.08731864	1.4815E-05		0.99994633
0.79	0.98333333	0.09349816	1.8519E-06		0.99999373
0.8	1	0.1	0		1

Table 53. Relative permeability-Excel data for core SK-R2

N_w	1.001		3.5		
N_o	2.49		2.8		
k_{rw}	0.07		0.12		
k_{ro}	0.82		0.2		
S_{wi}	0.2		0.2		
S_{or}	0.23		0.13		
μ_o	2.69		2.69		
μ_w	0.851		0.851		
S_w	S	k_{rw}	k_{ro}		fw
0.2	0	0	0.2		0
0.21	0.014925373	4.87438E-08	0.191753618		8.03523E-07
0.22	0.029850746	5.51473E-07	0.1837291		9.48779E-06
0.23	0.044776119	2.27952E-06	0.175923751		4.09566E-05
0.24	0.059701493	6.23921E-06	0.168334869		0.000117146
0.25	0.074626866	1.36243E-05	0.160959746		0.000267488
0.26	0.089552239	2.57898E-05	0.153795662		0.000529782
0.27	0.104477612	4.42346E-05	0.14683989		0.000951323
0.28	0.119402985	7.05886E-05	0.140089692		0.001590229
0.29	0.134328358	0.000106603	0.133542324		0.002516967
0.3	0.149253731	0.000154141	0.127195031		0.003816028
0.31	0.164179104	0.000215176	0.121045047		0.005587738
0.32	0.179104478	0.000291779	0.115089599		0.007950125
0.33	0.194029851	0.000386119	0.109325904		0.011040766
0.34	0.208955224	0.000500458	0.103751165		0.01501846
0.35	0.223880597	0.000637146	0.09836258		0.020064536
0.36	0.23880597	0.000798619	0.093157332		0.026383534
0.37	0.253731343	0.000987394	0.088132595		0.034202884
0.38	0.268656716	0.001206072	0.083285534		0.043771173
0.39	0.28358209	0.001457327	0.078613297		0.055354461
0.4	0.298507463	0.001743911	0.074113027		0.069230094
0.41	0.313432836	0.00206865	0.06978185		0.08567747
0.42	0.328358209	0.002434439	0.065616882		0.104965316
0.43	0.343283582	0.002844244	0.061615226		0.127335334
0.44	0.358208955	0.003301101	0.057773972		0.152982473
0.45	0.373134328	0.00380811	0.054090197		0.182032754
0.46	0.388059701	0.004368438	0.050560964		0.214520338
0.47	0.402985075	0.004985315	0.047183323		0.250366316
0.48	0.417910448	0.005662035	0.043954308		0.289362354
0.49	0.432835821	0.006401952	0.040870939		0.331162496
0.5	0.447761194	0.007208482	0.037930221		0.375286026

0.51	0.462686567	0.008085099	0.035129143		0.42113303
0.52	0.47761194	0.009035337	0.032464676		0.468012491
0.53	0.492537313	0.010062786	0.029933777		0.515180554
0.54	0.507462687	0.011171092	0.027533383		0.5618847
0.55	0.52238806	0.01236396	0.025260415		0.607408419
0.56	0.537313433	0.013645146	0.023111774		0.651110928
0.57	0.552238806	0.015018462	0.021084342		0.692457572
0.58	0.567164179	0.016487774	0.019174981		0.731038351
0.59	0.582089552	0.018056998	0.017380531		0.76657416
0.6	0.597014925	0.019730105	0.015697811		0.798912092
0.61	0.611940299	0.021511116	0.014123617		0.828012409
0.62	0.626865672	0.0234041	0.012654721		0.853930247
0.63	0.641791045	0.025413181	0.011287871		0.876794999
0.64	0.656716418	0.027542528	0.010019787		0.896789799
0.65	0.671641791	0.029796362	0.008847164		0.914132784
0.66	0.686567164	0.032178948	0.007766665		0.929061125
0.67	0.701492537	0.034694604	0.006774926		0.941818225
0.68	0.71641791	0.037347692	0.005868548		0.952644024
0.69	0.731343284	0.04014262	0.005044099		0.961768133
0.7	0.746268657	0.043083845	0.00429811		0.969405331
0.71	0.76119403	0.046175866	0.003627075		0.975752967
0.72	0.776119403	0.049423232	0.003027444		0.980989799
0.73	0.791044776	0.052830532	0.002495623		0.985275885
0.74	0.805970149	0.056402402	0.002027972		0.988753186
0.75	0.820895522	0.060143521	0.001620795		0.991546635
0.76	0.835820896	0.064058613	0.00127034		0.99376547
0.77	0.850746269	0.068152444	0.000972793		0.995504689
0.78	0.86567164	0.07242982	0.00072427		0.99684654
0.79	0.88059701	0.0768956	0.0005208		0.99786195
0.8	0.89552239	0.08155467	0.00035834		0.9986119
0.81	0.91044776	0.08641196	0.00023273		0.99914871
0.82	0.92537313	0.09147246	0.00013968		0.99951715
0.83	0.94029851	0.09674118	7.4781E-05		0.99975552
0.84	0.95522388	0.10222317	3.3416E-05		0.99989659
0.85	0.97014925	0.10792354	1.0738E-05		0.99996853
0.86	0.98507463	0.11384742	1.5418E-06		0.99999572
0.87	1	0.12	0		1

Table 54. Relative permeability-Excel data for core SK-C3

N_w	3.85		3.85		
N_o	2.3		3.39		
k_{rw}	0.12		0.23		
k_{ro}	0.61		1		
S_{wi}	0.2		0.2		
S_{or}	0.26		0.17		
μ_o	2.69		2.69		
μ_w	0.851		0.851		
S_w	S	k_{rw}	k_{ro}		fw
0.2	0	0	1		0
0.21	0.015873016	2.71811E-08	0.947203654		9.07081E-08

0.22	0.031746032	3.91951E-07	0.896403778		1.38214E-06
0.23	0.047619048	1.86717E-06	0.847555753		6.96362E-06
0.24	0.063492063	5.65194E-06	0.800615247		2.23145E-05
0.25	0.079365079	1.33445E-05	0.755538215		5.58269E-05
0.26	0.095238095	2.69246E-05	0.712280899		0.000119473
0.27	0.111111111	4.8741E-05	0.670799838		0.000229628
0.28	0.126984127	8.1501E-05	0.631051865		0.000408078
0.29	0.142857143	0.000128263	0.592994115		0.000683244
0.3	0.158730159	0.000192427	0.556584023		0.001091652
0.31	0.174603175	0.000277734	0.521779332		0.00167971
0.32	0.19047619	0.000388253	0.488538095		0.002505816
0.33	0.206349206	0.000528383	0.456818677		0.00364286
0.34	0.222222222	0.000702845	0.426579763		0.00518115
0.35	0.238095238	0.000916681	0.397780356		0.007231782
0.36	0.253968254	0.001175246	0.370379785		0.00993047
0.37	0.26984127	0.001484209	0.34433771		0.013441754
0.38	0.285714286	0.001849549	0.319614121		0.017963471
0.39	0.301587302	0.002277551	0.296169349		0.023731222
0.4	0.317460317	0.002774803	0.273964065		0.031022377
0.41	0.333333333	0.003348197	0.252959289		0.040158956
0.42	0.349206349	0.004004922	0.233116391		0.05150833
0.43	0.365079365	0.004752465	0.214397101		0.065480371
0.44	0.380952381	0.005598607	0.196763507		0.082519225
0.45	0.396825397	0.006551425	0.18017807		0.103087631
0.46	0.412698413	0.007619283	0.16460362		0.12764164
0.47	0.428571429	0.008810838	0.15000337		0.156594148
0.48	0.444444444	0.010135032	0.136340916		0.190267008
0.49	0.46031746	0.011601096	0.123580249		0.228833995
0.5	0.476190476	0.013218542	0.111685757		0.272260403
0.51	0.492063492	0.014997167	0.100622236		0.320249035
0.52	0.507936508	0.016947051	0.090354894		0.372205445
0.53	0.523809524	0.019078551	0.080849361		0.427235657
0.54	0.53968254	0.021402305	0.072071697		0.484185666
0.55	0.555555556	0.023929228	0.063988402		0.541723534
0.56	0.571428571	0.026670512	0.056566421		0.598453945
0.57	0.587301587	0.029637622	0.049773157		0.653045487
0.58	0.603174603	0.0328423	0.043576482		0.704346876
0.59	0.619047619	0.036296559	0.037944746		0.751471593
0.6	0.634920635	0.040012684	0.032846788		0.793839598
0.61	0.650793651	0.044003231	0.02825195		0.831176018
0.62	0.666666667	0.048281026	0.02413009		0.863475727
0.63	0.682539683	0.052859162	0.020451597		0.89094734
0.64	0.698412698	0.057751002	0.017187402		0.913950079
0.65	0.714285714	0.062970175	0.014309002		0.932933967
0.66	0.73015873	0.068530575	0.011788468		0.948389617
0.67	0.746031746	0.074446361	0.009598476		0.960810144
0.68	0.761904762	0.080731958	0.007712318		0.970665001
0.69	0.777777778	0.087402052	0.00610393		0.978384037
0.7	0.793650794	0.094471593	0.004747921		0.984349477
0.71	0.80952381	0.101955791	0.003619595		0.98889356
0.72	0.825396825	0.109870119	0.002694987		0.992299882
0.73	0.841269841	0.118230307	0.001950902		0.994806946
0.74	0.857142857	0.127052348	0.001364953		0.996612817

0.75	0.873015873	0.136352491	0.00091561		0.997880159
0.76	0.888888889	0.146147242	0.000582261		0.998741198
0.77	0.904761905	0.156453367	0.000345277		0.999302318
0.78	0.920634921	0.167287887	0.000186099		0.999648194
0.79	0.936507937	0.178668078	8.73412E-05		0.999845374
0.8	0.952380952	0.190611472	3.29364E-05		0.999945339
0.81	0.968253968	0.203135855	8.33158E-06		0.999987025
0.82	0.984126984	0.216259266	7.94759E-07		0.999998837
0.83	1	0.23	0		1

B.12: Capillary pressure curve- Excel data

Table 55. Capillary pressure curve data for chalk core SK-R1

c_w	15053				
a_w	0.251				
c_o	0				
a_o	0.251				
S_{wi}	0.2				
S_{or}	0.25				
S_w			W	O	P_c
0.2	0	0.925104211		0	
0.21	0.33290814	0.920853317	45216.6776	0	45216.6776
0.22	0.39617124	0.916543045	37996.196	0	37996.196
0.23	0.43861335	0.912171423	34319.5207	0	34319.5207
0.24	0.47145633	0.907736371	31928.726	0	31928.726
0.25	0.49861563	0.903235699	30189.5874	0	30189.5874
0.26	0.52196379	0.898667093	28839.1652	0	28839.1652
0.27	0.54255531	0.894028109	27744.6366	0	27744.6366
0.28	0.56104798	0.889316162	26830.1476	0	26830.1476
0.29	0.57788215	0.884528516	26048.5635	0	26048.5635
0.3	0.5933684	0.879662268	25368.7254	0	25368.7254
0.31	0.60773462	0.874714337	24769.0349	0	24769.0349
0.32	0.62115346	0.869681447	24233.9471	0	24233.9471
0.33	0.63375908	0.864560112	23751.9279	0	23751.9279
0.34	0.64565802	0.859346616	23314.1997	0	23314.1997
0.35	0.65693639	0.854036989	22913.9385	0	22913.9385
0.36	0.66766487	0.848626988	22545.742	0	22545.742
0.37	0.67790228	0.843112068	22205.2654	0	22205.2654
0.38	0.68769808	0.83748735	21888.9661	0	21888.9661
0.39	0.69709436	0.831747589	21593.9203	0	21593.9203
0.4	0.7061272	0.825887137	21317.6889	0	21317.6889
0.41	0.71482784	0.819899896	21058.2174	0	21058.2174
0.42	0.72322346	0.813779269	20813.7606	0	20813.7606
0.43	0.73133793	0.807518104	20582.824	0	20582.824
0.44	0.7391923	0.801108626	20364.119	0	20364.119
0.45	0.74680524	0.794542363	20156.5271	0	20156.5271
0.46	0.75419339	0.787810057	19959.0717	0	19959.0717
0.47	0.76137168	0.780901557	19770.8956	0	19770.8956
0.48	0.76835351	0.773805706	19591.2426	0	19591.2426
0.49	0.775151	0.766510191	19419.4422	0	19419.4422
0.5	0.78177513	0.759001379	19254.8976	0	19254.8976
0.51	0.78823588	0.751264115	19097.0754	0	19097.0754
0.52	0.79454236	0.743281476	18945.497	0	18945.497
0.53	0.80070292	0.735034486	18799.7316	0	18799.7316
0.54	0.8067252	0.726501752	18659.3899	0	18659.3899
0.55	0.81261623	0.717659027	18524.1193	0	18524.1193
0.56	0.81838251	0.708478665	18393.5993	0	18393.5993
0.57	0.82403004	0.698928937	18267.5378	0	18267.5378
0.58	0.82956438	0.688973158	18145.6682	0	18145.6682
0.59	0.83499068	0.678568568	18027.7461	0	18027.7461
0.6	0.84031375	0.667664875	17913.5471	0	17913.5471

0.61	0.84553806	0.656202317	17802.8651	0	17802.8651
0.62	0.85066778	0.644109055	17695.5097	0	17695.5097
0.63	0.85570682	0.631297567	17591.3053	0	17591.3053
0.64	0.86065884	0.617659587	17490.0893	0	17490.0893
0.65	0.86552727	0.60305875	17391.7109	0	17391.7109
0.66	0.87031532	0.587319598	17296.0301	0	17296.0301
0.67	0.87502604	0.570210499	17202.9167	0	17202.9167
0.68	0.87966227	0.551415832	17112.2493	0	17112.2493
0.69	0.88422671	0.530488027	17023.9146	0	17023.9146
0.7	0.8887219	0.506758561	16937.8069	0	16937.8069
0.71	0.89315026	0.479155724	16853.8271	0	16853.8271
0.72	0.89751404	0.445776385	16771.8824	0	16771.8824
0.73	0.90181542	0.402641144	16691.8858	0	16691.8858
0.74	0.90605643	0.338344891	16613.7555	0	16613.7555
0.75	0.91023902	0	16537.4146	#DIV/0!	

Table 56. Capillary pressure curve data for chalk core SK-R2

c_w	14812				
a_w	0.251				
c_o	0.04				
a_o	2				
S_{wi}	0.2				
S_{or}	0.23				
S_w			W	O	P_c
0.2	0	0.547984483	0	0.072994768	
0.21	0.332908139	0.52892562	44492.75417	0.075625	44492.67855
0.22	0.396171238	0.510204082	37387.87321	0.0784	37387.79481
0.23	0.438613352	0.491819868	33770.06178	0.08133059	33769.98045
0.24	0.47145633	0.47377298	31417.54402	0.084428622	31417.45959
0.25	0.498615626	0.456063417	29706.24914	0.087707101	29706.16143
0.26	0.521963791	0.438691179	28377.44733	0.091180315	28377.35615
0.27	0.542555314	0.421656266	27300.44223	0.094864	27300.34737
0.28	0.561047976	0.404958678	26400.5943	0.09877551	26400.49553
0.29	0.577882154	0.388598415	25631.52347	0.102934028	25631.42053
0.3	0.593368399	0.372575476	24962.56968	0.107360797	24962.46232
0.31	0.60773462	0.356889863	24372.48019	0.112079395	24372.36811
0.32	0.621153456	0.341541575	23845.95924	0.117116049	23845.84213
0.33	0.63375908	0.326530612	23371.65725	0.1225	23371.53475
0.34	0.64565802	0.311856974	22940.93705	0.128263926	22940.80878
0.35	0.656936389	0.297520661	22547.08407	0.134444444	22546.94962
0.36	0.667664875	0.283521673	22184.78246	0.141082689	22184.64138
0.37	0.677902277	0.26986001	21849.75697	0.148225	21849.60875
0.38	0.68769808	0.256535672	21538.52166	0.155923734	21538.36574
0.39	0.697094357	0.243548659	21248.19955	0.164238227	21248.03531
0.4	0.706127202	0.230898971	20976.39059	0.173235939	20976.21735
0.41	0.714827836	0.218586608	20721.07331	0.182993827	20720.89031
0.42	0.723223461	0.20661157	20480.53028	0.1936	20480.33668
0.43	0.731337933	0.194973857	20253.29103	0.205155709	20253.08587
0.44	0.739192301	0.183673469	20038.08749	0.217777778	20037.86971
0.45	0.746805238	0.172710406	19833.81911	0.231601563	19833.5875
0.46	0.754193393	0.162084669	19639.525	0.246784599	19639.27822

0.47	0.761371679	0.151796256	19454.36166	0.263511111	19454.09815
0.48	0.768353509	0.141845168	19277.58489	0.281997622	19277.30289
0.49	0.775150998	0.132231405	19108.53502	0.3025	19108.23252
0.5	0.781775126	0.122954967	18946.62481	0.325322359	18946.29949
0.51	0.788235878	0.114015854	18791.32938	0.350828402	18790.97855
0.52	0.794542363	0.105414066	18642.17779	0.379456	18641.79834
0.53	0.80070292	0.097149604	18498.74608	0.411736111	18498.33435
0.54	0.806725196	0.089222466	18360.65127	0.44831758	18360.20295
0.55	0.812616231	0.081632653	18227.54634	0.49	18227.05634
0.56	0.818382513	0.074380165	18099.11595	0.537777778	18098.57818
0.57	0.824030043	0.067465003	17975.07278	0.5929	17974.47988
0.58	0.82956438	0.060887165	17855.15429	0.656952909	17854.49734
0.59	0.834990683	0.054646652	17739.12009	0.731975309	17738.38811
0.6	0.840313752	0.048743464	17626.74949	0.820622837	17625.92886
0.61	0.84553806	0.043177602	17517.83946	0.92640625	17516.91306
0.62	0.850667783	0.037949064	17412.20286	1.054044444	17411.14881
0.63	0.855706824	0.033057851	17309.66679	1.21	17308.45679
0.64	0.860658842	0.028503964	17210.07125	1.403313609	17208.66794
0.65	0.865527267	0.024287401	17113.2679	1.646944444	17111.62096
0.66	0.870315321	0.020408163	17019.11898	1.96	17017.15898
0.67	0.875026036	0.016866251	16927.49631	2.3716	16925.12471
0.68	0.879662268	0.013661663	16838.28048	2.927901235	16835.35258
0.69	0.88422671	0.0107944	16751.36008	3.705625	16747.65445
0.7	0.888721904	0.008264463	16666.63095	4.84	16661.79095
0.71	0.893150257	0.00607185	16583.99568	6.587777778	16577.4079
0.72	0.897514043	0.004216563	16503.36295	9.4864	16493.87655
0.73	0.901815419	0.0026986	16424.64709	14.8225	16409.82459
0.74	0.90605643	0.001517963	16347.76765	26.35111111	16321.41654
0.75	0.910239019	0.00067465	16272.64893	59.29	16213.35893
0.76	0.91436503	0.000168663	16199.21969	237.16	15962.05969
0.77	0.918436219	3.75506E-31	16127.41276	1.06523E+29	

Table 57. Capillary pressure curve data for chalk core SK-C3

c_w	0				
a_w	0.251				
c_o	4348				
a_o	0.251				
S_{wi}	0.2				
S_{or}	0.26				
S_w			W	O	P_c
0.2	0	0.923961068		4705.82598	
0.21	0.33290814	0.91963625	0	4727.9563	-4727.9563
0.22	0.39617124	0.915249874	0	4750.61524	-4750.61524
0.23	0.43861335	0.910799854	0	4773.82597	-4773.82597
0.24	0.47145633	0.906283993	0	4797.61315	-4797.61315
0.25	0.49861563	0.901699968	0	4822.00305	-4822.00305
0.26	0.52196379	0.897045329	0	4847.02374	-4847.02374
0.27	0.54255531	0.89231748	0	4872.70517	-4872.70517
0.28	0.56104798	0.887513676	0	4899.07944	-4899.07944
0.29	0.57788215	0.882631005	0	4926.1809	-4926.1809
0.3	0.5933684	0.877666375	0	4954.04646	-4954.04646

0.31	0.60773462	0.8726165	0	4982.71577	-4982.71577
0.32	0.62115346	0.867477882	0	5012.23154	-5012.23154
0.33	0.63375908	0.86224679	0	5042.63982	-5042.63982
0.34	0.64565802	0.856919244	0	5073.99038	-5073.99038
0.35	0.65693639	0.851490986	0	5106.33709	-5106.33709
0.36	0.66766487	0.845957453	0	5139.73839	-5139.73839
0.37	0.67790228	0.840313752	0	5174.25782	-5174.25782
0.38	0.68769808	0.834554621	0	5209.96456	-5209.96456
0.39	0.69709436	0.82867439	0	5246.9342	-5246.9342
0.4	0.7061272	0.822666943	0	5285.24944	-5285.24944
0.41	0.71482784	0.81652566	0	5325.00106	-5325.00106
0.42	0.72322346	0.810243364	0	5366.28893	-5366.28893
0.43	0.73133793	0.803812256	0	5409.22332	-5409.22332
0.44	0.7391923	0.797223833	0	5453.92626	-5453.92626
0.45	0.74680524	0.790468805	0	5500.53332	-5500.53332
0.46	0.75419339	0.783536991	0	5549.19557	-5549.19557
0.47	0.76137168	0.776417192	0	5600.08208	-5600.08208
0.48	0.76835351	0.769097056	0	5653.38271	-5653.38271
0.49	0.775151	0.761562903	0	5709.31171	-5709.31171
0.5	0.78177513	0.753799526	0	5768.11188	-5768.11188
0.51	0.78823588	0.745789947	0	5830.05981	-5830.05981
0.52	0.79454236	0.737515125	0	5895.47231	-5895.47231
0.53	0.80070292	0.728953594	0	5964.7144	-5964.7144
0.54	0.8067252	0.720081026	0	6038.20938	-6038.20938
0.55	0.81261623	0.710869682	0	6116.4516	-6116.4516
0.56	0.81838251	0.701287725	0	6200.02297	-6200.02297
0.57	0.82403004	0.691298346	0	6289.61436	-6289.61436
0.58	0.82956438	0.680858642	0	6386.05392	-6386.05392
0.59	0.83499068	0.66991815	0	6490.34512	-6490.34512
0.6	0.84031375	0.658416909	0	6603.71862	-6603.71862
0.61	0.84553806	0.646282833	0	6727.70462	-6727.70462
0.62	0.85066778	0.633428108	0	6864.23596	-6864.23596
0.63	0.85570682	0.619744102	0	7015.79892	-7015.79892
0.64	0.86065884	0.605093989	0	7185.66055	-7185.66055
0.65	0.86552727	0.589301719	0	7378.22385	-7378.22385
0.66	0.87031532	0.57213488	0	7599.60658	-7599.60658
0.67	0.87502604	0.553276783	0	7858.63447	-7858.63447
0.68	0.87966227	0.53227835	0	8168.65837	-8168.65837
0.69	0.88422671	0.5084688	0	8551.16381	-8551.16381
0.7	0.8887219	0.480772808	0	9043.77271	-9043.77271
0.71	0.89315026	0.447280818	0	9720.96237	-9720.96237
0.72	0.89751404	0.404000002	0	10762.3762	-10762.3762
0.73	0.90181542	0.339486758	0	12807.5688	-12807.5688
0.74	0.90605643	0	0	0	

B.13: Skjæveland exponent values summary

Table 58. Summary of Skjæveland exponents

	SK-R1	*SK-R2*	*SK-C3*
c_w	15053	14812	14812
a_w	0.251	0.251	0.251

c_o	0	0.04	4348
a_o	0.251	0.251	0.251
S_{wi}	0.2	0.2	0.2
S_{or}	0.25	0.23	0.26